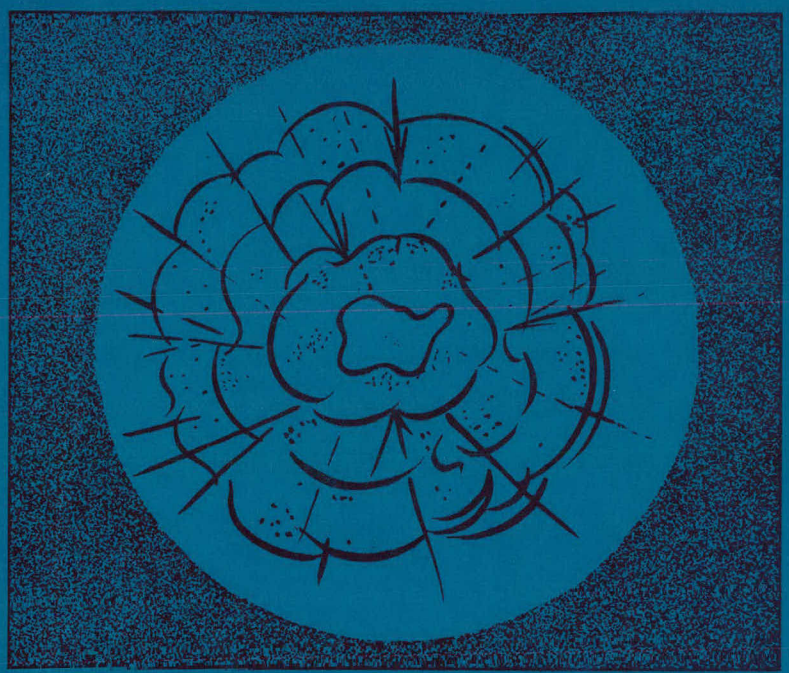

U.S. ATOMIC ENERGY COMMISSION
Albuquerque Operations Office
and
University of California
Lawrence Radiation Laboratory

FINAL REPORT

Project

COWBOY

Winnfield, Louisiana

DECEMBER 1959 - MARCH 1960

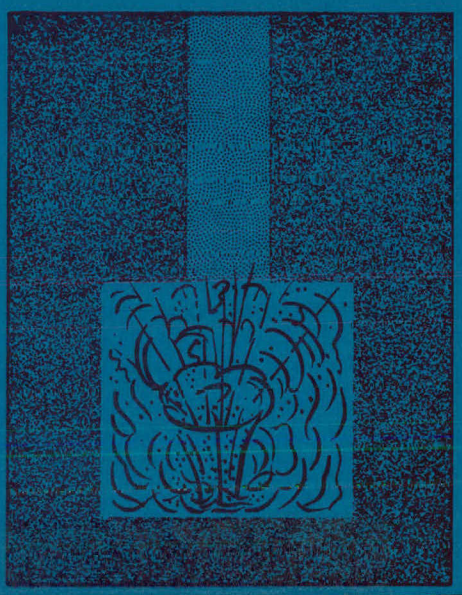

DYNAMIC ROCK MECHANICS INVESTIGATIONS

U.S. BUREAU OF MINES
APPLIED PHYSICS RESEARCH LABORATORY
COLLEGE PARK, MD.

DISCLAIMER

U. S. BUREAU OF MINES
APPLIED PHYSICS RESEARCH LABORATORY
COLLEGE PARK, MARYLAND

Contract No. AT(29-2)-914

DYNAMIC ROCK MECHANICS INVESTIGATIONS

PROJECT COWBOY

by

Harry R. Nicholls, Verne Hooker and Wilbur I. Duvall

September 1, 1960

NOTICE

This report, Dynamic Rock Mechanics Investigations- Project COWBOY, is presented in lieu of the two scheduled Applied Physics Research Laboratory reports listed in the "Titles for Final Project COWBOY Reports", given at end of this report. The interdependence of the various parts of this investigation prompted the submission of this combined report.

TABLE OF CONTENTS

FIGURES

FIGURES

TABLES

DYNAMIC ROCK MECHANICS INVESTIGATIONS

Project COWBOY

by

Harry R. Nicholls[1/], Verne Hooker[1/] and Wilbur I. Duvall[2/]

INTRODUCTION

This investigation was performed by APRL under Memorandum of Understanding AT (29-2)-914, Schedule 4, Appendix A- Rock Mechanics Studies, Item 1.a (1) Dynamic Stress Investigations in Rock Mechanic Studies in the Carey Salt Mine. This investigation included the following:

1. Strain gage instrumentation of three COWBOY shots to measure the strain produced in salt by coupled and decoupled detonations.
2. Linear array tests to develop a propagation law for strain, particle velocity and acceleration in salt; to compare explosives; to determine the effect of impedance coupling between explosive and rock; and to investigate other seismic effects.
3. Crater tests to determine the dynamic tensile breaking strength of salt.
4. Tests to measure in situ, longitudinal (P) and shear (S) wave velocities and to calculate the dynamic elastic constants therefrom.
5. Laboratory tests on core to determine the dynamic compressive and tensile breaking strength of salt.
6. Physical properties tests under laboratory conditions for comparison with dynamic results.

INSTRUMENTATION

The APRL instrumentation used in the linear array and other tests at Project COWBOY consisted of various gages, preamplifiers, a magnetic tape recorder, and a direct playback oscillograph. Figure 1 is a block diagram of the overall seismic recording and readout system. Most of

---

1/ Geophysicist, Applied Physics Research Laboratory, Bureau of Mines, Region V, College Park, Maryland.

2/ Supervisory Physicist, Applied Physics Research Laboratory, Bureau of Mines, Region V, College Park, Maryland.

this equipment was commercially available except the strain gages and preamplifiers. The strain gages and preamplifiers were designed and fabricated by APRL.

The APRL borehole strain gages used in the linear array consisted of Baldwin-Lima Hamilton Type C-1 resistance strain gage elements mounted on selected limestone cores (1)3/ . The limestone cores were chosen to match the characteristic impedance of the salt because salt cores were unavailable at the time the gages were prepared.

Type C-7 resistance strain gage elements were used in the dynamic core studies. These elements were cemented along the cores at various distances and were unshielded.

The strain gage output depends on the preamplifier input circuit, the gage characteristics, and the gage current. Figure 2 is a schematic diagram of the preamplifier input. The change in voltage, ΔE, generated by the gage is given by the equation:

$$\Delta E = \frac{(R_g R_1)}{(R_g + R_1)} f I \Delta \epsilon \qquad (1)$$

where

R_g = gage resistance= 505 ohms

R_1 = Shunt resistance= 3100 ohms

f= gage factor=3.24

I= gage current= 0.025 ampere

$\Delta\epsilon$= change in applied strain

For these circuit constants, the voltage generated by a type C-1 strain gage is 35.2 micro-volts per micro-inch per inch of strain.

3/ Underlined numbers in parentheses refer to items in the bibliography at the end of the publication.

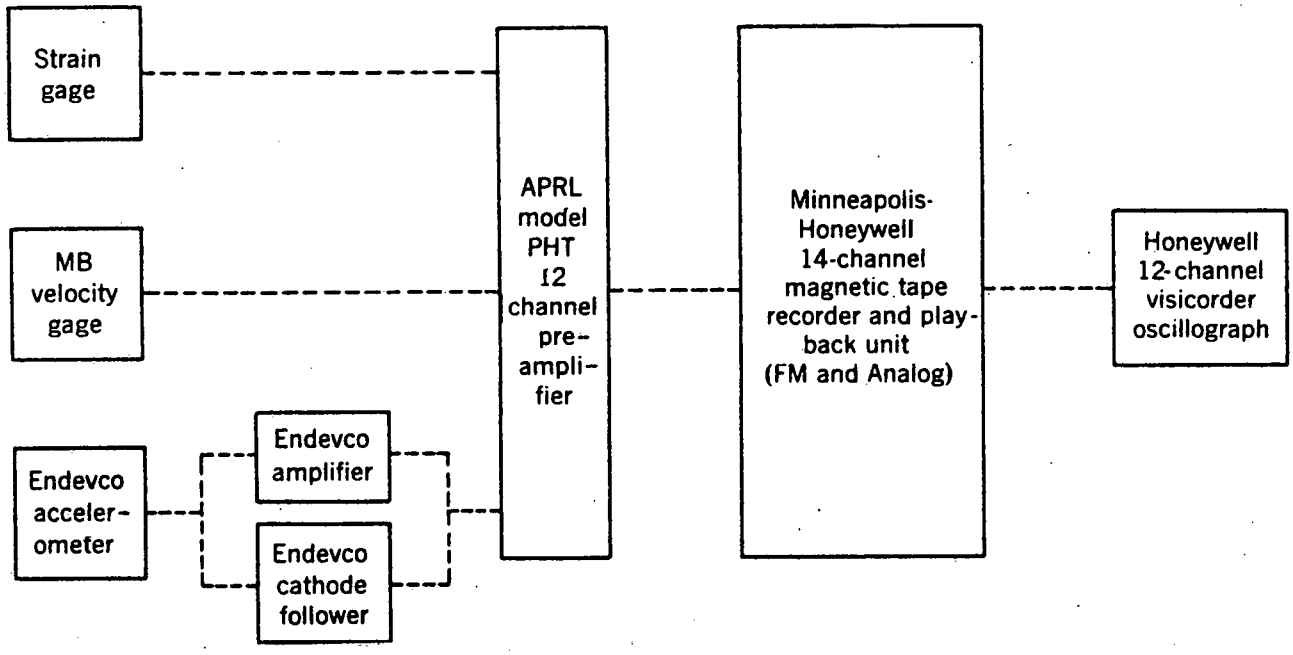

FIGURE 1. - Seismic Recording and Readout System.

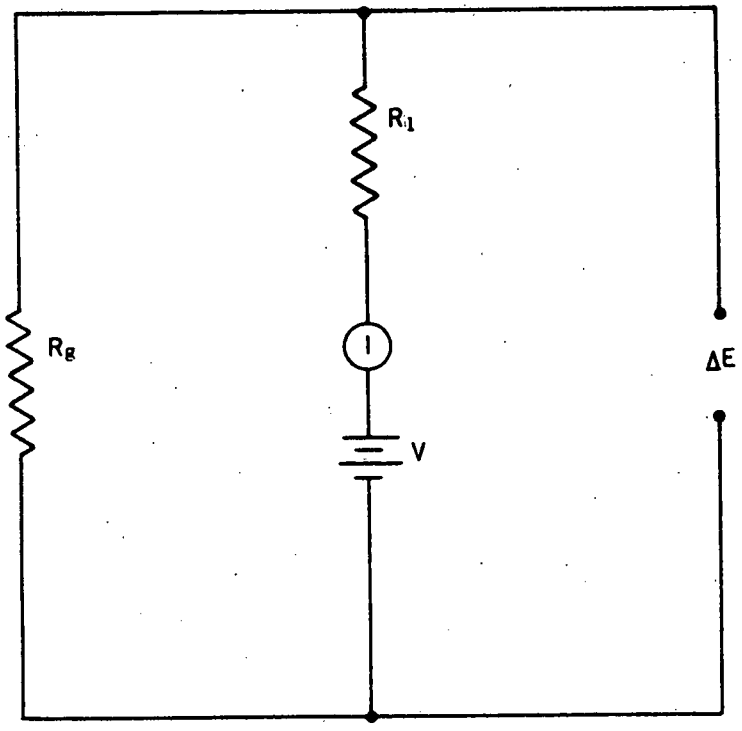

FIGURE 2. - Input Circuit for Strain Gage.

FIGURE 3. - Typical Response of MB Type 124 Velocity Gage.

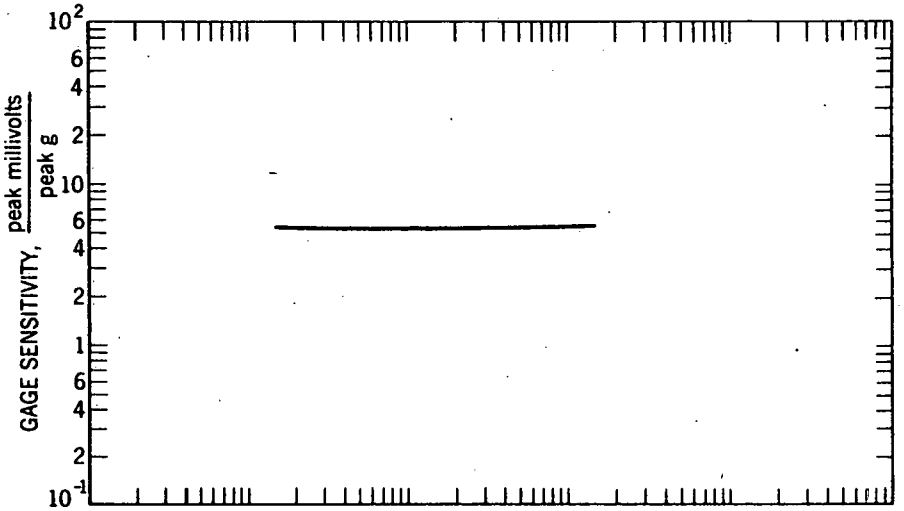

FIGURE 4. - Typical Response of Endevco Model 2215 Accelerometer.

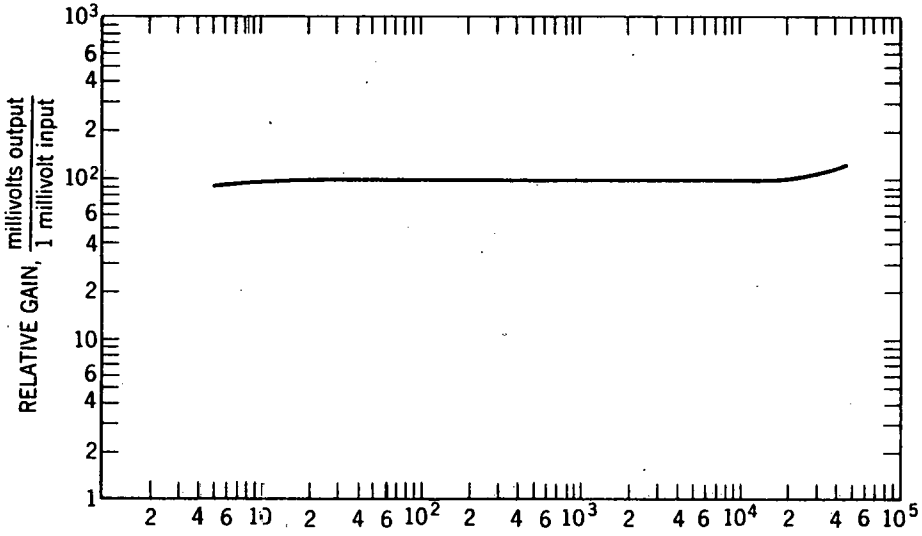

FIGURE 5. - Typical Response of Endevco Model 2607 Amplifier.

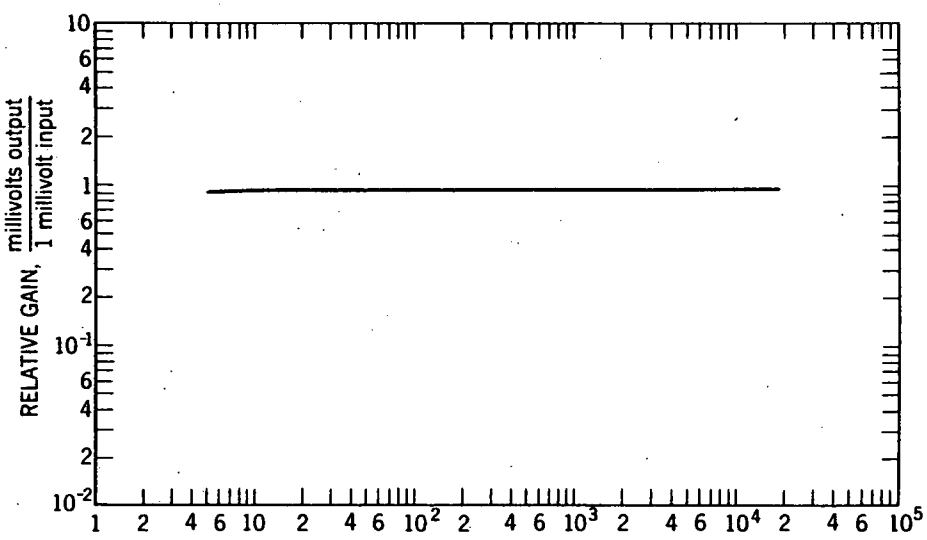

FIGURE 6. - Typical Response of Endevco Model 2608M3 Cathode Follower.

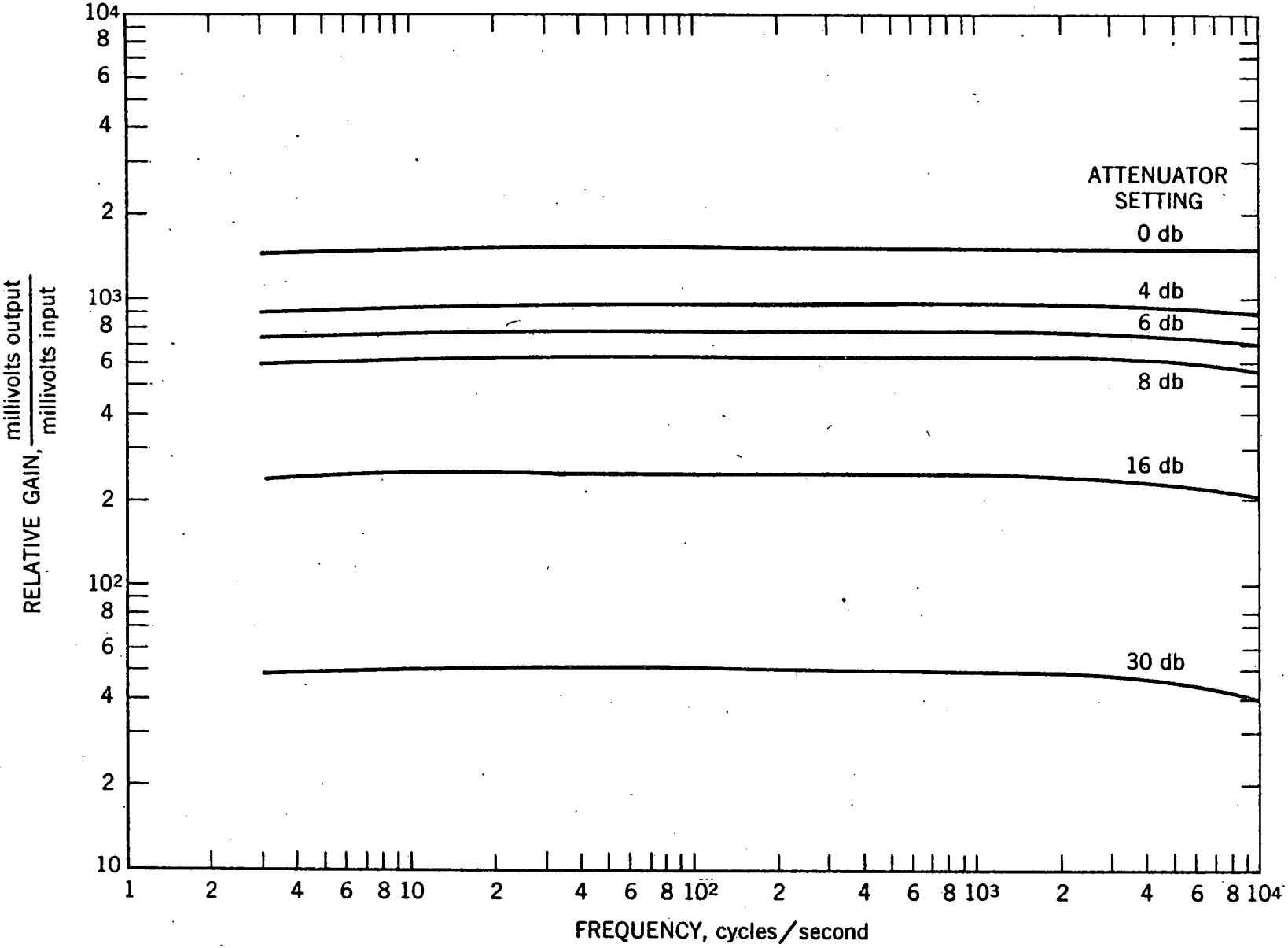

FIGURE 7. - Typical Frequency Response at Various Gain Settings, PHT Amplifiers.

Particle velocity measurements were made with MB Type 124 gages having a frequency response as shown in figure 3. The amplitude response is linear from 0 to 0.4 inch depending upon frequency. The gages will withstand accelerations to 50 g.

Endevco accelerometers Model 2215 were used. Figure 4 shows a typical frequency response curve. The amplitude linearity of these accelerometers is within 1% and the maximum acceleration tolerable to 10,000 g. These gages were chosen primarily because their high internal capacitance permits the use of long cable leads. In this gage, the Piezite crystal is not mechanically isolated from the case.

Calibration of the velocity and acceleration gages were made on MB Model C-11 vibration pickup calibration. Table 1 illustrates typical characteristics for the various gages.

TABLE 1.- Typical gage characteristics

Gage type	Sensitivity	Frequency range, cps
Borehole strain (APRL)	35μ volts/μinch/inch	0-20,000
Velocity (MB 124)	96,000 μ volts/ inch/ sec.	10-2000
Accelerometer (Endevco 2215)	700 μ volts/ g	0-10,000
Strain gage C-7	32 μ volts/ μ inch/inch	0-40,000

To match the accelerometer gage impedance and to provide gain, Endevco Model 2607 amplifiers or Endevco Model 2608 M3 cathode followers were used. These amplifiers provide high level outputs at low impedance. At low g levels, the Model 2607 amplifier was used at an amplification of 10, 30, or 100. The Model 2608 M3 cathode follower was used where seismic signals were large and additional amplification was unnecessary. Figures 5 and 6 show typical frequency responses for the amplifier and cathode follower, respectively.

Preamplifiers (APRL Model PHT) were designed to amplify signals from strain or velocity gages, or from accelerometer amplifiers or followers and to deliver up to 1 volt to the tape recording system. A maximum gain of 2000 was available. Gain control was accomplished by a 60 db switch attenuator (in two 30 db steps) and a 38 db attenuator (in two db steps), providing a total attenuation of 98 db. Figure 7 shows the frequency response of these preamplifiers at various gain settings.

The output of the preamplifier was recorded with a Minneapolis-Honeywell Series 3170 magnetic tape recorder. This recorder had been modified by placing the tape transport and recording and playback amplifiers in two separate cases for portability. The recorder includes both FM and analog record and playback units. The frequency response for FM recording and playback was from DC to 10,000 cycles per second and for AM recording and playback from 100 to 100,000 cps.

Readout of signals from the tape was accomplished by using a direct writing oscillograph (Visicorder). High frequency galvanometers were used to prevent frequency limiting in the playback system.

The overall system was calibrated immediately before each shot. A 1 millivolt signal was recorded simultaneously on each channel with preamplifier gain setting at 16 db below maximum.

Figure 8 shows the recording system on site at Project COWBOY.

INSTRUMENTATION OF COWBOY COUPLED AND DECOUPLED SHOTS

Procedure

Shot 8, a 477.4 pound decoupled charge of Pelletol at Station 2.1 was instrumented with two radial strain gages at Stations 2.1-13 and 2.1-16, as shown in figure 9.

Shot 10, a 954 pound decoupled charge of Pelletol at Station 2.1 was instrumented with four radial strain gages at Stations 2.1-13, 2.1-14, 2.1-15 and 2.1-16, as shown in figure 9.

Four radial strain gages were installed in slant holes to measure radial strain from Shot 11, a 1,003 pound coupled charge of Pelletol at Station 2.4. The strain gages are shown at Stations 2.4-9, 2.4-10, 2.4-11 and 2.4-12, in figure 9 (Plan and Section AA').

In addition, two accelerometers, R-53A and R-53B, and two velocity gages, R-53C, R-53D, were installed for Shot 11 in the main haulageway to the shaft. Gages R-53A and R-53C were mounted on the floor and R-53B and R-53D were wall mounted.

Data and Analysis

Table 2 presents the data from Shots 8, 10 and 11. Tracings of the strain records from Shot 11 are given in figure 10.

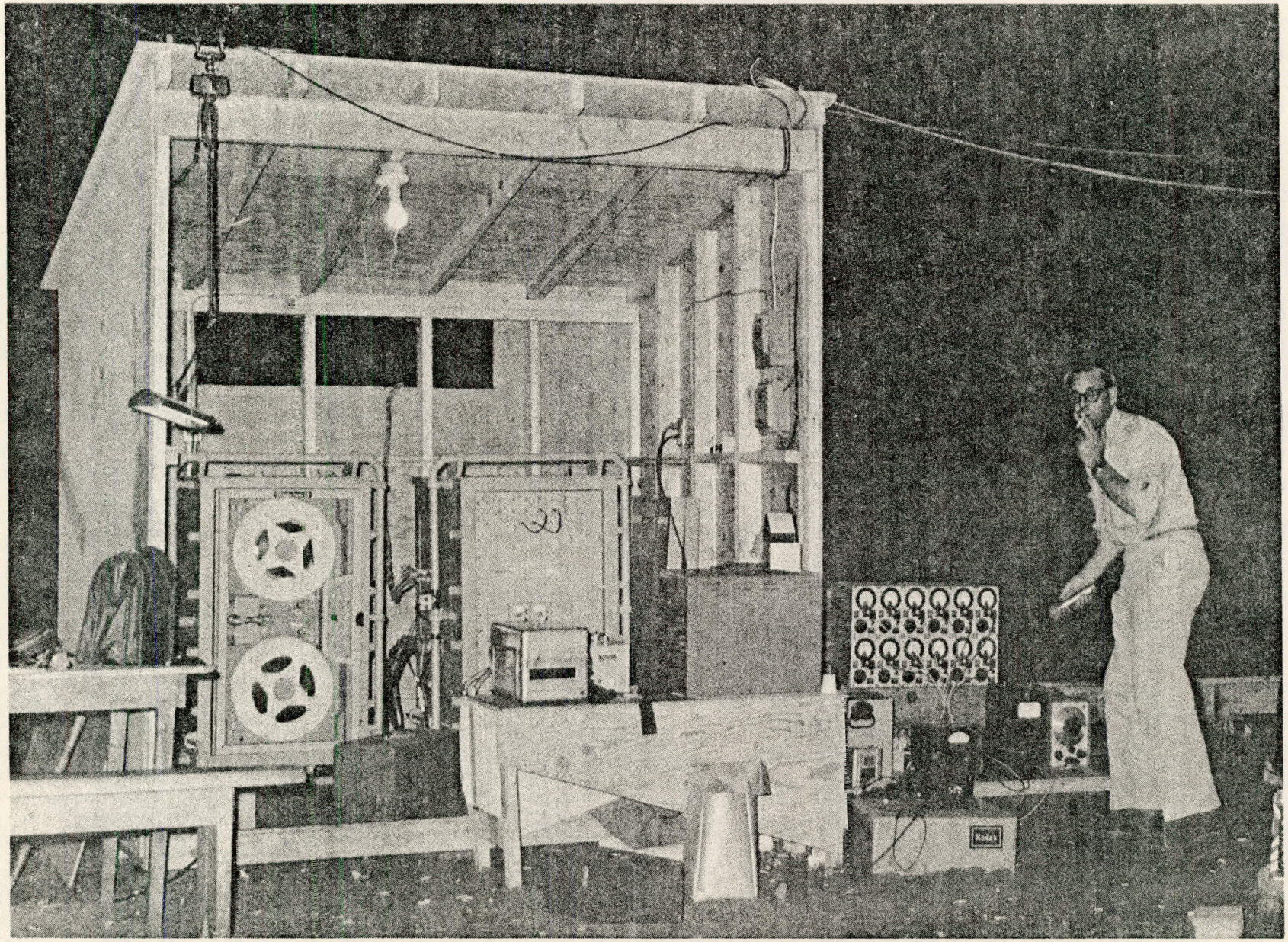

FIGURE 8. - 14 Channel FM and Analog Recording Unit.

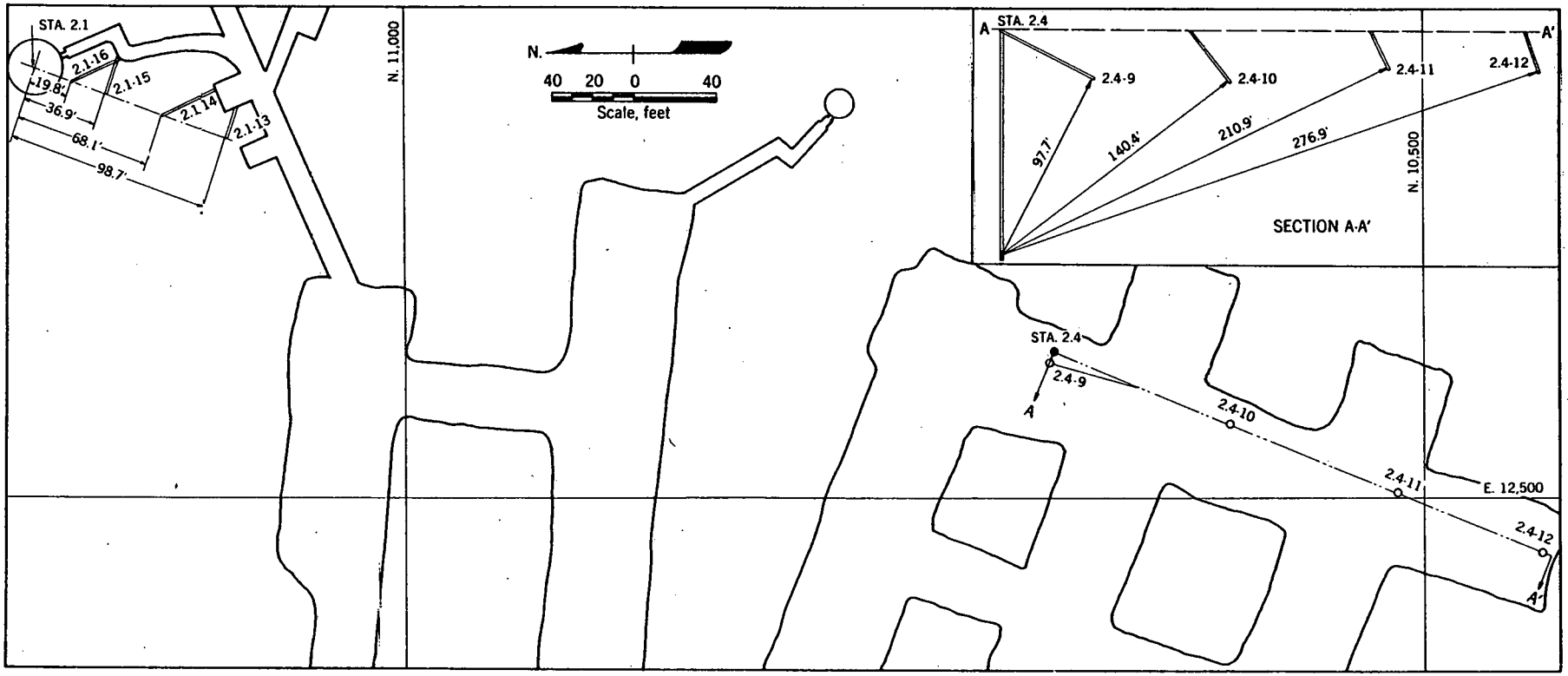

FIGURE 9. - Location of APRL Instrumentation for Cowboy Shots.

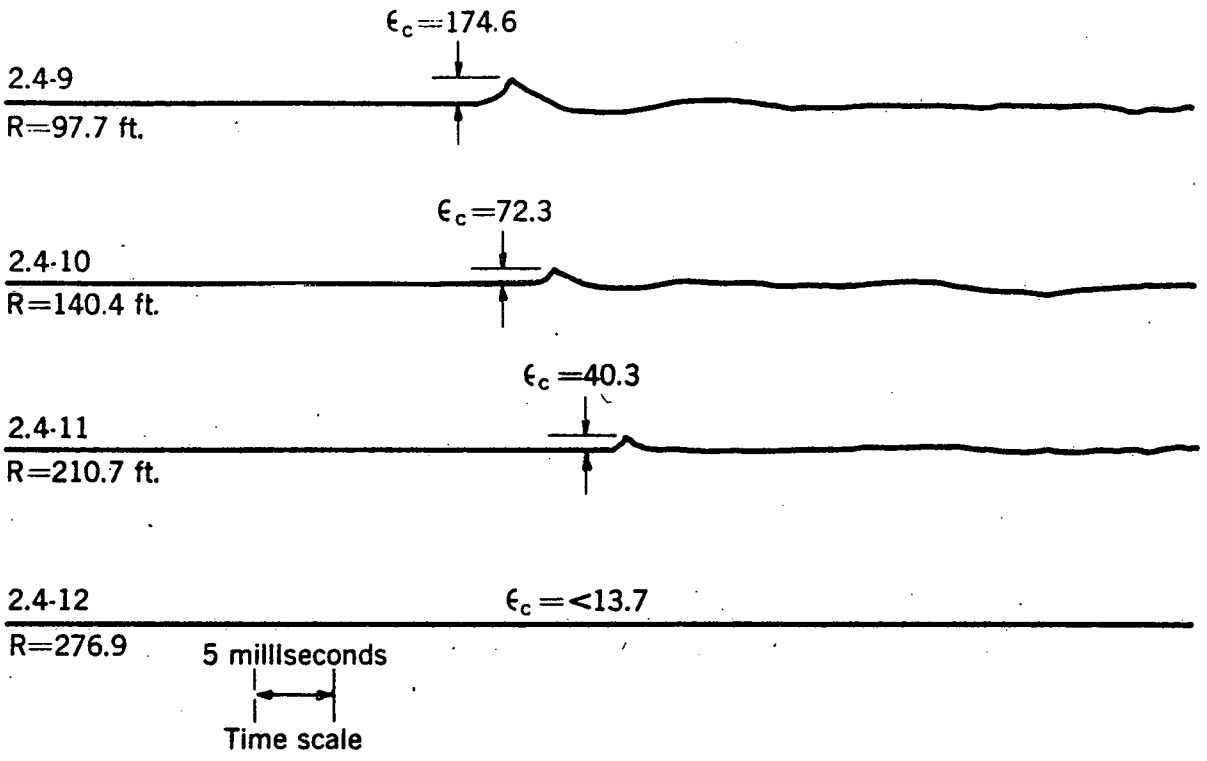

ϵ_c. Peak compressive strain in microinches/inch
R. Distance from shotpoint to gage
2.4-9. Gage No.

FIGURE 10. - Typical Strain Records, Cowboy Shot 11.

TABLE 2.- Data from COWBOY Shots 8, 10 and 11

Shot No.	Gage No.	Shot to gage distance R ft.	Scaled distance $R/W^{1/3}$ $ft/lb^{1/3}$	Peak compression ϵ_c in/in.	Peak acceleration A g's	Peak velocity v in/sec.	Frequency f cps	Decoupling factor ϵ_p/ϵ_c
8	2.1-13	98.7	-	.6*				123*
	2.1-16	19.8	-	10.6*				86*
10	2.1-13	98.7	-	11.4*				9.5*
	2.1-14	68.1	-	21.5*				8.9*
	2.1-15	36.9	-	54.0*				9.3*
	2.1-16	19.8	-	97.4*				14*
11	2.4-9	97.7	9.77	174.6			115	
	2.4-10	140.4	14.0	72.3			115	
	2.4-11	210.7	21.1	40.3			133	
	2.4-12	276.9	27.7	13.7*				
	R-53A	597	59.7		.1			
	R-53B	597	59.7		.01			
	R-53C	597	59.7			.39	133	
	R-53D	597	59.7			.79		

* Inferred

Although the equipment worked satisfactorily, no strain records were obtained for the decoupled Shots 8 and 10. This was due to setting the amplifier gain at a level estimated on the basis of a decoupling factor of 100, whereas the actual decoupling factor was greater than 100. The inferred value of peak compression strain, ϵ_c, given in table 2 indicates the minimum value of the peak compressive strain, ϵ_c, which would have produced a record.

An inferred decoupling factor is given in table 2 for Shots 8 and 10. This decoupling factor was computed by taking the linear array results for Pelletol (see figure 17) and calculating the strain, ϵ_p, that would have been recorded from each strain gage, assuming Shots 8 and 10 to be coupled. This calculated peak strain was then divided by ϵ_c in table 2 to give the inferred decoupling factor. It can readily be seen that gain settings were too low to evaluate the true decoupling factor.

The velocity gages and accelerometers installed at R-53 were grouted to the salt with Hydrostone. The linear array results presented later indicate

that Hydrostone does not provide a satisfactory bond to the COWBOY salt, see figure 26. Hence, the velocity and acceleration data from Shot 11 are considered questionable.

Interpretation of Results

The peak strain data from coupled Shot 11 has been plotted with the Pelletol strain data from the linear array test, see figure 17. The strain data from Shot 11 is in good agreement with the data obtained from smaller linear array shots. A more detailed discussion of this point is included in a later section of the report.

LINEAR ARRAY STUDIES

Procedure

To effect the linear array test, a total of 16 gage holes (G 1 to G 10 A 1 to A3, V 1 to V 3) and 8 shot holes (S 1-S 8) were drilled in Carey Drift #4. These holes were 3 inches in diameter, vertical, and approximately 25 feet deep. The depth of these holes was adjusted so that the center of each gage and the centers of gravity of the initial charge in each shot hole were on a horizontal plane.

Figure 11 shows the detail plan of the test area. Holes S 1 through S 8 were used as shot holes. APRL borehole strain gages were cemented in holes G 1 through G 10 and oriented to record radial strain waves from either end of the array. Accelerometers, mounted on the same cores, were cemented in gage holes G 7 and G 10, and are referred to hereafter as G 7A and G 10A. Gages in G 1 through G 6, G 9 and G 10, were cemented in with the salt grout developed by Waterways Experiment Station which was used by other Project COWBOY participants. Gages G 7 and G 8 were cemented in with Hydrostone for comparison.

Velocity gages were installed in V 1 and V 2. The V 1 gage was mounted on a mechanical clamp, consisting of a segmented cylinder with a fixed cone on one end and a moveable cone on the other. Gage V 2 was cemented in with salt grout.

Accelerometers were placed in A 1, A 2 and A 3. Gage A 3 was grouted in with salt grout. Gage A 1 was mounted on a mechanical clamp as described for Gage V 1, and Gage A 2 was mounted on a rubber packer-type clamp.

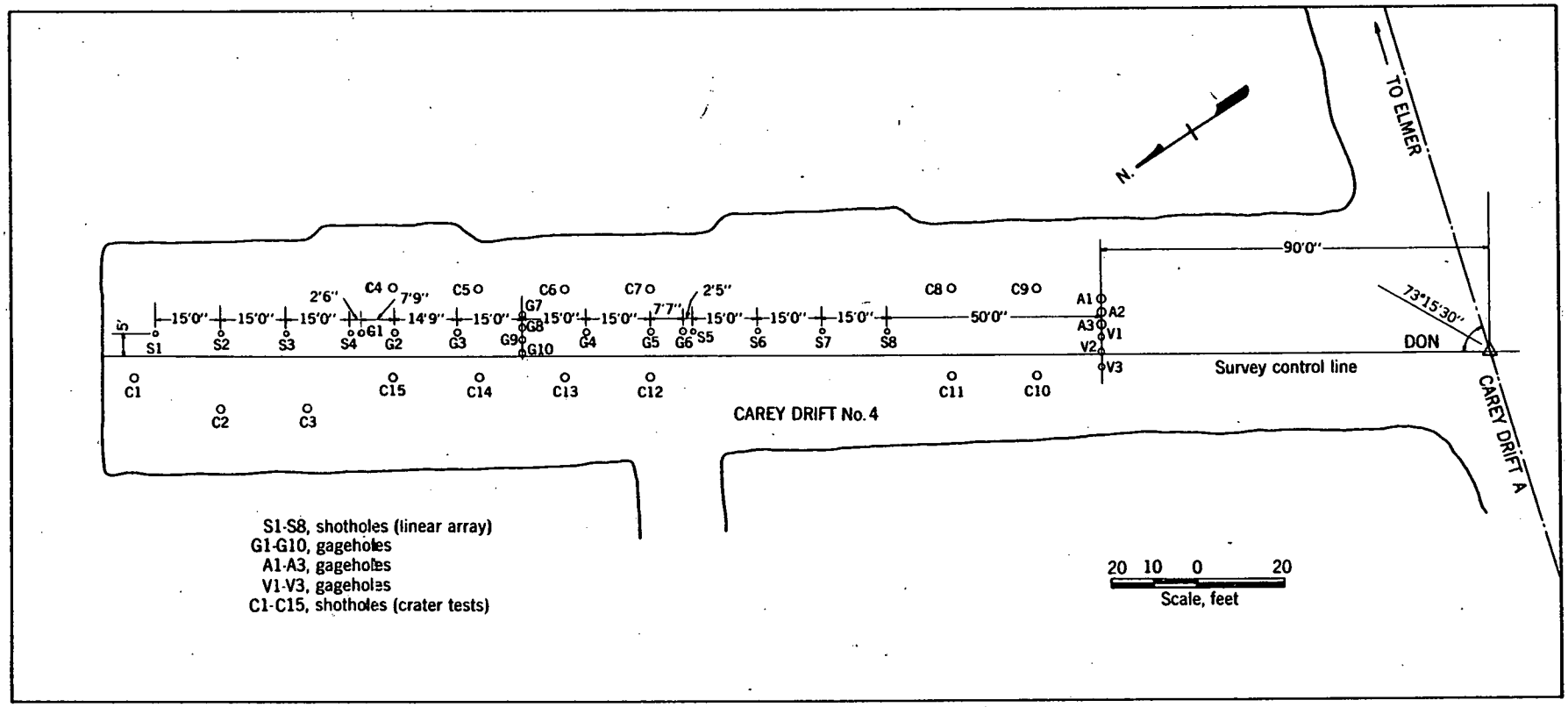

FIGURE 11. - Linear Array and Crater Test Area.

Three shots were fired in each shot hole, making a total of 24 shots. Two-pound charges were fired first. The cavity was cleaned with compressed air, and the cavity volume measured by adding known increments of sand and measuring the corresponding hole depth. The sand was then cleaned from the hole and the cavity completely filled with explosive for the second shot (2). This procedure was repeated for the third shot. The explosives used were Red HL, Gelamite 2, and 60% high pressure gelatin (60% HP), in 1-1/4 by 8 inch sticks in Hercules Tamp-tite cartridges and granular Pelletol. Pelletol was used so that the linear array results could be compared with the large COWBOY shots. Red HL, Gelamite 2 and 60% HP were used to give a good spread in detonation pressure, velocities, and densities. All shots were tamped to give loading densities equivalent to the density calculated for a single stick of explosive. Second and third shot charge sizes were calculated on the basis of the nominal densities of the explosives so as to completely fill the cavity.

The shots were detonated with No. 6 electric blasting caps. To insure detonation of the Pelletol, a booster consisting of 1/4 stick of 60% HP was used. The end holes in the array were fired first, then the next closer hole to the center of the array was fired, etc. This technique avoids any propagation through broken rock. The properties of the four explosives are as shown in table 3.

TABLE 3. - Properties of explosives[1/]

Explosive	Weight density ρ	Detonation velocity C	Characteristic impedance $(\rho C)_e$	Impedance ratio $\frac{(\rho C)_e}{(\rho C)_r}$	Detonation pressure P
	lb/ft^3	ft/sec	$lb\text{-}sec/in^3$		$lb/in^2 \times 10^6$
Red HL	41.2	10,300	7.6	.22	.28
Pelletol	62.4	15,000	16.8	.48	.76
Gelamite 2	69.9	15,400	19.4	.55	.92
60% HP	89.9	17,850	28.6	.82	1.48

1/ The properties of Red HL, Gelamite 2, and 60% HP are based on previous Bureau studies. The properties of Pelletol were furnished by the Explosives Branch, Bureau of Mines, Pittsburgh, Pa.

A factorial design was employed to randomize the effects of variations in the salt, shot to gage distance, and repeated shooting in the same hole. This design was modified as shown in table 4 to keep the third shot in each hole at 40 pounds or less. In this table the type of explosive is noted, preceded by a number indicating the order in the sequence of shooting. Thus, the second shot in hole S 4 was Red HL and this shot was the 21st shot in the series.

TABLE 4. - Factorial design, linear array shooting

Shot # \ Hole #	S 1	S 2	S 3	S 4	S 5	S 6	S 7	S 8
1	1-Red*	7-Pel*	13-Gel*	19-60%*	20-Gel	14-Pel	8-Gel	2-60%
2	4-Pel	9-Gel	15-60%	21-Red	22-Pel	16-Gel	10-60%	3-Red
3	6-Red	11-Red	17-Red	23-60%	24-Pel	18-Red	12-Red	5-Pel

*Red= Red HL, 60%= 60% HP, Gel= Gelamite 2, Pel= Pelletol

Seismic records were played back immediately after each shot and a preliminary analysis made. This preliminary analysis permitted setting the preamplifier attenuators at an appropriate level for the next shot.

Linear array data and analysis

Figure 12 shows two typical strain records and indicates the quantities that were measured. Figures 13, 14, 15 are tracings of strain records from three different charge weights. Several interesting features appear on these records. For a given charge weight, no large change in pulse duration with increased shot-to-gage distance is evident. A definite increase in pulse duration is indicated with increasing charge size. The strain pulse for large shot-to-gage distances consists of a compressive phase followed by a tensile phase. As the shot-to-gage distance decreases and/or charge size increases, the relative amplitudes of the tensile phase with respect to the compressive phase decreases until the strain pulse consists of only a compressive phase. A secondary arrival is present on records from gages at distances greater than 25 or 30 feet. As discussed later, these large amplitude second arrivals are identified as reflections from the salt-air interface.

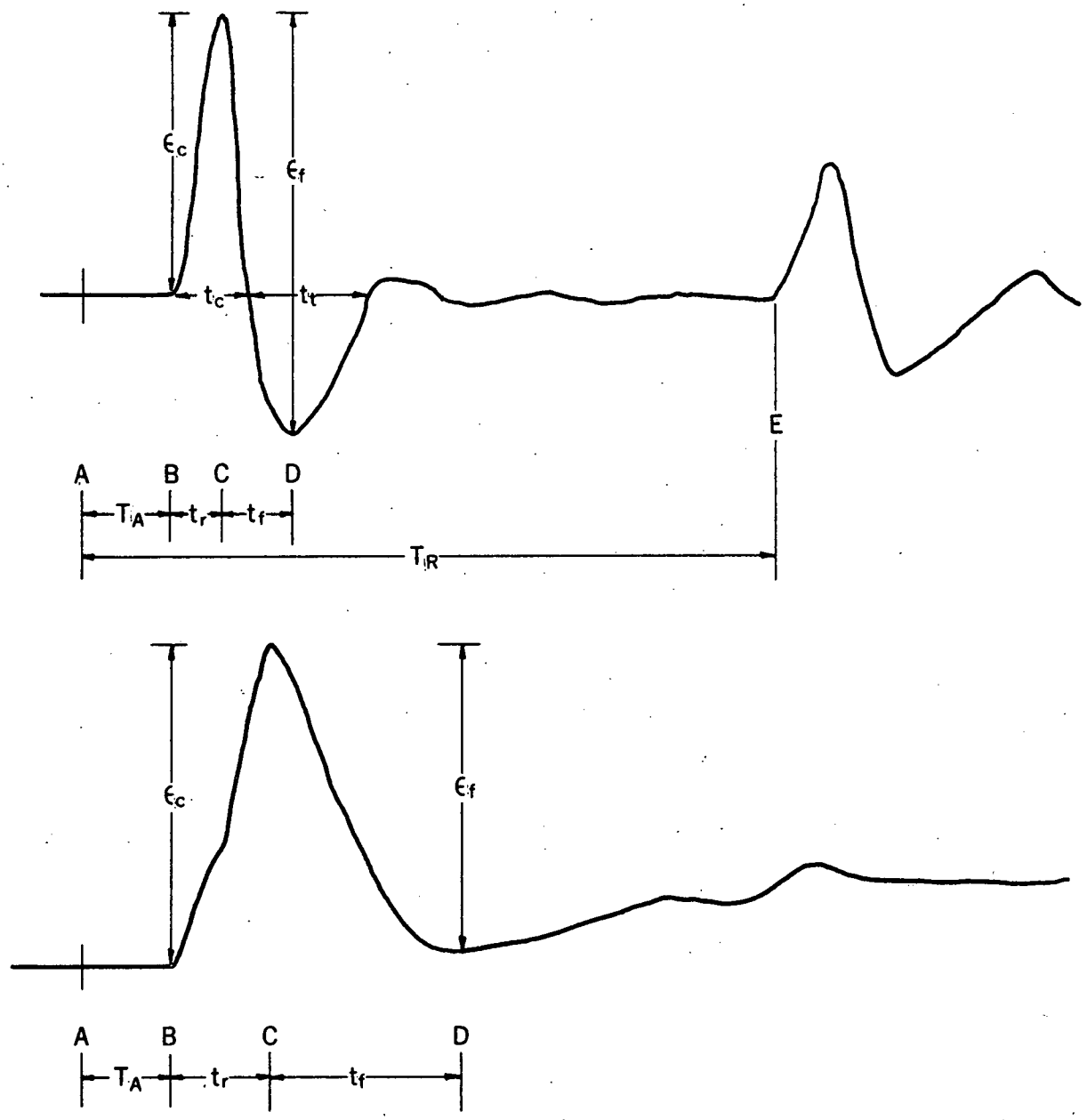

A. Detonation of charge
B. Start of strain pulse
C. Peak of compressive strain
D. End of fall strain
E. Start of reflected S-P pulse
T_A. Arrival time for primary pulse
T_R. Time for reflected pulse

t_r. Rise time
t_f. Fall time
t_c. Compressive time
t_t. Tensile time
ϵ_c. Peak compressive strain
ϵ_f. Fall strain

FIGURE 12. - Strain Record Measurements.

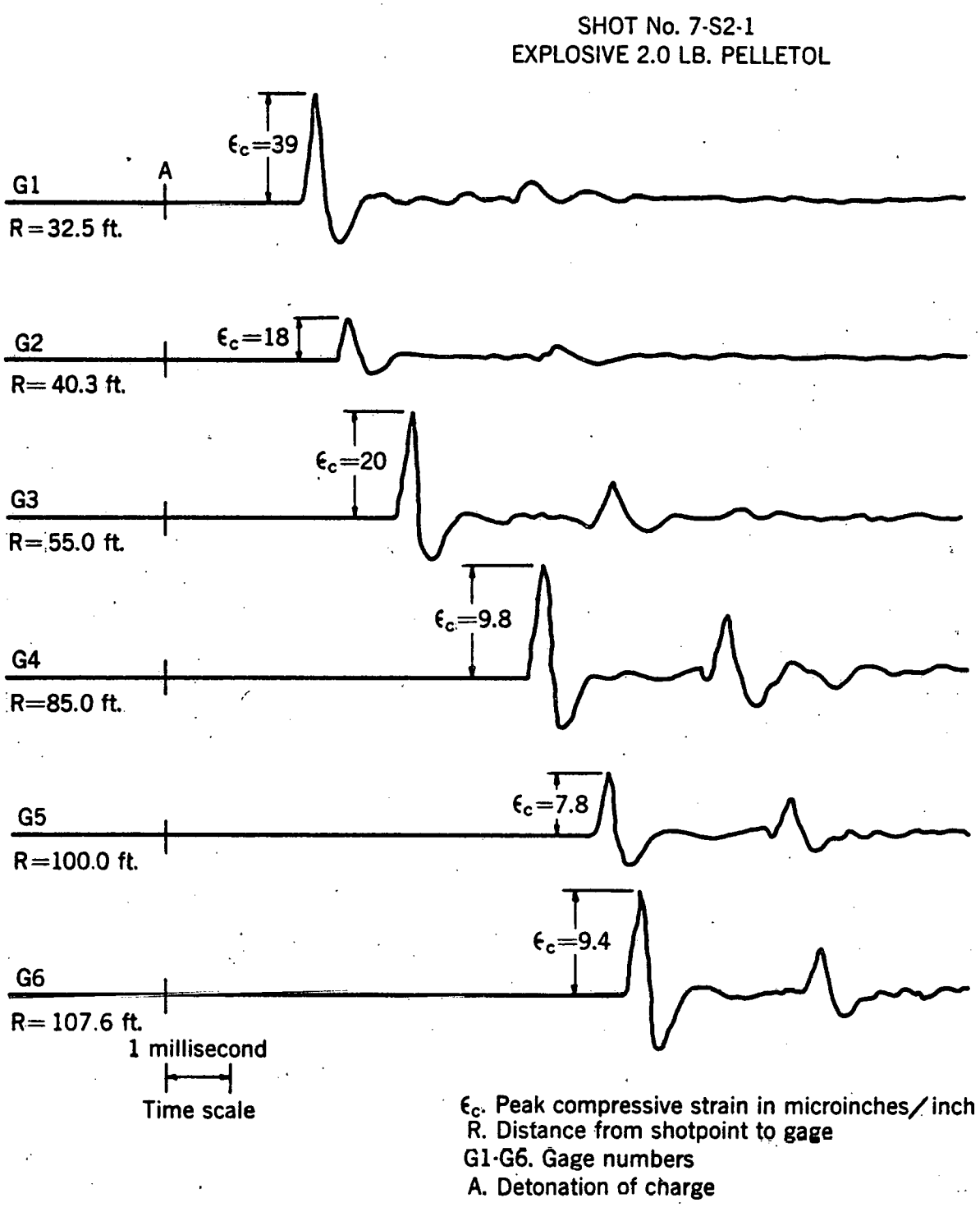

FIGURE 13. - Typical Strain Records.

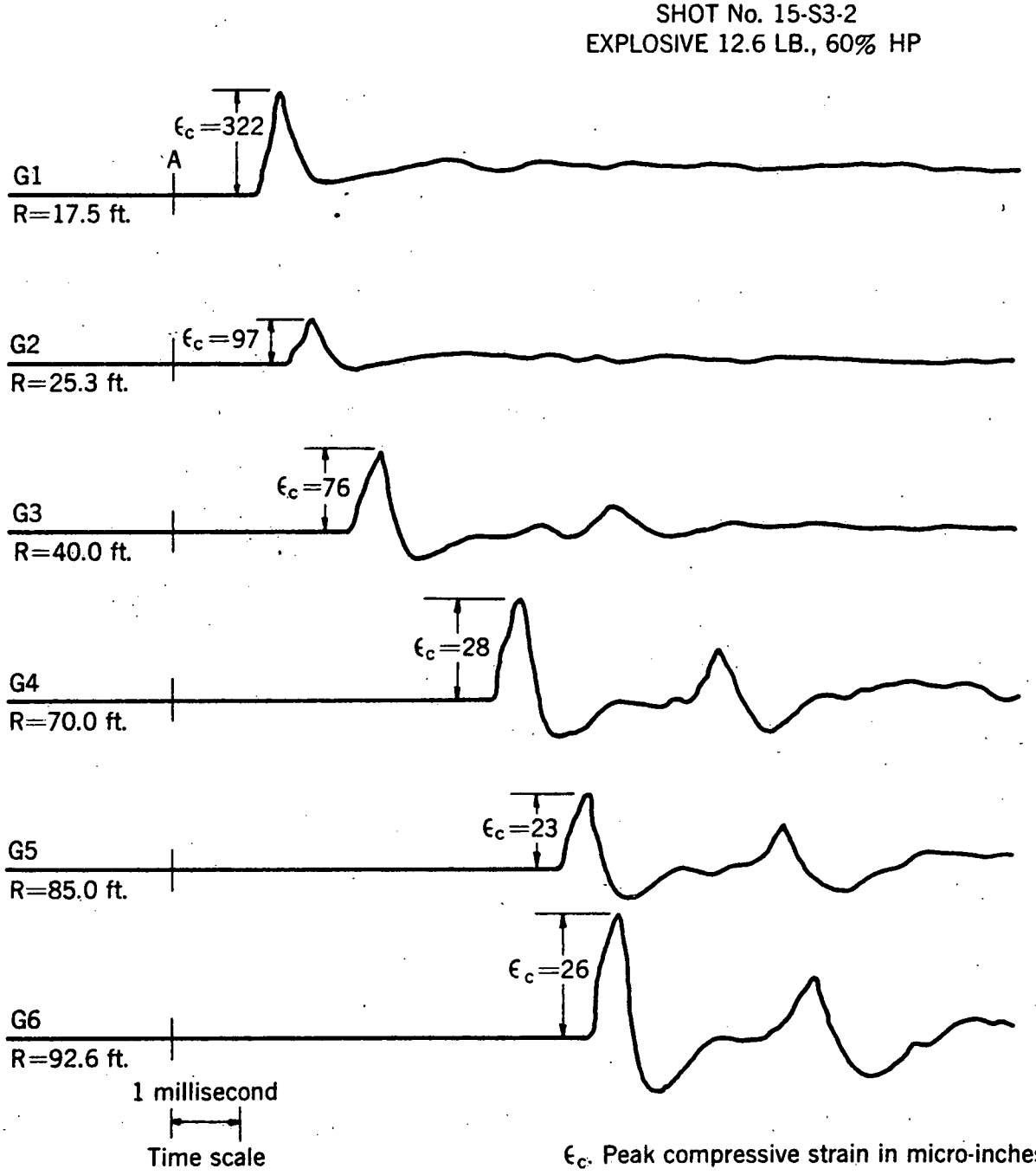

ϵ_c. Peak compressive strain in micro-inches/inch
R. Distance from shotpoint to gage
G1-G6. Gage number
A. Detonation of charge

FIGURE 14. - Typical Strain Records.

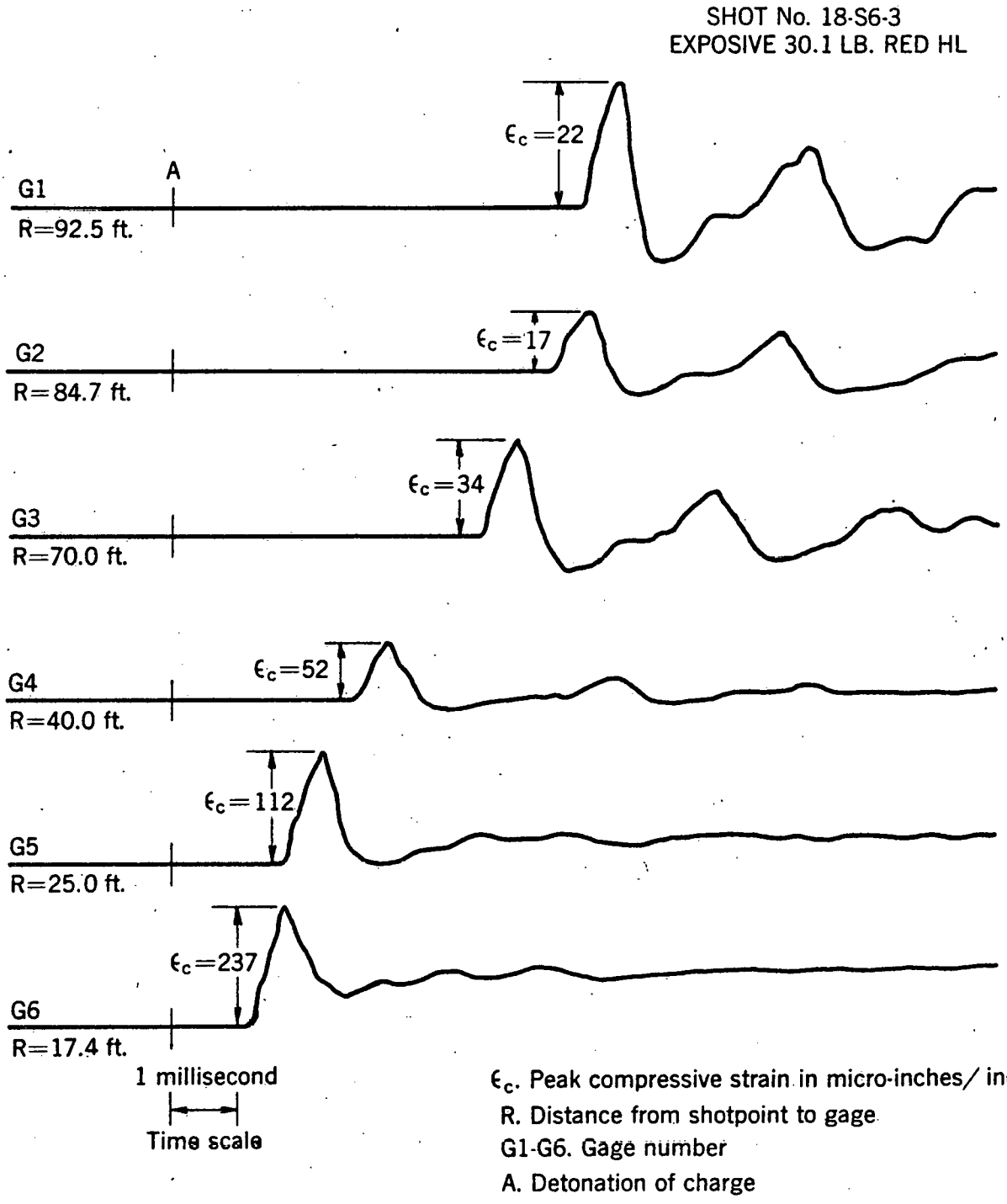

FIGURE 15. - Typical Strain Records.

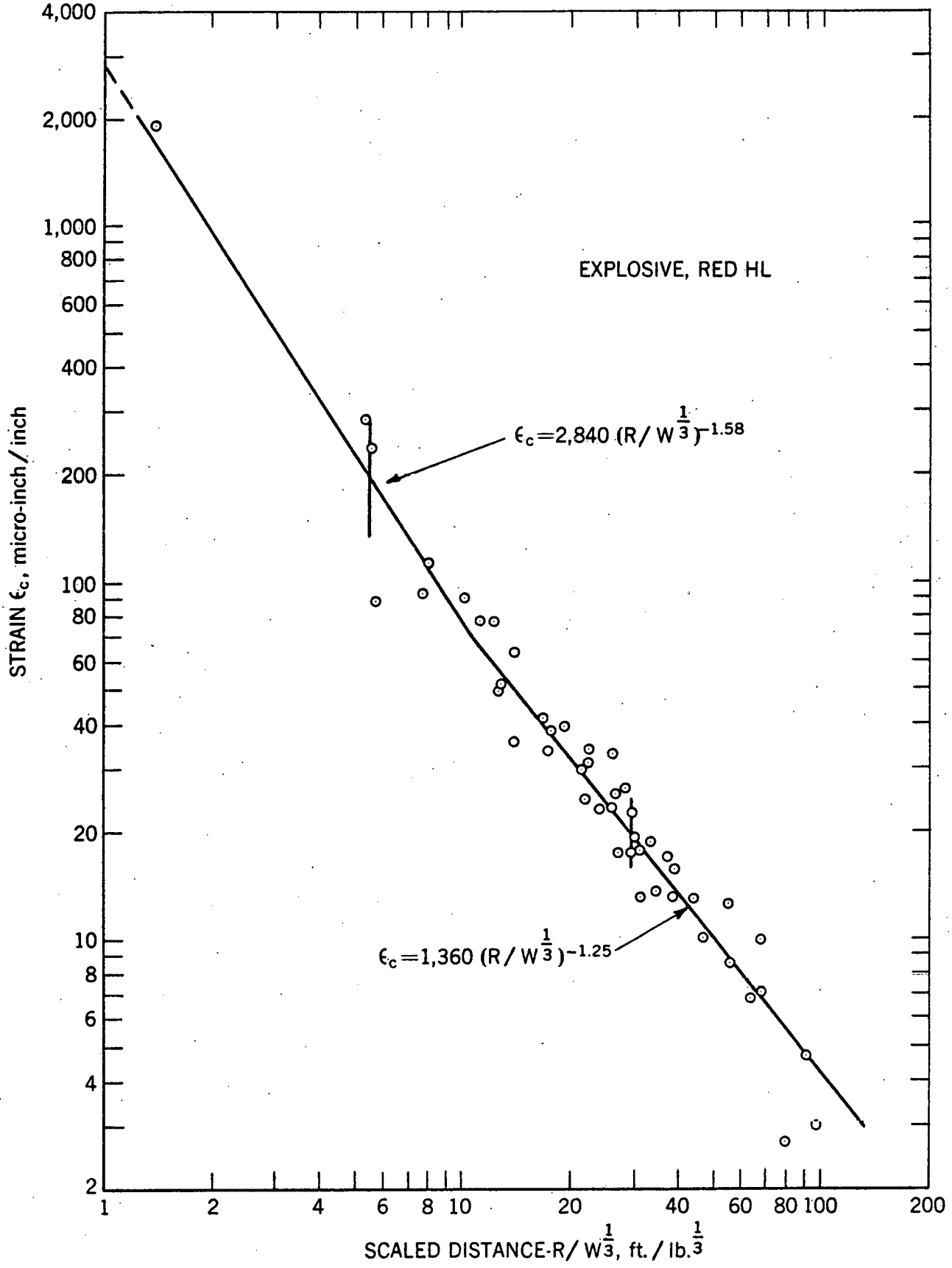

FIGURE 16. - Strain vs. Scaled Distance.

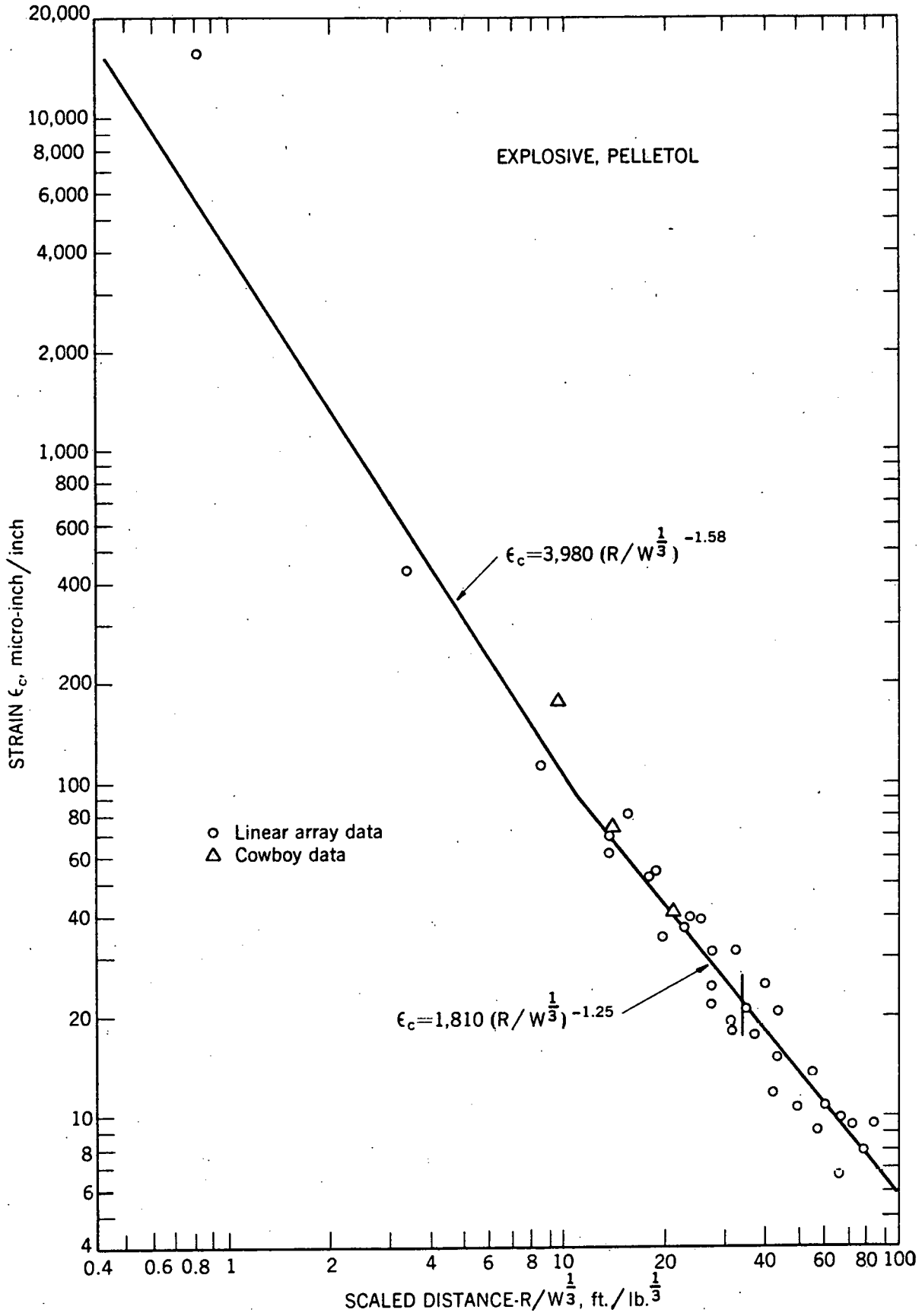

FIGURE 17. - Strain vs. Scaled Distance.

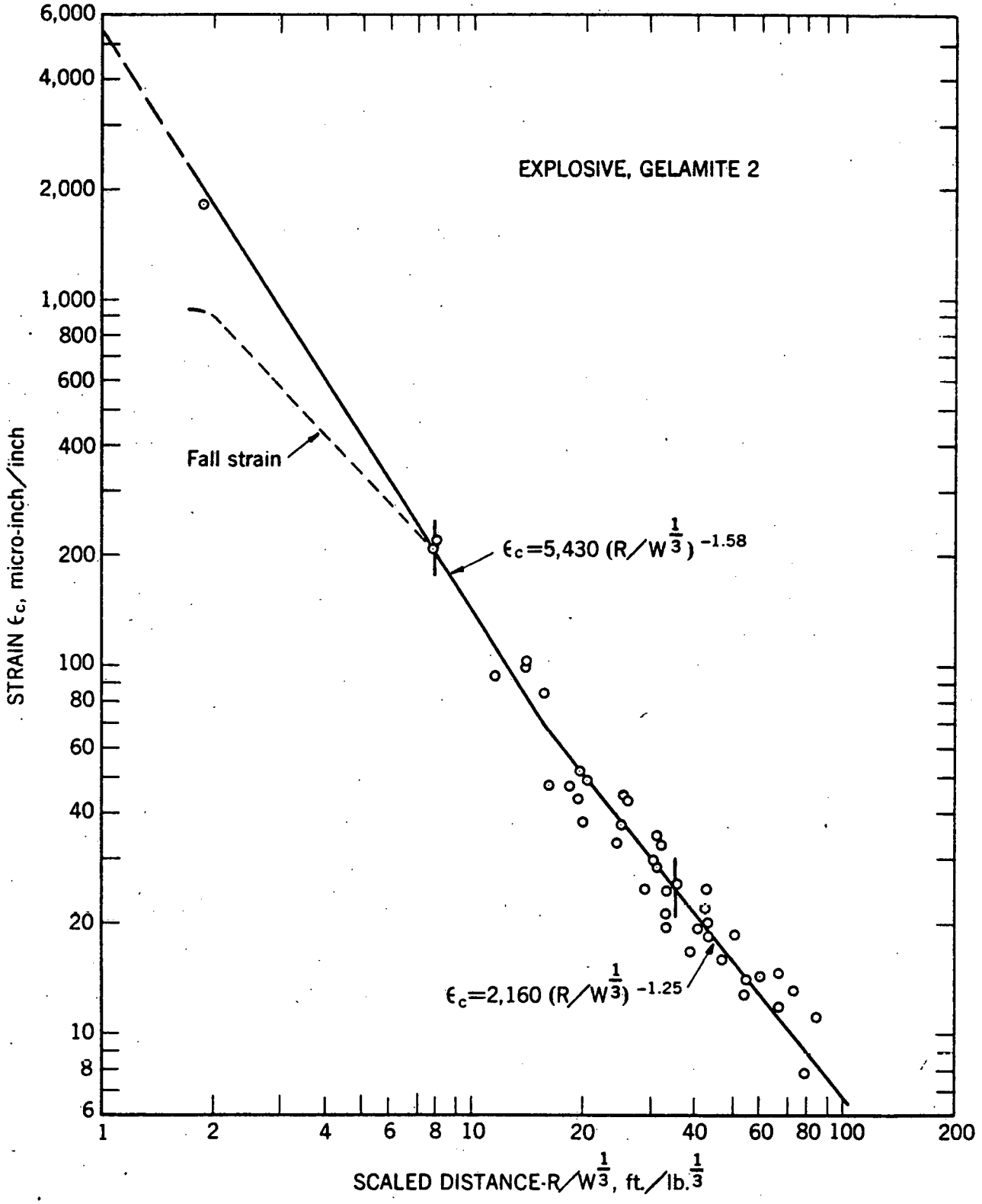

FIGURE 18. - Strain vs. Scaled Distance.

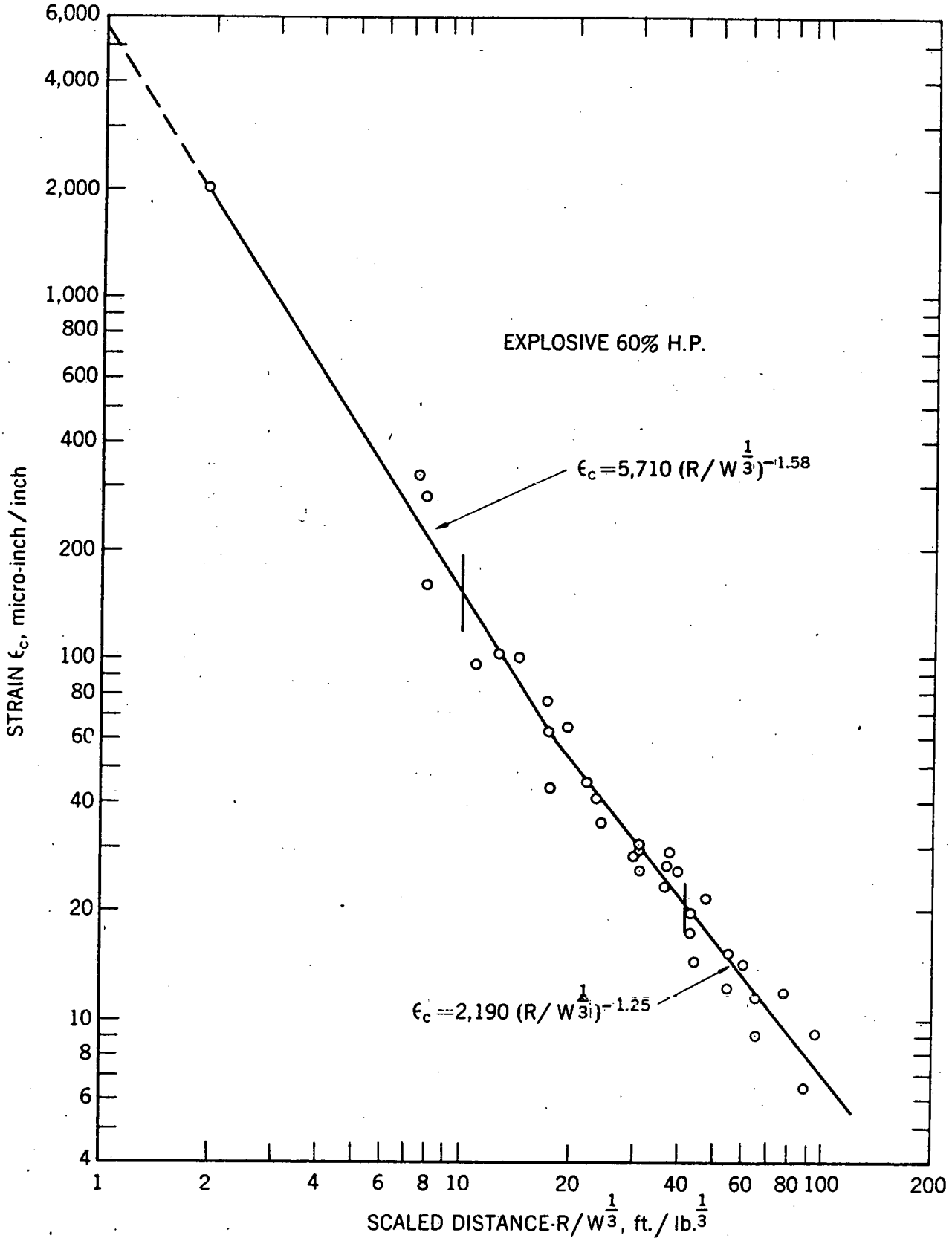

FIGURE 19. - Strain vs. Scaled Distance.

Tables 5a, b, c, d, present the linear array strain data grouped by explosives. The first column gives the shot designation, for example, Shot No. 18-S6-3 is the 18th shot in the series, fired in Hole S-6 and it was the third shot in Hole S-6. The charge weight, W, is given under the shot designation. In the second column, the gage number represents the position of the gage noted in figure 11. The third column gives the shot-to-gage distance, R. The scaled distance, $R/W^{1/3}$, is given in the fourth column. The quantities in the other columns are defined in figure 12.

Figures 16, 17, 18 and 19 show, on log-log coordinates, the peak compressive strain versus scaled distance. The straight lines through the data were determined by using standard methods of regression analysis. Peak compressive strain can be expressed as a function of a scaled distance through the following equation:

$$\epsilon_c = K(R/W^{1/3})^n \qquad (2)$$

where

ϵ_c = peak compressive strain

K= strain intercept constant at a scaled distance of 1.

$R/W^{1/3}$= scaled distance

n= exponent or slope of regression curve

The standard deviations of the data about the straight lines were calculated and are shown as vertical lines near the center for each set of data.

Two conclusions are immediately evident. First, the peak strain depends on the type of explosive; and second, for each explosive the slope of the propagation curve becomes steeper for scaled distances where the peak strain is greater than 60 micro-inches per inch. The slopes and intercepts (n and K), and the standard error in each (S_n and S_k) are shown in table 6. There are two sets of constants for each explosive representing peak strain propagation at the two different strain levels.

In most rock types the pulse duration increases with increasing shot-to-gage distance because the rock absorbs the higher frequencies in the pulse. In the COWBOY salt the change in the pulse duration with increasing distance was small, indicating a very low absorption (see figures 13, 14, 15).

TABLE 5a.- Linear array strain data

Explosive-Red HL

Shot designation and charge weight	Gage No.	Shot-to-gage distance R ft.	Scaled distance $R/W^{1/3}$ ft/lb$^{1/3}$	Peak compressive strain ϵ_c in/in. x10^{-6}	Fall strain ϵ_f in/in. x10^{-6}	Rise time t_r sec. x10^{-3}	Fall time t_f sec. x10^{-3}	Compression time t_c sec. x10^{-3}	Tension time t_t sec. x10^{-3}	Arrival time T_A sec. x10^{-3}	Reflection time T_R sec. x10^{-3}
	G 1	47.5	37.7	No record							
1-S1-1	G 2	55.3	43.9	13	17	.25	.34	.38	.74	-	2.96
	G 3	70.0	55.6	8.5	12	.25	.35	.37	.64	1.03	3.99
W= 2 lb.	G 4	100.0	79.4	2.7	3.8	.26	.30	.38	.61	3.05	5.94
	G 5	115.0	91.3	4.7	7	.23	.30	.36	.71	4.15	6.95
$W^{1/3}$= 1.26 lb$^{1/3}$	G 6	122.6	97.3	3	4.4	.24	.31	.37	.65	4.63	7.44
	G 7	85.0	67.5	2.3	2.9	-	-	-	-	2.07	-
	G 8	85.0	67.5	7.1	10	.26	.30	.38	.70	2.07	5.03
	G 10	85.0	67.5	No time break G 2 is reference for arrival times							
	G 1	122.5	67.4	9.9	15	.28	.38	.45	.83	8.47	11.25
3-S8-2	G 2	114.7	63.1	6.8	11	.27	.41	.45	.72	7.91	10.64
	G 3	100.0	55.0	12	18	.27	.38	.45	.83	6.89	9.69
W= 6.0 lb.	G 4	70.0	38.5	13	20	.27	.40	.45	.83	4.81	7.65
	G 5	55.0	30.3	19	28	.27	.38	.43	.71	3.82	6.73
$W^{1/3}$= 1.82 lb$^{1/3}$	G 6	47.4	26.1	33	48	.27	.39	.45	.76	3.29	6.28
	G 7	85	46.8	2.8	6	-	-	-	-	-	-
	G 9	85	46.8	10	16	.25	.41	.43	.71	5.87	8.71
	G 1	32.5	11.2	78	90	.51	.63	.90	.86	2.39	-
11-S2-3	G 2	40.3	13.9	36	43	.49	.65	.89	1.01	2.86	5.96
	G 3	55.0	19.0	40	52	.49	.65	.79	1.14	3.89	6.86
W= 24.5 lb.	G 4	85.0	29.3	17	24	.45	.65	.76	1.20	6.07	8.86
	G 5	100.0	34.5	14	19	.47	.67	.76	1.14	7.13	9.80
$W^{1/3}$= 2.90 lb$^{1/3}$	G 6	107.6	37.1	17	24	.48	.62	.76	1.01	7.60	10.30
	G 10	70.0	24.1	23	31	.48	.66	.74	1.04	4.95	7.85

Linear array strain data

Explosive- Red HL (Continued)

Shot designation and charge weight	Gage No.	Shot-to-gage distance R ft.	Scaled distance $R/W^{1/3}$ $ft/lb^{1/3}$	Peak compressive strain ϵ_c in/in. $x10^{-6}$	Fall strain ϵ_f in/in. $x10^{-6}$	Rise time t_r sec. $x10^{-3}$	Fall time t_f sec. $x10^{-3}$	Compression time t_c sec. $x10^{-3}$	Tension time t_t sec. $x10^{-3}$	Arrival time T_A sec. $x10^{-3}$	Reflection time T_R sec. $x10^{-3}$
12-S7-3	G 1	107.5	33.6	19	27	.65	.80	.97	1.07	7.48	10.23
	G 2	99.7	31.2	13	18	.63	.82	.98	.96	6.98	9.69
W= 32.9 lb.	G 3	85.0	26.6	25	37	.65	.82	.97	1.07	5.93	8.64
$W^{1/3}$= 3.20 $lb^{1/3}$	G 4	55.0	17.2	34	44	.62	1.00	1.01	1.08	3.88	6.78
	G 5	40.0	12.5	50	61	.62	.91	.99	1.10	2.85	6.06
	G 6	32.4	10.1	90	104	.62	.92	1.04	1.00	2.33	5.76
	G 10	70.0	21.9	25	34	.65	.84	1.01	1.10	4.92	-
	G 1	17.5	5.35	283	221	.47	.91	-	-	1.32	-
17-S3-3	G 2	25.3	7.74	93	97	.47	.88	-	-	1.86	-
	G 3	40.0	12.2	77	105	.49	.79	.90	-	2.84	6.05
W= 34.9 lb.	G 4	70.0	21.4	30	43	.49	.72	.84	1.19	4.89	7.69
	G 5	85.0	26.0	23	35	.48	.78	.82	1.17	5.91	8.73
$W^{1/3}$= 3.27 $lb^{1/3}$	G 6	92.6	28.3	26	39	.47	.75	.82	1.08	6.40	8.98
	G 7	55.0	16.8	7.4	10	-	-	-	-	3.83	-
	G 10	55.0	16.8	42	60	.49	.72	.84	1.32	3.88	-
18-S6-3	G 1	92.5	29.6	22	31	.52	.73	.81	1.14	6.42	-
	G 2	84.7	27.1	17	24	.52	.78	.82	1.07	5.94	8.70
W= 30.1 lb.	G 3	70.0	22.4	34	48	.52	.82	.87	1.21	4.88	7.64
	G 4	40.0	12.8	52	62	.52	.83	.92	1.13	2.87	5.99
$W^{1/3}$= 3.12 $lb^{1/3}$	G 5	25.0	8.01	112	109	.51	.81	-	-	1.93	-
	G 6	17.4	5.58	237	174	.52	.99	-	-	1.37	-
	G 10	55.0	17.6	38	49	.50	.93	.85	1.20	3.82	6.78
21-S4-2	G 1	2.5	1.39	1920	240	.21	.14	-	-	.26	-
	G 2	10.3	5.72	88	79	.29	.35	.63	-	.79	-
W= 5.8 lb.	G 3	25.0	13.9	63	86	.29	.47	.50	.69	1.82	5.48
	G 4	55.0	30.6	18	26	.27	.47	.48	.77	3.80	6.88
$W^{1/3}$= 1.80 $lb^{1/3}$	G 5	70.0	38.9	16	23	.27	.40	.41	.74	4.89	7.78
	G 6	77.6	43.1	6.7	11	.26	.38	.38	.76	5.40	8.33
	G 10	40.0	22.2	31	46	.27	.49	.48	.78	2.87	6.00

TABLE 5b.- Linear array strain data

Explosive- Pelletol

Shot designation and charge weight	Gage No.	Shot-to-gage distance R ft.	Scaled distance $R/W^{1/3}$ ft/lb$^{1/3}$	Peak compressive strain ϵ_c in/in. x10^{-6}	Fall strain ϵ_f in/in. x10^{-6}	Rise time t_r sec. x10^{-3}	Fall time t_f sec. x10^{-3}	Compression time t_c sec. x10^{-3}	Tension time t_t sec. x10^{-3}	Arrival time T_A sec. x10^{-3}	Reflection time T_R sec. x10^{-3}
4-S1-2	G 1	47.5	23.8	40	52	.35	.45	.53	.72	3.24	6.13
	G 2	55.3	27.7	21	29	.34	.44	.61	.85	3.74	6.55
W= 8.0 lb.	G 3	70.0	35.0	21	31	.35	.48	.53	1.01	4.70	7.55
	G 4	100.0	50.0	11	16	.35	.44	.51	.89	6.62	9.36
$W^{1/3}$= 2.0 lb$^{1/3}$	G 5	115.0	57.5	9.1	13	.33	.44	.51	.77	7.64	10.25
	G 6	122.6	61.3	11	16	.34	.41	.52	.75	8.12	10.74
	G 7	85.0	42.5	3.6	4.9	-	-	-	-	5.74	-
	G 9	85.0	42.5	12	16	.32	.45	.52	.76	5.65	8.39
5-S8-3	G 1	122.5	40.0	25	32	.51	.76	.88	1.01	4.89	7.55
	G 2	114.7	37.5	17	23	.53	.75	.88	.69	4.38	7.00
W= 28.8 lb.	G 3	100.0	32.7	31	43	.51	.88	.88	.88	3.40	5.98
	G 4	70.0	22.9	37	51	.52	.87	.92	.97	1.50	4.18
$W^{1/3}$= 3.06 lb$^{1/3}$	G 5	55.0	18.0	52	68	.50	.88	.89	1.12	.52	3.31
	G 6	47.4	15.5	80	102	.53	.79	.97	1.30	-	2.86
	G 7	85.0	27.8	2.8	4.9	.38	.44	-	-	-	-
	G 8	85.0	27.8	3.3	6.6	-	-	-	-	-	-
	G 9	85.0	27.8	25	35	.51	.91	.85	.89	2.58	5.33
	G 10	85.0	27.8	31	43	.50	.89	.88	1.14	2.58	5.33
		No time break, G6 is reference for arrival times									
7-S2-1	G 1	32.5	25.8	39	52	.26	.36	.36	.56	2.28	5.64
	G 2	40.3	32.0	18	24	.25	.31	.36	.60	2.82	6.02
W= 2.0 lb.	G 3	55.0	43.7	21	29	.26	.28	.36	.60	3.83	6.92
	G 4	85.0	67.5	9.8	14	.26	.28	.34	.54	5.82	8.68
$W^{1/3}$= 1.26 lb$^{1/3}$	G 5	100.0	79.4	7.8	11	.23	.28	.34	.57	6.88	9.71
	G 6	107.6	85.4	9.4	14	.25	.28	.36	.60	7.38	10.21

Linear array strain data

Explosive- Pelletol (Continued)

Shot designation and charge weight	Gage No.	Shot-to-gage distance R ft.	Scaled distance $R/W^{1/3}$ $ft/lb^{1/3}$	Peak compressive strain ϵ_c in/in. $x10^{-6}$	Fall strain ϵ_f in/in. $x10^{-6}$	Rise time t_r sec. $x10^{-3}$	Fall time t_f sec. $x10^{-3}$	Compression time t_c sec. $x10^{-3}$	Tension time t_t sec. $x10^{-3}$	Arrival time T_A sec. $x10^{-3}$	Reflection time T_R sec. $x10^{-3}$
14-S6-1	G 1	92.5	73.4	9.5	15	.23	.39	.38	.61	6.40	9.24
	G 2	84.7	67.2	6.6	10	.25	.35	.38	.61	5.85	8.70
W= 2.0 lb.	G 3	70.0	55.6	13	20	.26	.32	.39	.56	4.85	7.71
	G 4	40.0	31.7	19	27	.25	.38	.39	.54	2.82	6.03
$W^{1/3}$= 1.26 $lb^{1/3}$	G 5	25.0	19.8	34	47	.25	.38	.39	.56	1.78	5.42
	G 6	17.4	13.8	69	91	.23	.41	.43	.58	1.27	5.25
	G 10	55.0	43.7	15	22	.23	.39	.38	.61	3.79	6.85
22-S5-2	G 1	77.5	39.1	5.8	8.8	.34	.39	.42	.81	5.39	8.29
	G 2	69.7	35.2	2.7	3.9	-	-	-	-	4.87	-
W= 7.8 lb.	G 3	55.0	27.8	18	25	.32	.40	.51	.82	3.84	6.83
	G 4	25.0	12.6	31	37	.32	.39	.54	.60	1.78	5.36
$W^{1/3}$= 1.98 $lb^{1/3}$	G 5	10.0	5.05	138	90	.27	.38	-	-	.78	-
	G 6	2.4	1.21	1050	-	.27	-	-	-	.25	-
	G 7	40.0	20.2	1.7	3.4	-	-	-	-	2.99	-
	G 8	40.0	20.2	3.5	5.1	-	-	-	-	2.83	-
	G 9	40.0	20.2	18	24	.30	.41	.53	.66	2.83	6.06
	G 10	40.0	20.2	21	28	.29	.42	.52	.68	2.83	6.08
24-S5-3	G 3	55.0	18.8	54	70	.57	.60	8.91	1.40	3.87	6.97
	G 4	25.0	8.56	113	111	.54	.62	1.11	-	1.91	-
W= 24.8 lb.	G 5	10.0	3.42	434	250	.39	.67	-	-	.80	-
	G 6	2.4	.82	15000	-	-	-	-	-	.32	-
$W^{1/3}$= 2.92 $lb^{1/3}$	G 7	40.0	13.7	5.8	15	-	-	-	-	2.98	-
	G 10	40.0	13.7	61	74	.58	.65	.92	.93	2.85	6.13

TABLE 5c.- Linear array strain data

Explosive- Gelamite 2

Shot designation and charge weight	Gage No.	Shot-to-gage distance R ft.	Scaled distance $R/W^{1/3}$ ft/lb$^{1/3}$	Peak compressive strain ϵ_c in/in. x10^{-6}	Fall strain ϵ_f in/in. x10^{-6}	Rise time t_r sec. x10^{-3}	Fall time t_f sec. x10^{-3}	Compression time t_c sec. x10^{-3}	Tension time t_t sec. x10^{-3}	Arrival time T_A sec. x10^{-3}	Reflection time T_R sec. x10^{-3}
6-S1-3	G 1	47.5	13.9	103	115	.59	-	1.01	-	3.28	-
	G 2	55.3	16.2	48	55	.59	-	1.01	-	3.78	-
W= 40 lb.	G 3	70.0	20.5	49	61	.59	-	1.03	1.65	4.83	-
	G 4	100.0	29.2	25	30	.59	-	1.07	1.68	6.84	-
$W^{1/3}$= 3.02 lb$^{1/3}$	G 5	115.0	33.6	20	25	.59	-	1.01	1.55	7.88	-
	G 6	122.6	35.8	26	33	.62	-	1.08	1.68	8.39	11.10
	G 7	85.0	24.9	56	10	-	-	-	-	6.05	-
	G 10	85.0	24.9	33	40	.62	-	1.08	1.65	5.84	-
5-S7-1	G 1	107.5	85.3	11	17	.26	.30	.37	.65	7.40	10.13
	G 2	99.7	79.1	7.8	12	.26	.34	.36	.62	6.88	9.60
W= 2.0 lb.	G 3	85.0	67.5	15	22	.26	.30	.36	.70	5.81	8.59
	G 4	55.0	43.7	18	27	.26	.35	.37	.65	3.78	6.78
$W^{1/3}$= 1.26 lb$^{1/3}$	G 5	40.0	31.7	28	41	.23	.30	.37	.60	2.77	5.92
	G 6	32.4	25.7	44	64	.23	.35	.37	.71	2.24	5.57
9-S2-2	G 1	32.5	15.6	84	103	.33	.44	.61	1.08	2.28	-
	G 2	40.3	19.3	44	51	.36	.43	.61	1.10	2.80	6.02
W= 9.1 lb.	G 3	55.0	26.3	43	61	.37	.48	.62	1.28	3.80	6.91
	G 4	85.0	40.7	19	27	.37	.46	.60	1.01	5.83	8.77
$W^{1/3}$= 2.09 lb$^{1/3}$	G 5	100.0	47.8	16	22	.37	.46	.55	.91	6.89	-
	G 6	107.6	51.5	19	26	.38	.46	.58	1.00	7.35	10.33
	G 7	70.0	33.5	6.4	9.2	-	-	-	-	4.86	-
	G 8	70.0	33.5	4.7	7.8	-	-	-	-	4.86	-
	G 9	70.0	33.5	21	29	.37	.46	.60	1.06	4.85	7.79
	G 10	70.0	33.5	24	34	.33	.45	.56	1.20	4.86	7.92

Linear array strain data

Explosive- Gelamite 2 (Continued)

Shot designation and charge weight	Gage No.	Shot-to-gage distance R ft.	Scaled distance $R/W^{1/3}$ ft/lb$^{1/3}$	Peak compressive strain ϵ_c in/in. x10^{-6}	Fall strain ϵ_f in/in. x10^{-6}	Rise time t_r sec. x10^{-3}	Fall time t_f sec. x10^{-3}	Compression time t_c sec. x10^{-3}	Tension time t_t sec. x10^{-3}	Arrival time T_A sec. x10^{-3}	Reflection time T_R sec. x10^{-3}
13-S3-1	G 1	17.5	13.9	100	129	.25	.38	.37	.67	1.28	-
	G 2	25.3	20.1	38	51	.23	.39	.37	.66	1.77	-
W= 2.0 lb.	G 3	40.0	31.7	35	50	.23	.34	.37	.66	2.80	5.99
	G 4	70.0	55.6	14	21	.25	.34	.37	.63	4.78	7.65
$W^{1/3}$= 1.26 lb$^{1/3}$	G 5	85.0	67.5	12	17	.25	.34	.37	.58	5.85	8.66
	G 6	92.6	73.5	13	19	.25	.34	.38	.57	6.34	9.18
	G 10	55.0	43.7	20	31	.22	.36	.34	.61	3.79	6.85
16-S6-2	G 1	92.5	42.6	22	31	.35	.64	.54	1.01	6.47	9.45
	G 2	34.7	39.0	17	23	.36	.54	.57	1.05	5.92	8.79
W= 10.2 lb.	G 3	70.0	32.3	32	46	.36	.54	.54	1.17	4.85	7.77
	G 4	40.0	18.4	49	63	.38	.54	.61	1.13	2.90	6.04
$W^{1/3}$= 2.17 lb$^{1/3}$	G 5	25.0	11.5	94	110	.38	.59	.69	.92	1.84	-
	G 6	17.4	8.0	219	202	.35	.66	-	-	1.29	-
	G 7	55.0	25.3	2	4	-	-	-	-	3.91	-
	G 10	55.0	25.3	37	48	.38	.54	.57	1.02	3.87	3.86
20-S5-1	G 1	77.5	60.5	14	22	.20	.38	.33	.63	5.40	8.33
	G 2	69.7	54.5	13	18	.20	.41	.38	.76	4.82	7.77
W= 2.1 lb.	G 3	55.0	43.0	25	35	.24	.40	.38	.76	3.79	6.75
	G 4	25.0	19.5	52	65	.23	.41	.38	.76	1.80	5.46
$W^{1/3}$= 1.28 lb$^{1/3}$	G 5	10.0	7.81	208	202	.20	.43	-	-	.76	-
	G 6	2.4	1.88	1830	839	.13	.35	-	-	.22	-
	G 10	40.0	31.3	30	41	.25	.39	.38	.77	2.81	6.10

TABLE 5d.- Linear array strain data

Explosive- 60% High Pressure Gelatin

Shot designation and charge weight	Gage No.	Shot-to-gage distance R ft.	Scaled distance $R/W^{1/3}$ ft/lb$^{1/3}$	Peak compressive strain ϵ_c in/in. x10^{-6}	Fall strain ϵ_f in/in. x10^{-6}	Rise time t_r sec. x10^{-3}	Fall time t_f sec. x10^{-3}	Compression time t_c sec. x10^{-3}	Tension time t_t sec. x10^{-3}	Arrival time T_A sec. x10^{-3}	Reflection time T_R sec. x10^{-3}
2-S8-1	G 1	122.5	95.6	9	13	.26	.30	.35	.69	8.39	11.18
	G 2	114.7	89.5	6.4	10	.26	.30	.34	.71	7.86	10.58
W= 2.1 lb.	G 3	100.0	78.1	12	18	.25	.30	.35	.76	6.81	9.57
	G 4	70.0	54.6	12	18	.26	.35	.35	.72	4.79	7.70
$W^{1/3}$= 1.28 lb$^{1/3}$	G 5	55.0	42.9	17	25	.26	.29	.37	.69	3.70	6.71
	G 6	47.4	37.0	27	40	.25	.27	.37	.69	3.22	6.28
	G 7	85.0	66.4	2.1	4.1	-	-	-	-	5.95	-
	G 8	85.0	66.4	1.4	2.5	.25	-	-	-	5.95	-
	G 9	85.0	66.4	9	13	.25	.29	.37	.71	5.81	8.73
	G 10	85.0	66.4	11	17	.25	.30	.37	.76	5.81	8.73
10-S7-2	G 1	107.5	47.6	22	30	.38	.53	.57	.96	7.47	10.22
	G 2	99.7	44.1	14	20	.34	.57	.57	.98	6.94	9.61
W= 11.6 lb.	G 3	85.0	37.6	29	40	.38	.56	.57	1.02	5.94	8.66
	G 4	55.0	24.3	35	46	.32	.49	.57	1.21	3.88	6.77
$W^{1/3}$= 2.26 lb$^{1/3}$	G 5	40.0	17.7	44	66	.34	.53	.59	.88	2.86	5.91
	G 6	32.4	14.3	101	119	.38	.51	.64	1.02	2.29	5.60
	G 8	70.0	31.0	6.5	7.9	-	-	-	-	4.91	7.75
	G 9	70.0	31.0	26	36	.37	.54	.58	1.13	4.89	7.68
	G 10	70.0	31.0	30	41	.36	.52	.59	1.08	4.98	7.75
15-S3-2	G 1	17.5	7.5	322	277	.33	.67	-	-	1.27	-
	G 2	25.3	10.9	97	104	.38	.66	.77	-	1.80	-
W= 12.6 lb.	G 3	40.0	17.2	76	102	.38	.56	.66	.99	2.82	6.06
	G 4	70.0	30.0	28	40	.39	.56	.65	1.13	4.80	7.74
$W^{1/3}$= 2.33 lb$^{1/3}$	G 5	85.0	36.5	23	33	.38	.63	.63	1.14	5.90	8.75
	G 6	92.6	39.7	26	37	.39	.54	.62	1.09	6.37	9.20
	G 7	55.0	23.6	7	11	-	-	-	-	3.87	-
	G 10	55.0	23.6	41	56	.40	.52	.63	.95	3.87	6.67

Linear array strain data

Explosive- 60% High Pressure Gelatin (Continued)

Shot designation and charge weight	Gage No.	Shot-to-gage distance R ft.	Scaled distance $R/W^{1/3}$ $ft/lb^{1/3}$	Peak compressive strain ϵ_c in/in. $x10^{-6}$	Fall strain ϵ_f in/in. $x10^{-6}$	Rise time t_r sec. $x10^{-3}$	Fall time t_f sec. $x10^{-3}$	Compression time t_c sec. $x10^{-3}$	Tension time t_t sec. $x10^{-3}$	Arrival time T_A sec. $x10^{-3}$	Reflection time T_R sec. $x10^{-3}$
19-S4-1	G 1	2.5	1.95	2039	1037	.14	.24	-	-	.19	-
	G 2	10.3	8.0	160	141	.23	.41	-	-	.76	-
W= 2.1 lb.	G 3	25.0	19.5	65	90	.25	.39	.38	.67	1.74	5.50
	G 4	55.0	43.0	20	28	.23	.34	.38	.63	3.83	6.82
$W^{1/3}$= 1.28 $lb.^{1/3}$	G 5	70.0	54.7	15	22	.25	.34	.36	.66	4.86	7.85
	G 6	77.6	60.6	14	21	.25	.35	.37	.76	5.38	8.38
	G 10	40.0	31.3	30	44	.25	.35	.37	.77	2.82	-
23-S4-3	G 1	2.5	.79	Gage failed						.22	
	G 3	25.0	7.89	281	263	.50	.94	-	-	1.77	-
W= 31.9 lb.	G 4	55.0	17.4	63	63	.52	-	.90	1.16	3.83	-
	G 5	70.0	22.1	46	63	.54	.91	.89	1.27	4.87	7.86
$W^{1/3}$= 3.17 $lb.^{1/3}$	G 6	77.6	24.5	21	27	.49	-	.76	1.27	5.36	-
	G 7	40.0	12.6	13	19	.84	.94	1.12	1.04	2.92	-
	G 10	40.0	12.6	103	122	.52	.91	1.01	1.32	2.85	-

TABLE 6.- Strain propagation law constants and standard deviations

Explosive	Range of $R/W^{1/3}$	Exponent		Intercept	
		n	S_n	K	S_k
Red HL	1-11	-1.58	±.092	2840	+1356 - 924
	11-100	-1.25	±.035	1360	+ 323 - 258
Pelletol	3-11	-1.58	±.092	3980 1/	
	11-100	-1.25	±.035	1810	+ 569 - 425
Gelamite 2	1-16	-1.58	±.092	5430	+1260 -1016
	16-100	-1.25	±.035	2160	+ 574 - 459
60% H.P.	1-18	-1.58	±.092	5710	+2092 -1524
	18-100	-1.25	±.035	2190	+ 747 - 552

1/ Intercept estimated because of insufficient data.

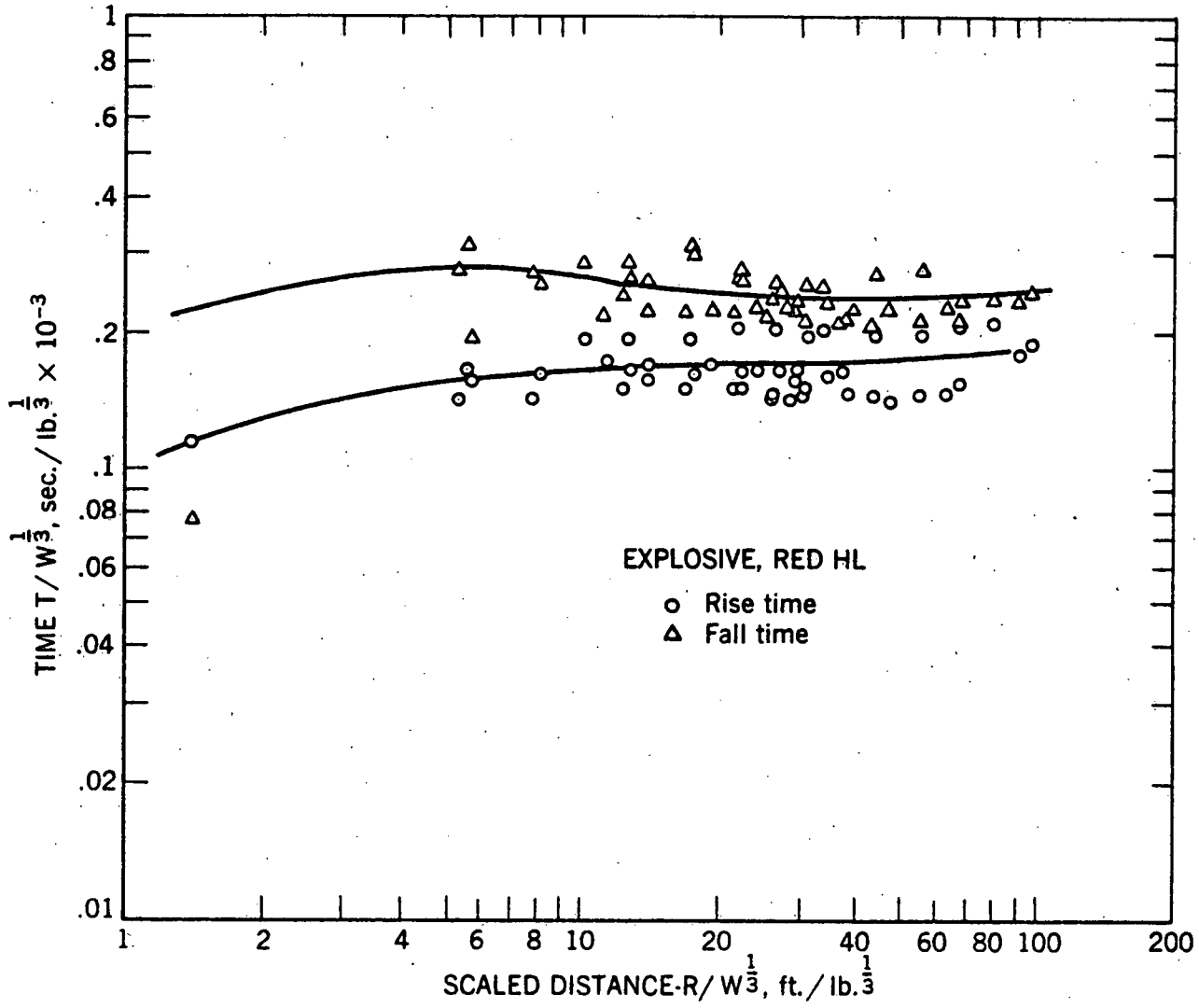

FIGURE 20. - Scaled Rise and Fall Times vs. Scaled Distance.

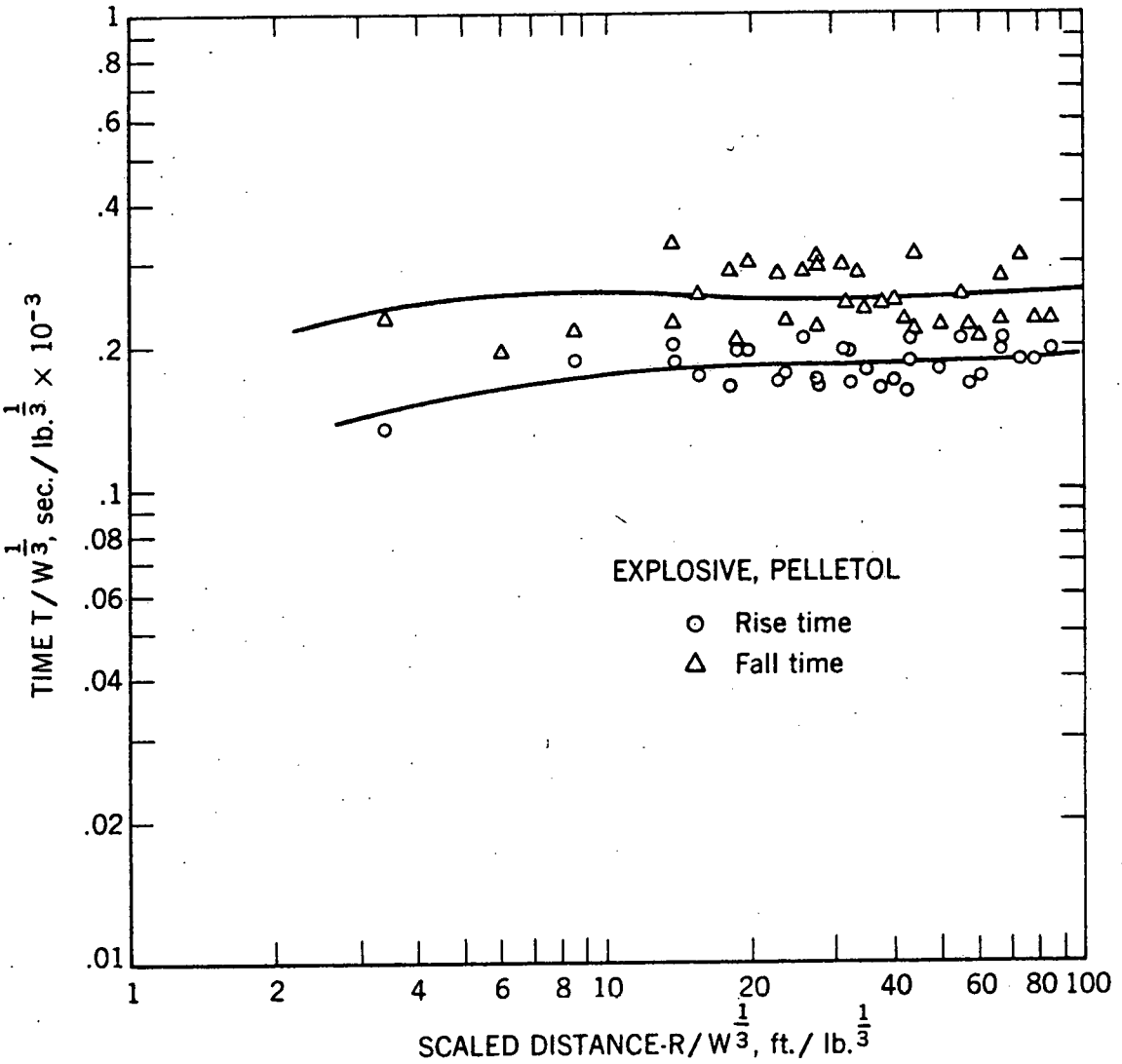

FIGURE 21. - Scaled Rise and Fall Times vs. Scaled Distance.

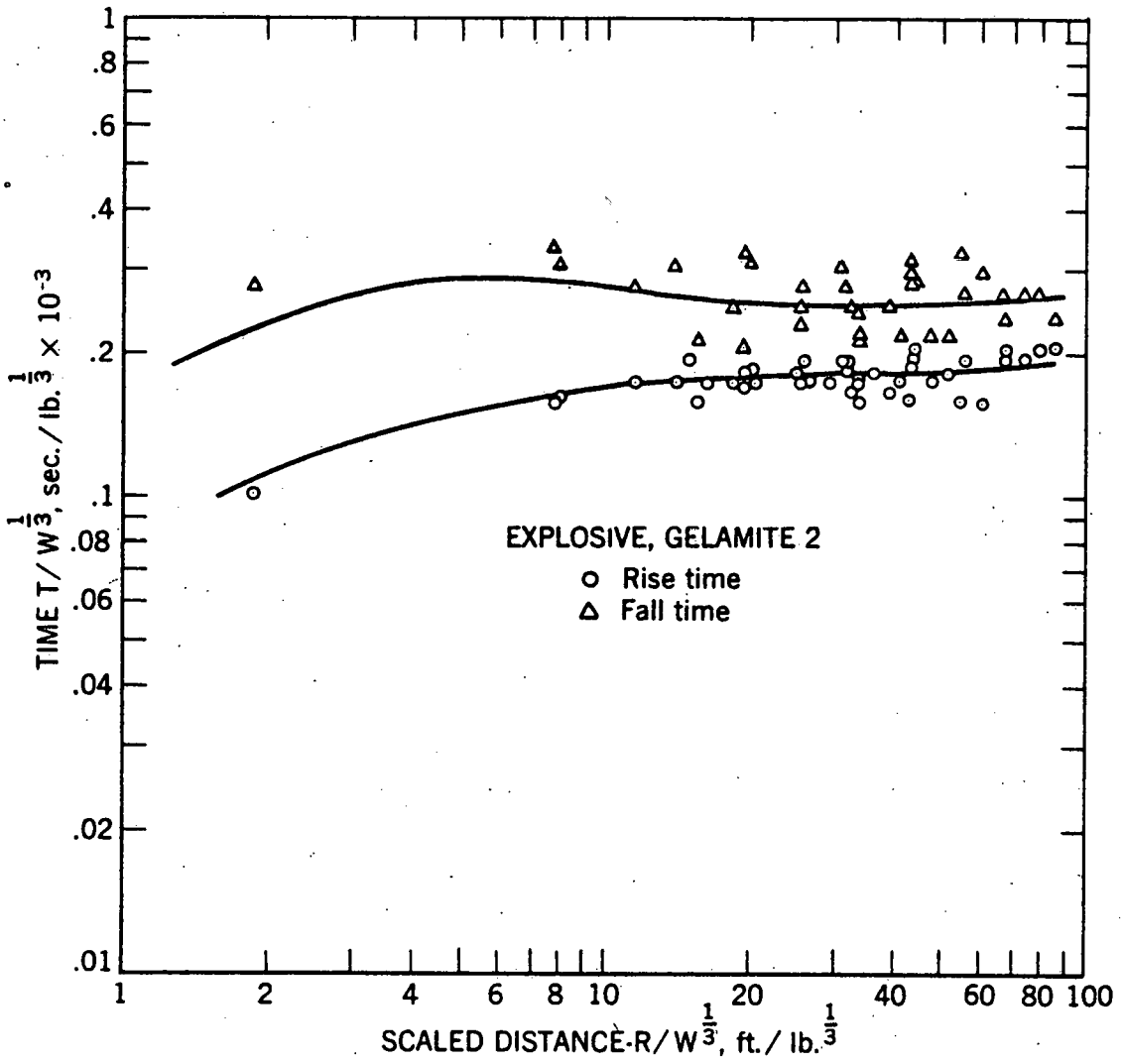

FIGURE 22. - Scaled Rise and Fall Times vs. Scaled Distance.

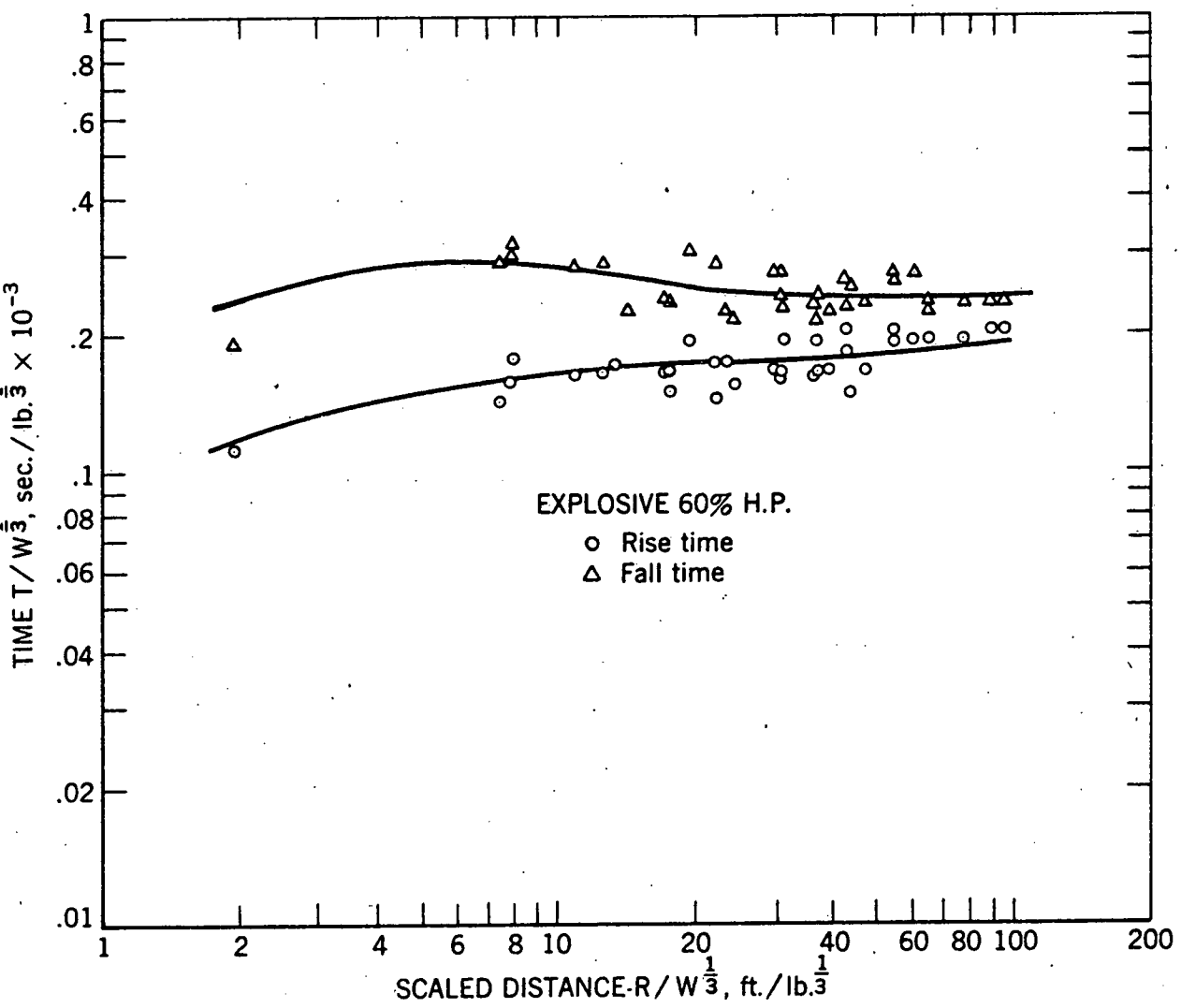

FIGURE 23. - Scaled Rise and Fall Times vs. Scaled Distance.

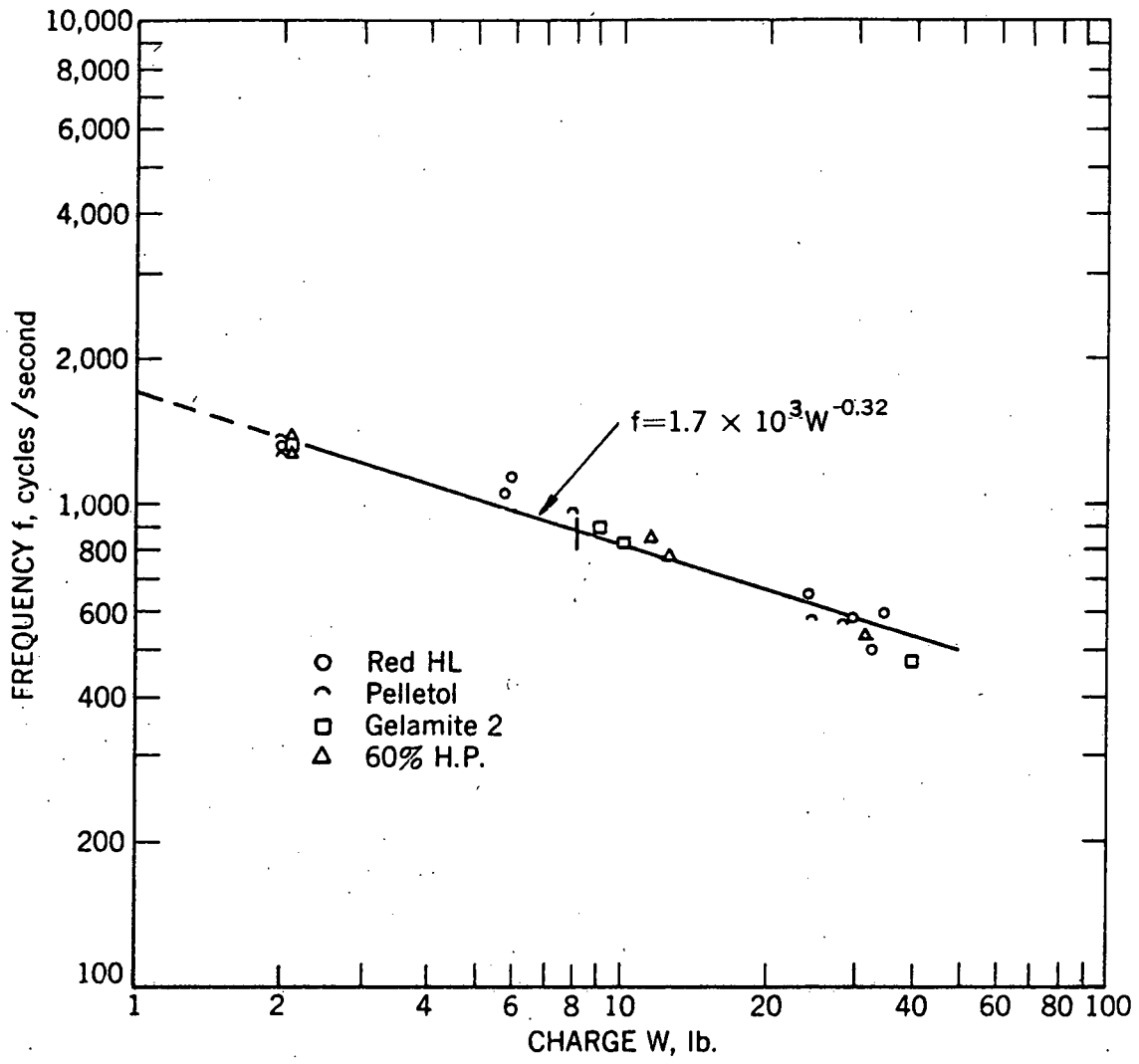

FIGURE 24. - Strain Data Frequency vs. Charge Size.

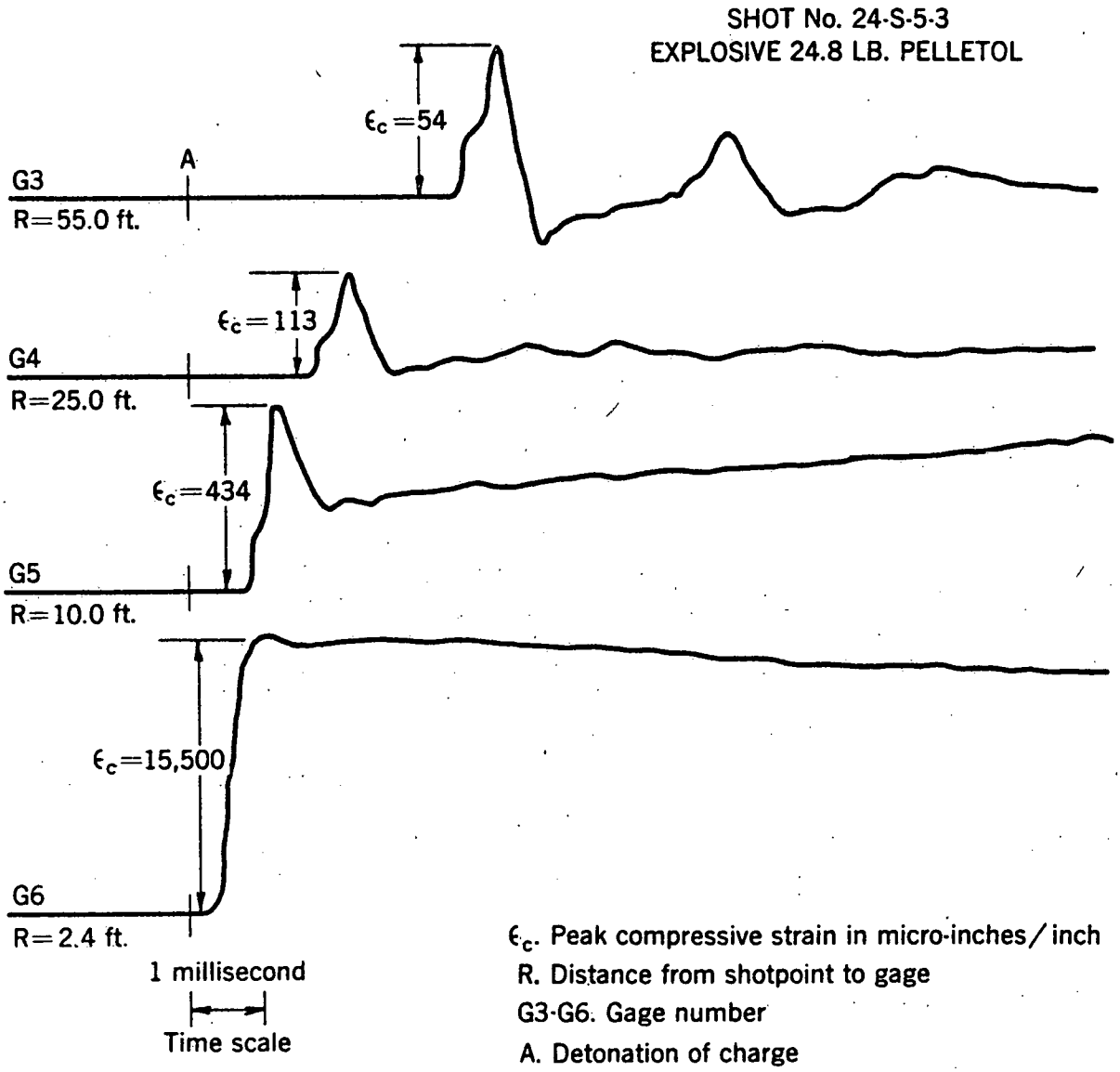

FIGURE 25. - Pulse Shape Near Shot Point.

Pulse duration may be considered in any of several ways. For a symmetric pulse, the rise time should represent one quarter of the pulse duration; the fall, compressive, and tensile times should each represent half the pulse duration. However, in most rock types the pulse is not symmetric; the fall time is more than twice the rise time and the tensile time is greater than the compressive time. Scaled rise time and fall time data are shown graphically in figures 20, 21, 22 and 23. These data show that the scaled fall times are not twice the rise times. Also there is no general increase in scaled rise or fall times with increased distance. Pulse duration, or period, is the reciprocal of frequency. Over the range of distances in these tests, the pulse duration (or frequency) was independent of distance in the COWBOY salt. These results indicate a minimum attenuation of high frequency components and a low rate of absorption.

Because no frequency change with distance was evident, an average frequency was calculated for each shot. Figure 24 shows the relationship between the frequency, f, and the charge weight to be:

$$f = 1700\ W^{-0.32} \qquad (3)$$

where

f= frequency

1700= frequency intercept constant at W=1

W= charge weight

-0.32= exponent or slope of regression curve

The results for frequency versus charge weight show the dependence of frequency on cube root scaling and indicate that this type of scaling is valid for the salt medium and the type of wave propagated.

Figure 25 illustrates the change in pulse shape which occurs with changing shot-to-gage distance. The strain record from Gage 3 (shot-to-gage distance of 55 feet) shows an initial compressive pulse followed by a tensile phase which in turn is followed by a reflected pulse. At Gage 4 (shot-to-gage distance of 25 feet), only the compressive phase of the initial pulse is present. At a distance of 10 feet from the shotpoint, Gage 5 experiences an apparent long period, gradual deformation or yielding in compression resulting in a permanent compressive strain. At Gage 6, at a distance of 2.4 feet, a definite yield occurs with the arrival of the strain wave. Thus, salt appears to behave plastically above

certain stress levels. This strain record (from Gage 6 in Shot 24) may contain some distortion because the strain level for this recording is at the point where distortion begins to occur in the recording equipment.

Strain Gages 7 and 8 were cemented in place with Hydrostone and Strain Gages 9 and 10 were cemented with salt grout. As these gages were always at the same distance from a given shot, the pulse shapes and amplitudes from these gages should be approximately the same. The data from Gages 7 and 8 (Hydrostone) showed that strain amplitudes were only one-fifth as large as those from Gages 9 and 10 (salt grout). Also, the wave forms obtained from Gages 7 and 10 or 8 and 9 (see figure 26) show no resemblance. Subsequent laboratory tests indicate that the bond between the COWBOY salt and Hydrostone is unsatisfactory. It is presumed that Hydrostone did not provide a satisfactory bond at the COWBOY site.

Table 7 lists the particle velocity data. The initial recorded peak is called the peak positive velocity and the following trough is called peak negative velocity. By this definition and the relationship between particle velocity and strain, the peak positive particle velocity compares with the peak compressive strain. Figure 27 shows a comparison of velocity and strain records. All time measurements correspond to those used for strain pulses (see figure 12).

Gage V 1 was used to record one shot and then was abandoned because of ringing in the mechanical clamp.

The velocity data from Gage V 2 is presented graphically in figure 28. No regression analysis was made because of the limited number of points for each explosive. The particle velocity and strain data vary with explosive type in the same manner, i.e., the highest peak amplitudes were obtained for 60% high pressure gelatin, etc. The recorded particle velocity amplitudes are in good agreement with amplitudes calculated from strain data by a procedure described in a later section of the report. The particle velocity rise and fall times show the same lack of dependence on distance as noted for the strain data.

Table 8 gives the acceleration data from gage A 2. The accelerometers at G7A, G10A, and A 3, did not function properly. These accelerometers were crystal type and the case and crystal are pre-stressed, with no isolation between case and crystal. In grouting the gages in place, an additional stress was applied to the case and crystal which changed the gage sensitivity and response. Accelerometer A 1 was mounted on a mechanical clamp and gave unreliable results because of

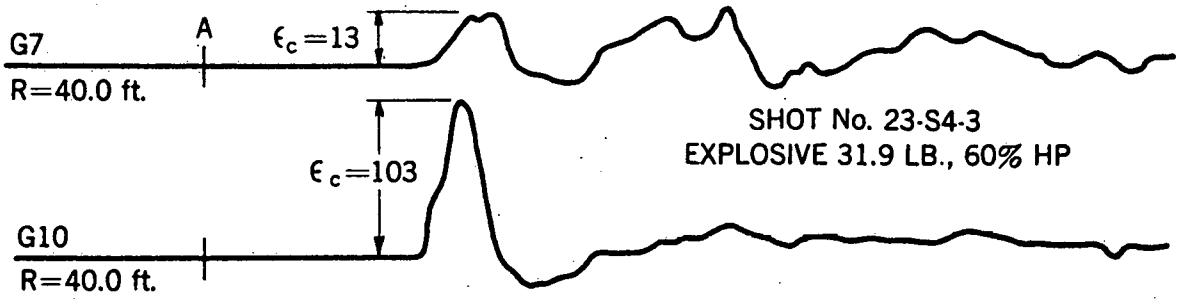

ϵ_c. Peak compressive strain in micro-inches/ inch
R. Distance from shotpoint to gage
A. Detonation of charge
G7. Gage in hydrostone
G10. Gage in saltgrout

FIGURE 26. - Strain Records From Saltgrout and Hydrostone Grouted Gage.

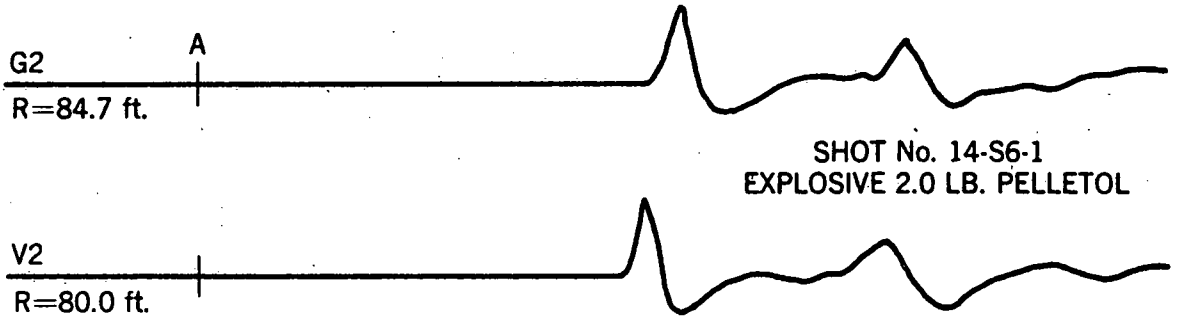

R. Distance from shotpoint to gage
A. Detonation of charge
G2. Strain gage record
V2. Velocity record

FIGURE 27. - Comparison of Velocity and Strain Records.

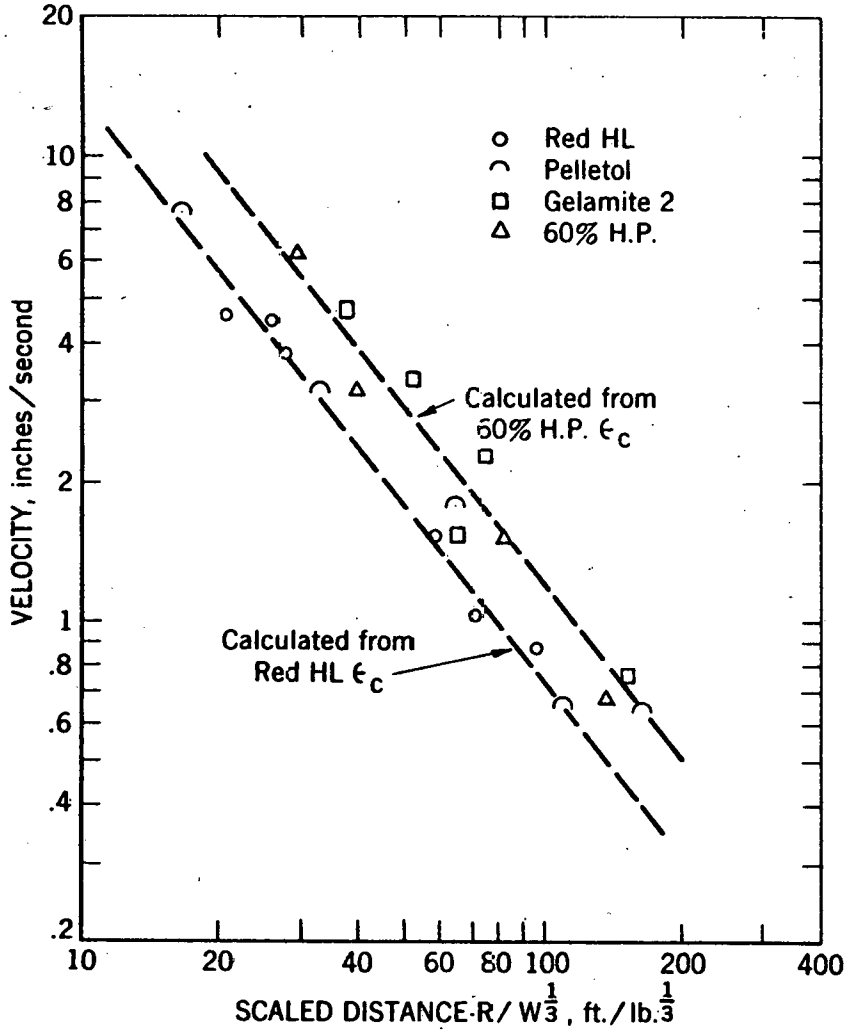

FIGURE 28. - Particle Velocity vs. Scaled Distance.

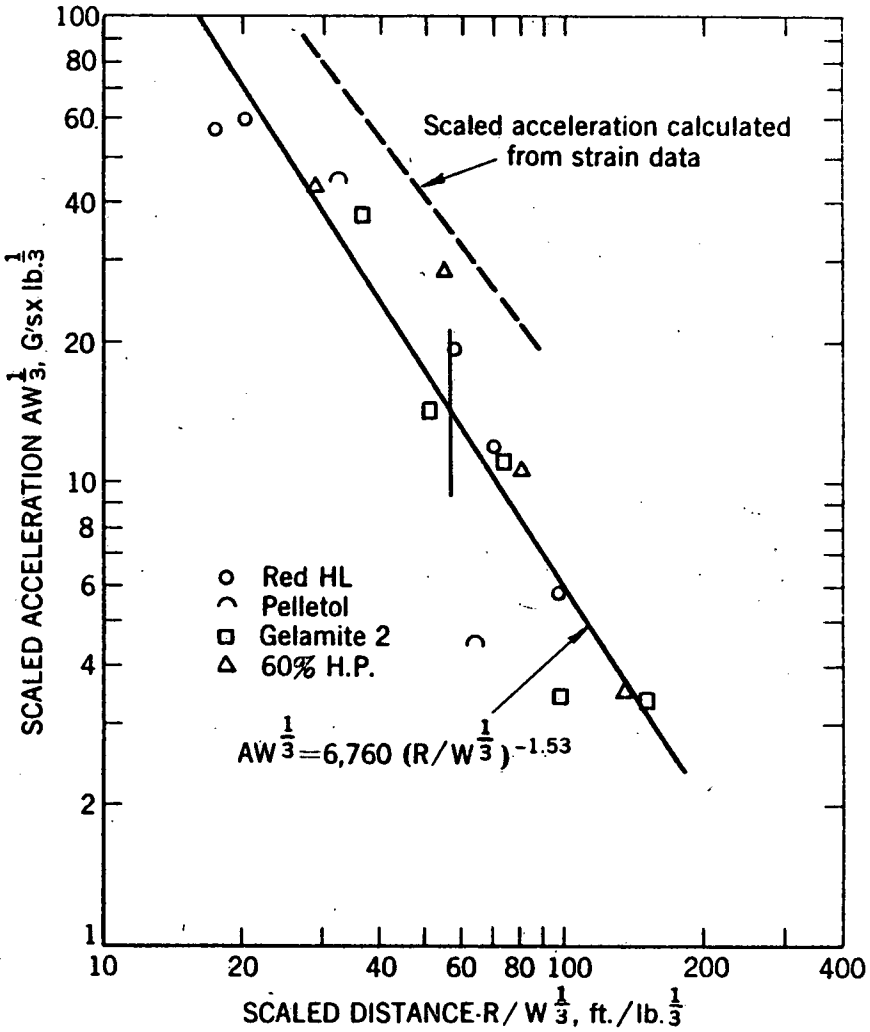

FIGURE 29. - Scaled Particle Acceleration vs. Scaled Distance.

TABLE 7.- Linear array particle velocity data

Shot designation	Explosive [1]	Charge size W lb.	Scaled charge size $W^{1/3}$ $lb.^{1/3}$	Distance R ft.	Scaled distance $R/W^{1/3}$ $ft/lb^{1/3}$	Peak positive velocity v in/sec.	Negative velocity v in/sec.	Rise time t_r sec. $x10^{-3}$	Fall time t_f sec. $x10^{-3}$	Positive time t_c sec. $x10^{-3}$	Negative time t_t sec. $x10^{-3}$	Arrival time T_A sec. $x10^{-3}$	Reflection time T_R sec. $x10^{-3}$
2-S8-1	60%	2.1	1.28	50	39.0	3.16	1.35	.25	.31	.38	.76	3.46	6.57
3-S8-2	Red	6.0	1.82	50	27.5	3.79	7.34	.24	.50	.45	.70	3.56	5.87
4-S1-2	Pel.	8.0	2.00	220	110	.66	.13	.29	.28	.49	.22	14.53	17.08
5-S8-3	Pel.	28.8	3.06	50	16.3	7.59	2.92	.50	.92	1.10	.17	3.39	
		No time break, G6 is reference for arrival time and was 2.6 feet from V2											
6-S1-3	Gel.	40.0	3.42	220	64.3	1.53	1.40	.51	-	.99	2.08	15.34	-
7-S2-1	Pel	2.0	1.26	205	162.7	.64	.45	.26	.36	.38	.51	14.09	16.83
8-S7-1	Gel.	2.0	1.26	65	51.6	3.35	1.70	.26	.26	.37	.52	4.63	7.56
10-S7-2	60%	11.6	2.26	65	28.8	6.17	2.92	.36	.52	.60	1.20	4.64	7.53
11-S2-3	Red	24.5	2.90	205	70.7	1.03	.54	.49	.65	.79	1.24	14.20	16.22
12-S7-3	Red	32.9	3.20	65	20.3	4.59	2.33	.56	.89	.90	1.27	4.72	-
13-S3-1	Gel.	2.0	1.26	190	150.8	.76	.60	.27	.34	.41	.53	13.03	15.95
14-S6-1	Pel.	2.0	1.26	80	635	1.79	1.55	.26	.31	.42	.55	5.66	8.59
15-S3-2	60%	12.6	2.33	190	81.5	1.51	.68	.40	.50	.63	.89	13.18	-
16-S6-2	Gel.	10.2	2.17	80	36.9	4.71	2.68	.34	.53	.54	1.06	5.68	8.44
17-S3-3	Red	34.9	3.27	190	58.1	1.52	.73	.48	.83	.85	-	13.20	-
18-S6-3	Red	30.1	3.12	80	25.6	4.44	2.19	.42	.76	.76	1.02	5.76	-
19-S4-1	60%	2.1	1.28	175	136.7	.68	.76	.26	.39	.44	.48	12.21	-
20-S5-1	Gel.	2.1	1.28	95	74.2	2.27	2.04	.27	.27	.42	.60	6.73	9.65
21-S4-2	Red	5.8	1.80	175	97.2	.88	.70	.35	.43	.53	.69	12.10	14.70
22-S5-2	Pel.	7.8	1.98	95	48	1.76	1.18	.25	.41	.44	.76	6.74	9.51
23-S4-3	60%	31.9	3.17	175	55.2	.31	74.7	-	-	-	-	12.10	-
24-S5-3	Pel.	24.8	2.92	95	32.5	3.14	3.36	.39	.60	.66	.99	6.82	9.58

[1] 60%= 60% HP, Red= Red HL, Pel.= Pelletol, Gel.= Gelamite 2.

TABLE 8.- Linear array particle acceleration data

Shot designation	Explosive	Charge size W lb.	Scaled charge size $W^{1/3}$ $lb.^{1/3}$	Gage	Distance R ft.	Scaled distance $R/W^{1/3}$ $ft/lb.^{1/3}$	Peak positive acceleration A g's	Scaled positive acceleration $AW^{1/3}$ $g\text{-}lb.^{1/3}$
8-S7-1	Gel.2	2.0	1.26	A2	65	51.6	11.2	14.1
9-S2-2	Gel.2	9.1	2.09	A2	205	98.1	4.1	-
10-S7-2	60% HP	11.6	2.26	A2	65	28.8	19.1	43.7
11-S2-3	Red HL	24.5	2.90	A2	205	70.7	4.1	11.89
12-S7-3	Red HL	32.9	3.20	A2	65	20.3	18.6	59.52
13-S3-1	Gel.2	2.0	1.26	A2	190	150.8	2.7	3.40
14-S6-1	Pelletol	2.0	1.26	A2	80	63.5	3.5	4.41
15-S3-2	60% HP	12.6	2.33	A2	190	81.5	4.5	10.49
16-S6-2	Gel.2	10.2	2.17	A2	80	36.9	17.0	36.89
17-S3-3	Red HL	34.9	3.27	A2	190	58.1	5.8	18.97
18-S6-3	Red HL	30.1	3.12	A2	80	25.6	18.1	56.47
19-S4-1	60% HP	2.1	1.28	A2	175	136.7	2.8	3.58
20-S5-1	Gel. 2	2.1	1.28	A2	95	74.2	8.6	11.01
21-S4-2	Red HL	5.8	1.80	A2	175	97.2	3.2	5.76
23-S4-3	60% HP	31.9	3.17	A2	175	55.2	9.0	28.53
24-S5-3	Pelletol	24.8	2.92	A2	95	32.5	15.1	44.09

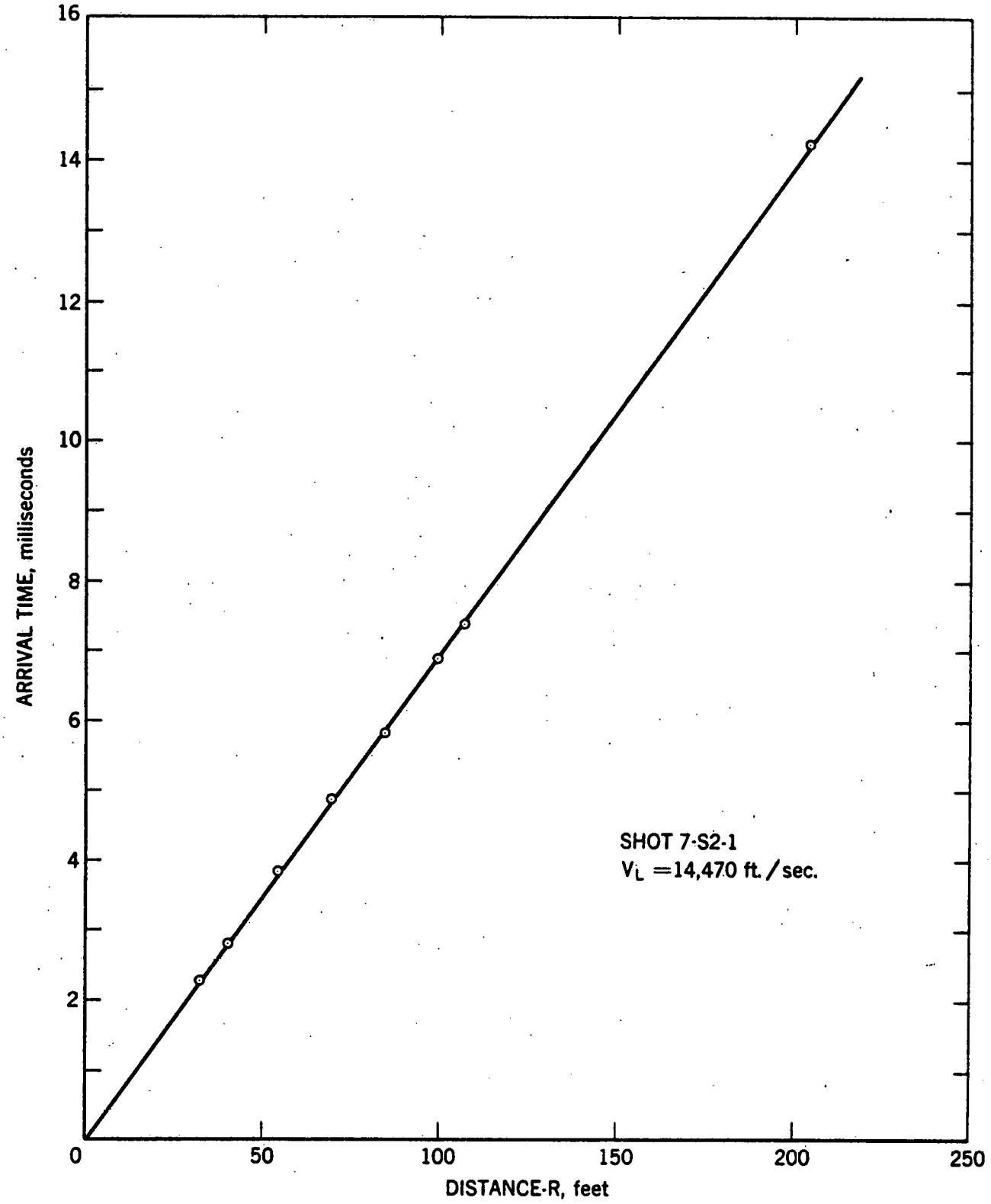

FIGURE 30. - Typical Linear Array Arrival Time vs. Distance.

excessive ringing. Only the initial arrival time, rise time, and initial peak acceleration was obtained from Gage A 2 records. Ringing in the clamp prevented any study of pulse shape or later arrival times. Figure 29 gives the results from all explosives. The relationship between the scaled acceleration and the scaled distance, obtained by regression analysis is:

$$AW^{1/3} = 6760\ (R/W^{1/3})^{-1.53} \qquad (4)$$

where

$AW^{1/3}$ = scaled acceleration

6760 = scaled acceleration intercept constant

$(R/W^{1/3})$ = scaled distance

-1.53 = exponent or slope of regression curve

The limited amount of data prevented comparing the peak acceleration values for the different explosives. The dashed lines indicate scaled acceleration values calculated from strain data.

Chronograph contactors or "targets" were placed in each charge as a means for determining the detonation time. The propagation time (difference between arrival time and detonation times) was determined for each shot-to-gage distance. A typical time-distance graph is shown in figure 30. Longitudinal propagation velocity, determined by least squares analysis, was 14,440 feet per second.

The size of the cavity after each shot was measured. The cavity size from each explosive varied approximately as the strain data. The cavity volume to charge volume ratio for each explosive is given in table 9.

TABLE 9.- Cavity volume to charge volume

Explosive							
Red HL		Pelletol		Gelamite 2		60% HP	
Shot No.	Cavity vol. Chg.vol.	Shot No.	Cavity vol. Chg.vol.	Shot No.	Cavity vol. Chg.vol.	Shot No.	Cavity vol. Chg.vol.
1-S1-1	2.7	4-S1-2	3.9	6-S1-3	4.8	2-S8-1	5.4
3-S8-2	2.7	5-S8-3	4.6	8-S7-1	4.5	10-S7-2	4.8
11-S2-3	2.8	7-S2-1	4.0	9-S2-2	4.7	15-S3-2	5.9
12-S7-3	3.0	14-S6-1	4.5	13-S3-1	5.1	19-S4-1	5.4
17-S3-3	2.8	22-S5-2	3.2	16-S6-2	4.8	22-S4-3	5.6
18-S6-3	2.7	24-S5-3	3.9	20-S5-1	4.5		
21-S4-2	2.8						
Average	2.8	Average	4.0	Average	4.7	Average	5.6

INTERPRETATION OF RESULTS

Introduction

The linear array data can be used to show:

1. Validity of scaling laws for comparing seismic amplitudes from small and large shots.
2. Relationship between strain amplitudes and shot hole cavities to the type of explosive used and its characteristic impedance.
3. Particle velocities can be predicted from strain data.
4. Particle accelerations can be predicted from strain data.
5. Particle displacements can be predicted from strain and velocity data.
6. Reflection events can be identified.
7. Cavity radii can be calculated from linear array data and elastic constants of the medium.

Scaling Law Validity

Pelletol was used both in the linear array tests and in Phase I and II of Project COWBOY. As shown in figure 17 the strain data (given as a function of scaled distance) for the linear array tests for 2-to-40 lb. shots are in good agreement with the strain data from COWBOY Shot 11. which was a 1000 lb. coupled shot. Thus, the cube root scaling is satisfactory over a scale factor range of 8, and the quality of the linear array data are such that extrapolation to even larger size charges should be possible.

Explosive to Rock Coupling

When an explosive charge is detonated in a cavity in rock, the resulting pressure is transferred to the interior surface of the cavity by some form of wave transmission. Thus, the pressure or stress transferred to the surrounding rock medium would be expected to depend on the gas pressure and the ratio of characteristic impedance of the gaseous medium to that of the rock medium. Shock phenomena are undoubtedly present in the medium immediately surrounding the point of pressure application. As a first approximation, the characteristic impedance of the gaseous medium for a closely coupled shot may be defined as the product of the density and the rate of detonation of explosive. Also the gas pressure may be estimated by the detonation pressure of the explosive. Detonation pressures may be calculated from the following equation:

$$P = \frac{\rho C^2}{4} \tag{5}$$

where:

P= detonation pressure of the explosive

ρ= average loading density

C= detonation velocity

For an elastic medium, the characteristic impedance is the product of the density and longitudinal propagation velocity. Thus, as a first approximation, assuming strain is directly proportional to stress, one would expect the following relationship to exist:

$$K = Pf\frac{[(\rho C)_e]}{[(\rho C)_r]} \tag{6}$$

which may also be written as:

$$K/P = f\frac{[(\rho C)_e]}{[(\rho C)_r]} \tag{7}$$

where:

K= intercept constant in the strain propagation equation

P= detonation pressure

$(\rho C)_e$ = characteristic impedance of explosive

$(\rho C)_r$ = characteristic impedance of rock

$f\frac{[(\rho C)_e]}{[(\rho C)_r]}$ = a function of the ratio of characteristic impedance of explosive to rock.

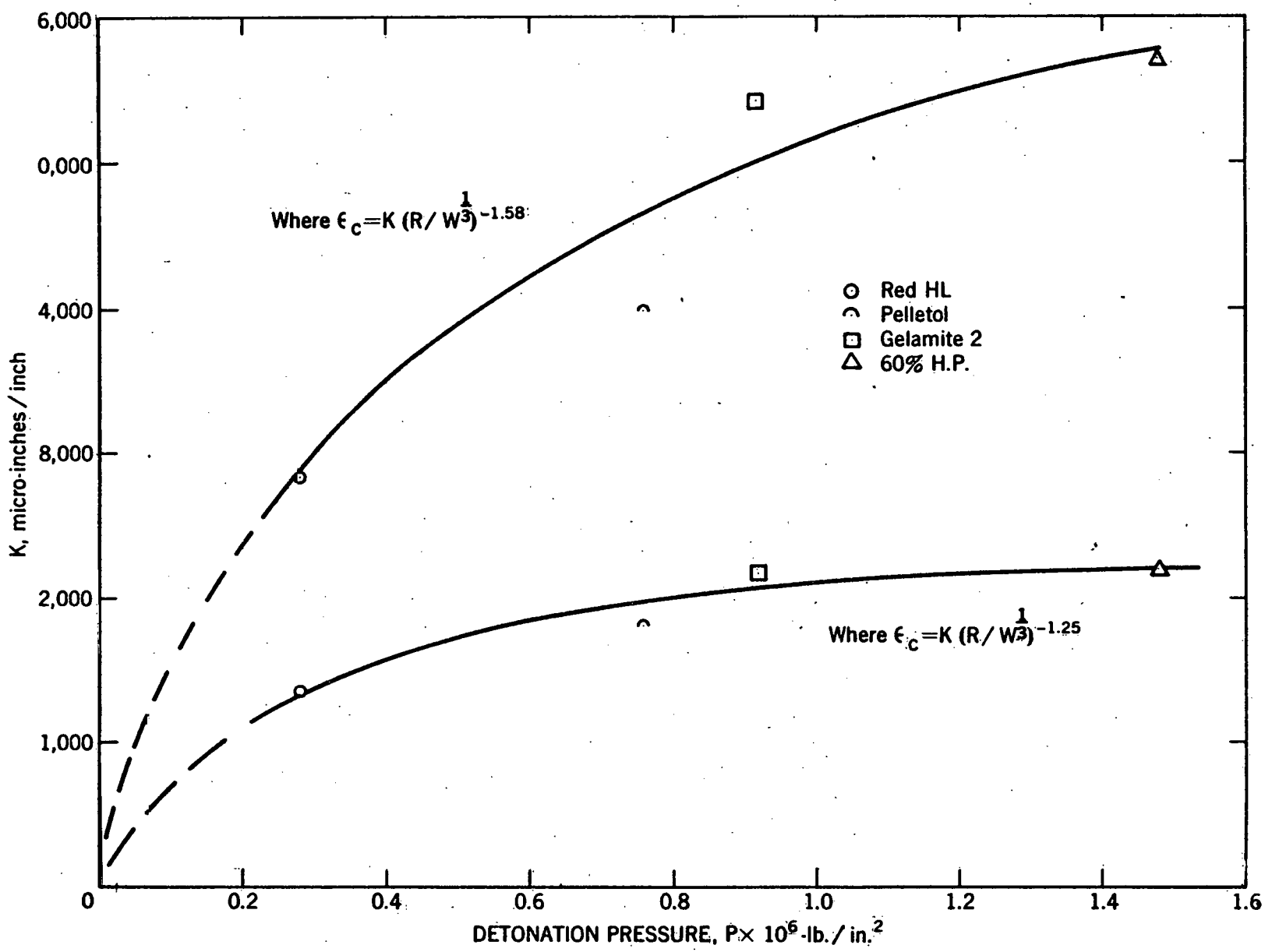

FIGURE 31. - Peak Strain Data vs. Detonation Pressure.

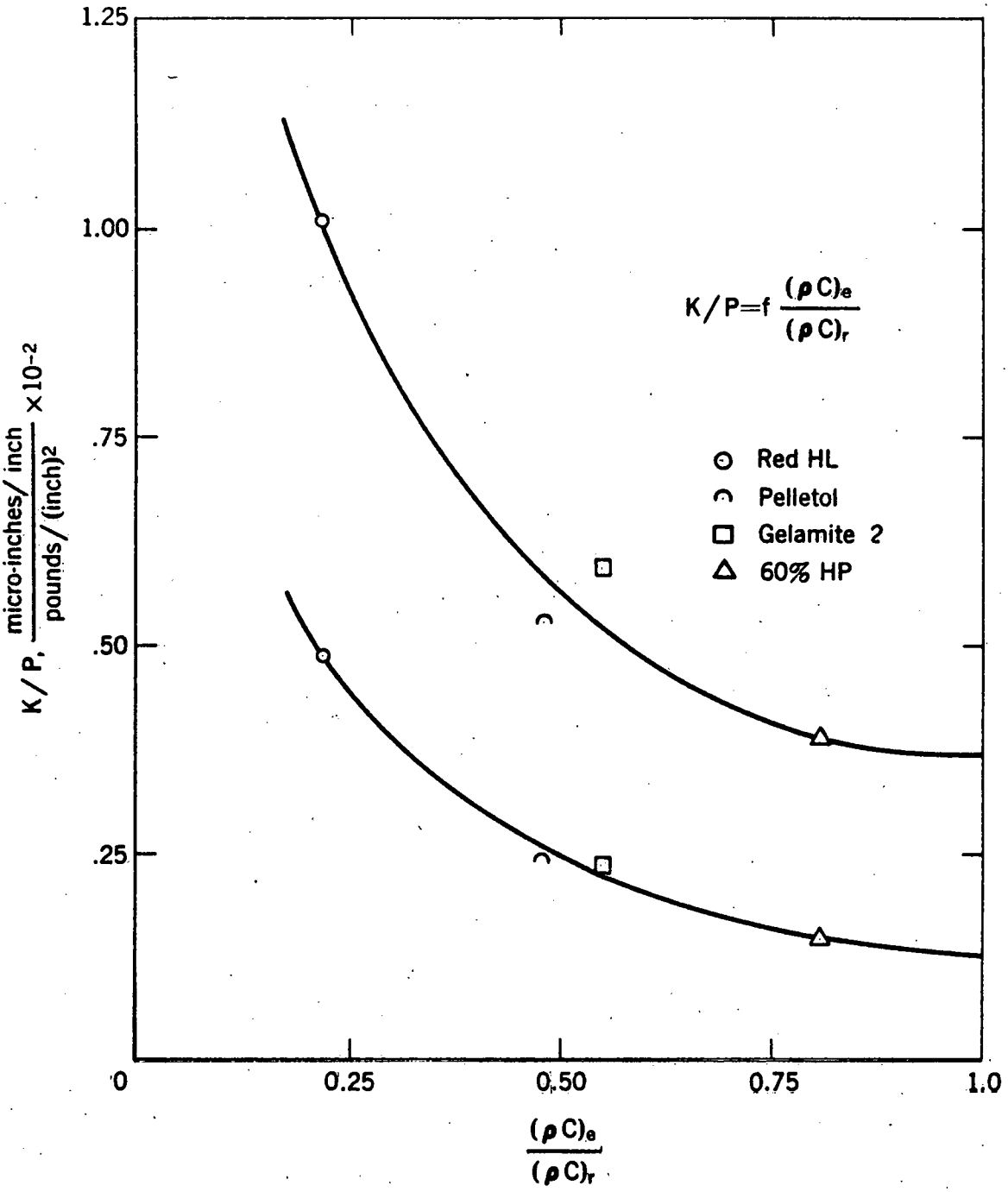

FIGURE 32. - Peak Strain/Detonation Pressure vs. Ratio of Characteristic Impedances.

Unfortunately, it is not possible to select explosives having a wide variation in pressure with constant charactersitic impedance, or constant pressure with wide variation in characteristic impedance. Consequently, both P and $(\rho C)_e$ vary from explosive to explosive.

The product of P and f in equation (6) represents the stress produced at the boundary of the hole. Assuming that strain is directly proportional to stress, the relationship between K and Pf should be a straight line through the origin. An evaluation of equation (7) may be made for the four explosives used in the linear array test. Figure 31 shows the strain intercept constant, which is the strain at a scaled distance of 1 ft/lb$^{1/3}$, plotted as a function of detonation pressure. Two curves are shown corresponding to the two sets of K values given in table 6.

The fact that the strain-pressure curves are not straight lines indicates that there exists some function f, which relates the gas pressure in the cavity to the stress in the rock at the boundary of the cavity. Figure 32 shows graphically the relationship (from equation 7) between K/P and $(\rho C)_e$ / $(\rho C)_r$. The function, f, of the ratio of characteristic impedances is represented by the curves in figure 32. The curves in figure 32 permit the calculation of the stress in the medium for each explosive. If the ratio of characteristic impedances is 1.0, the medium stress equals the detonation pressure. If the ratio is less than 1.0, the medium stress is greater than the detonation pressure. The medium stress is calculated from the following equation using values from the curves in figure 32.

$$P_m = \frac{[(K/P)_{z=1}]}{[(K/P)_{z=a}]} \quad P \qquad (8)$$

where

P_m = medium stress

P= detonation pressure

z= ratio of characteristic impedances

$(K/P)_{z=1}$ = value from the curve where z=1

$(K/P)_{z=a}$ = value from the curve where z=a represents the z value for each explosive.

For each curve in figure 32, the medium stress for each explosive is calculated by means of equation 8 and plotted versus K in figure 33. Straight lines can be drawn through these points and the origin indicating that dynamic strain is directly proportional to stress for the salt.

Elastic wave theory predicts that:

$$K/P = \frac{2}{1+\frac{(\rho C)_e}{(\rho C)_r}} \tag{9}$$

Since the ratio of the characteristic impedances of the explosives used varies from about .20 to .80, elastic wave theory would predict a maximum range for K/P to be of the order of 1.5 fold from minimum to maximum. The data shows at least a 2.5 fold change in K/P indicating shock wave effects.

After each shot in the linear array, the cavity was cleaned, and the cavity volume measured by adding known increments of sand. The cavity volumes were scaled on a volume basis by dividing by the charge volume. Figure 34 shows this volume ratio plotted as a function of detonation pressure. The similarity of this curve with the upper strain-pressure curve of figure 31 at the higher rate of attenuation is striking. The ratio of cavity volume to the charge volume was divided by detonation pressure and plotted as a function of the ratio of the characteristic impedances of explosive to rock in figure 35. Again there is a similarity of this curve with the upper curve of figure 32, even though strain data is scaled by charge weight and cavity volume data is scaled by charge volume.

Particle Velocity

For a plane or spherical wave, at large distances from the origin, particle velocity, v, is related to strain, ϵ_c, by:

$$v = \epsilon_c C \tag{10}$$

where C is the longitudinal propagation velocity. This relationship indicates that strain and velocity should be similar for approximately the same shot-to-gage distance.

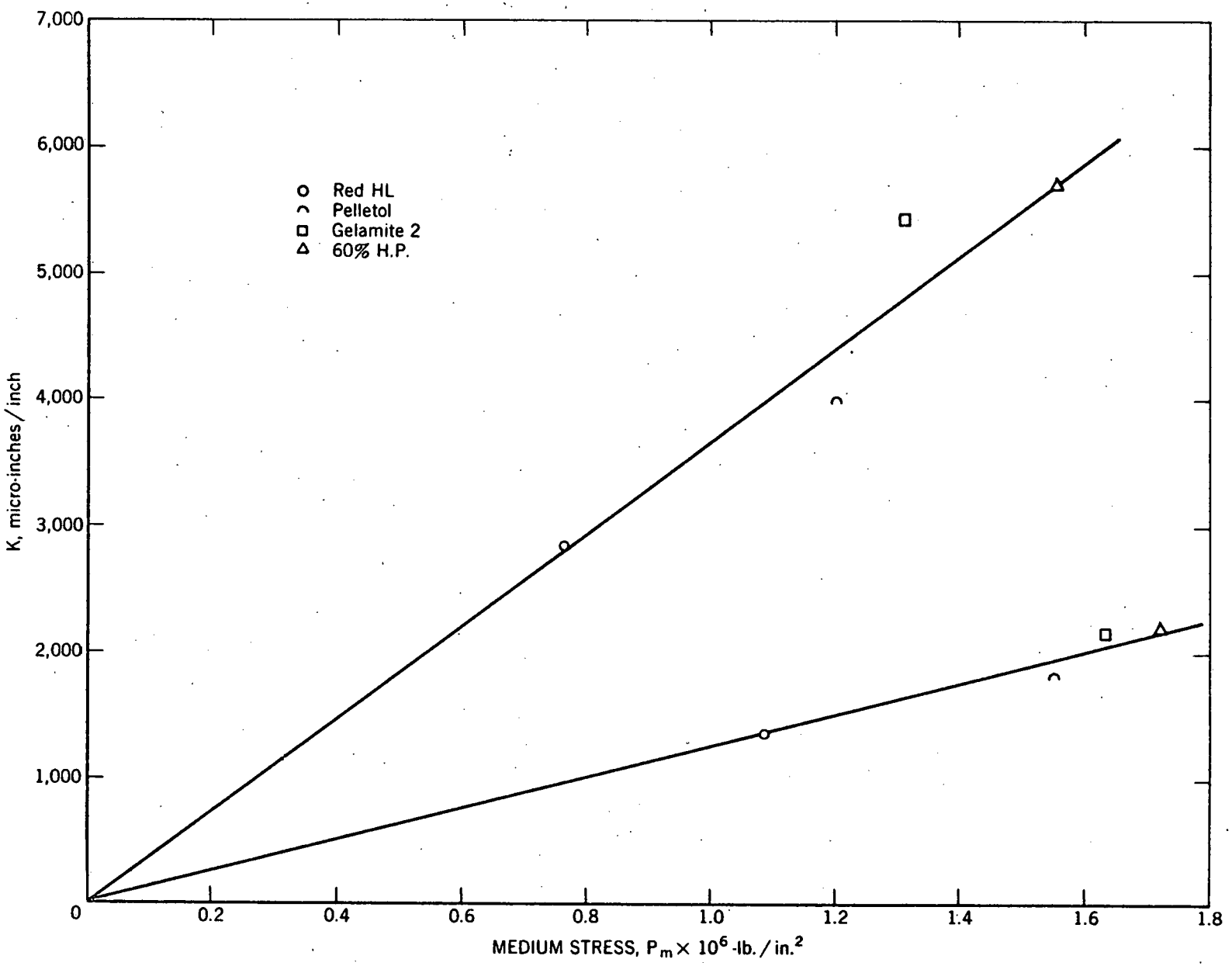

FIGURE 33. - Peak Strain vs. Medium Stress.

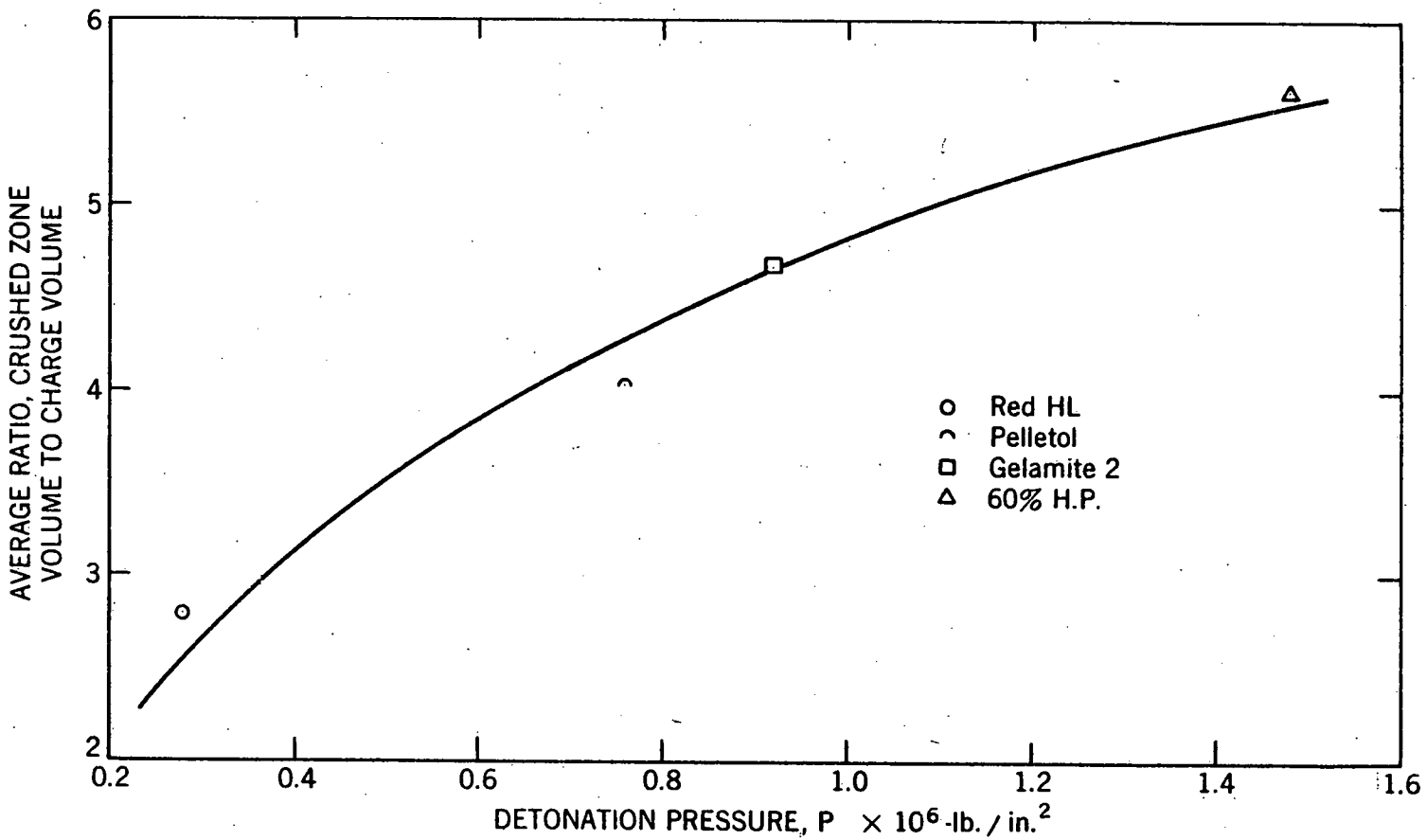

FIGURE 34. - Cavity Volume/Charge Volume vs. Detonation Pressure.

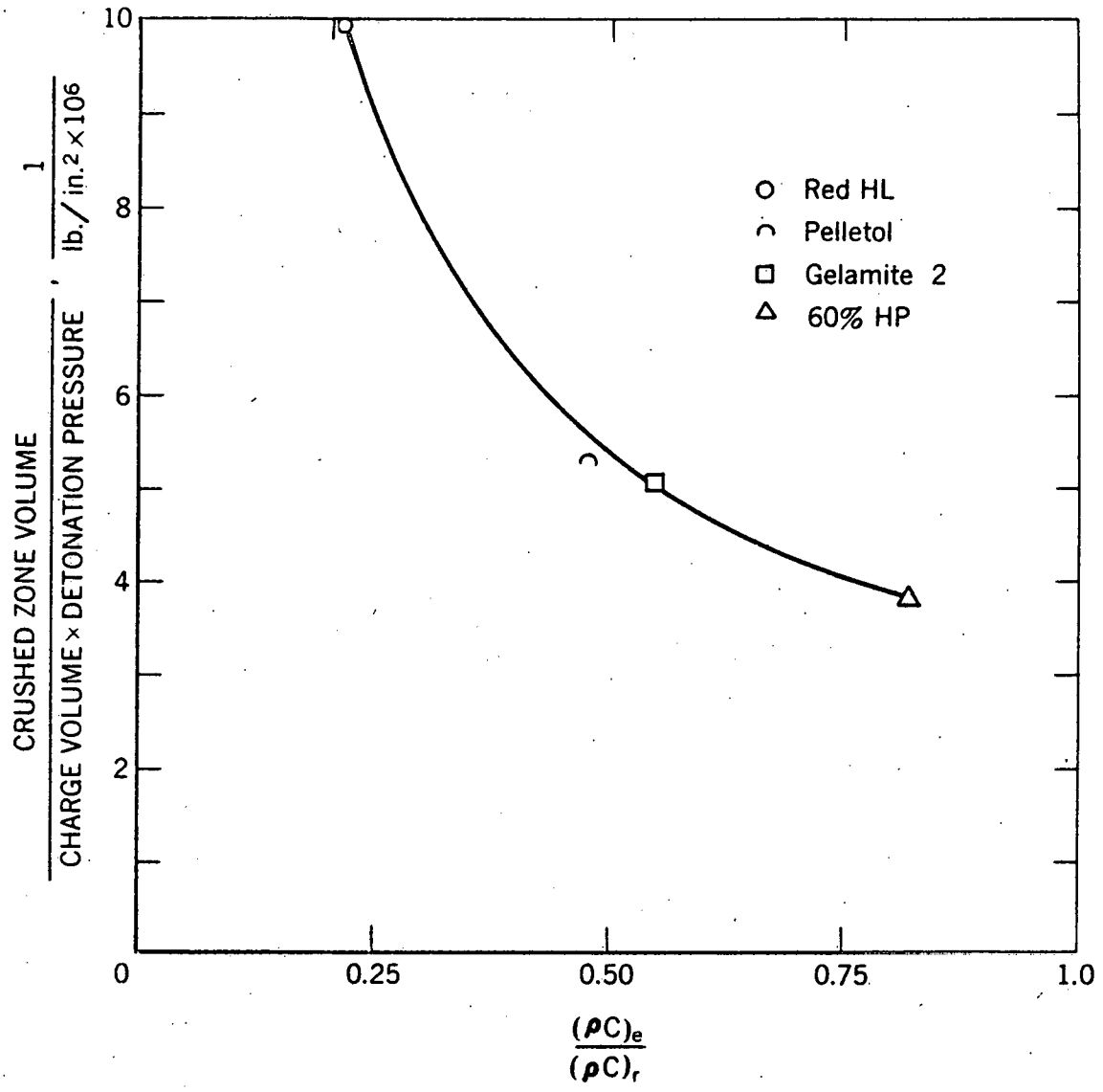

FIGURE 35. - Cavity Volume/Charge Volume x Pressure vs. Ratio of Characteristic Impedances.

The strain propagation laws

$$\epsilon_c = K(R/W^{1/3})^{-n} \qquad (11)$$

for 60% high pressure gelatin and Red HL were converted to particle velocity propagation laws by multiplying each by propagation velocity. Figure 28 shows these results. The velocity data from each explosive plots around these calculated curves with close agreement. No conversion from strain to particle velocity was made at close distances where particle velocity was not recorded.

Particle Acceleration

The peak particle acceleration can be approximated from the strain data by the following equation:

$$A = \frac{v}{t_r} = \frac{\epsilon_c C}{t_r} \qquad (12)$$

where

A= peak acceleration

v= peak particle velocity

t_r= rise time of strain pulse

ϵ_c= peak compressive strain

C= propagation velocity

In using the above equation, the assumption is made that the shape of the strain pulse from the first arrival to the initial peak is a straight line. A more accurate acceleration could be estimated if the maximum slope of the rising portion of the strain pulse was measured. The lack of accurate acceleration data with which to compare the estimated acceleration did not warrant these additional measurements. Acceleration is scaled by multiplying it by $W^{1/3}$, the cube root of charge weight. Scaled rise times were determined from the curves in figures 20, 21, 22, and 23, and the peak acceleration calculated from:

$$AW^{1/3} = \frac{\epsilon_c C}{t_r / W^{1/3}}. \qquad (13)$$

The dashed line in figure 29 represents a plot of these acceleration data. The peak accelerations calculated from the strain data are of the same magnitude as the measured accelerations, thus, the method appears to be valid as a first approximation.

Particle Displacement

Displacement, u, is related to strain, ϵ, by the following:

$$\epsilon = \frac{du}{dr} \tag{14}$$

Thus, to obtain displacement, it is necessary to have the shape of the strain pulse as a function of distance and to integrate this strain distance curve.

For mediums which show relatively small attenuation of high frequency waves with distance, such as salt at Winnfield, it is possible to obtain the strain as a function of distance from strain-time records.

The time scale on a strain record is converted to a distance scale by multiplying the time scale by the propagation velocity. The shape of the pulse must be corrected for attenuation with distance. When a pulse first arrives at a gage, the later portions of the record are actually of greater amplitude than the amplitude recorded because the pulse has traveled the added distance comparable to the time shown on the record. This decrease in amplitude is corrected for by multiplying the recorded amplitude by some number N. This number N is, the strain from the curve in figure 17 at a scaled distance of the gage minus the scaled pulse length to the peak, divided by the strain from the curve at the scaled distance of the gage. Intermediate points may be calculated in the same manner. Calculations were made for all strain records from Pelletol, from arrival at the gage, to the point at which strain again became zero. These new pulses are the strain in space at a particular instant. These pulses were hand integrated to give displacement values. Hand integration of velocity data gives comparable values for displacement. Figure 36 shows displacement as calculated from strain and velocity. Since no displacement measurements were taken, no comparisons of recorded and calculated displacements were made.

Identification of Reflection Events

The most prominent reflection on the records was identified as being S-P or P-S type reflected by the salt-air interface. Shear velocities were measured on the surface of the floor of the drift. Reflection arrival times

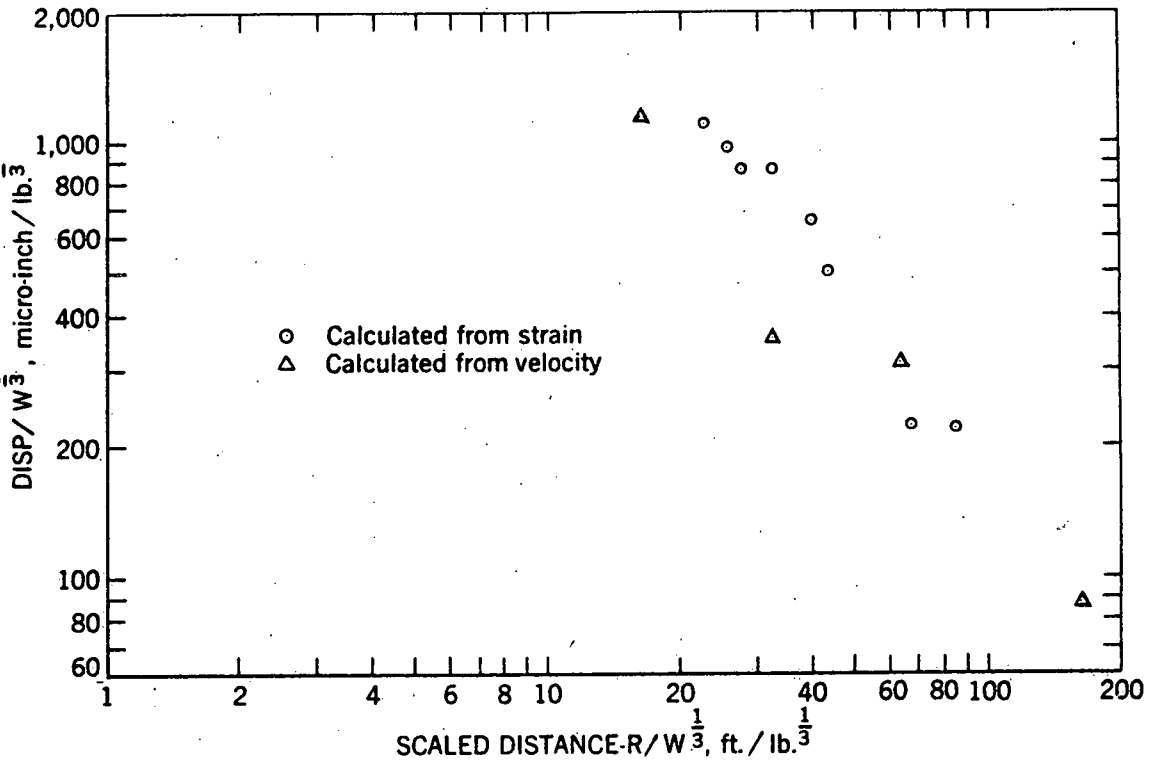

FIGURE 36. - Estimated Particle Displacements vs. Scaled Distance.

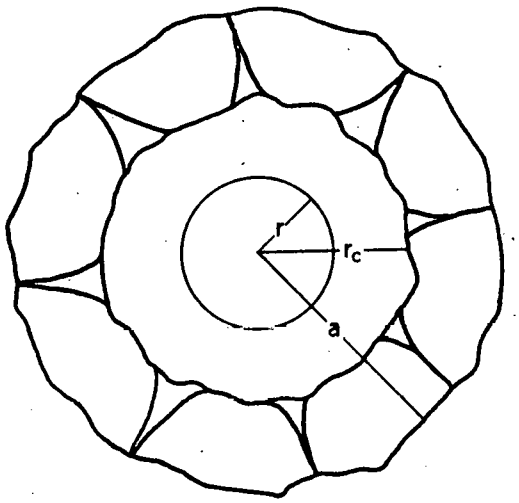

r=radius of charge

r_c=radius of zone of crushing

a=radius of zone of fracturing
(also equivalent radius of cavity)

FIGURE 37. - Zones Surrounding an Explosion in Rock.

indicate that part of the path has been traveled as a transverse wave and part as a longitudinal wave. Because it is impossible to calculate the amount of shear or longitudinal energy arriving at the surface reflecting point, generalizations have to be made as to the exact type of reflection. A consideration of the relative amplitudes of direct and reflected waves indicates the prominent reflection noted to be of the S-P type. P-P and S-S reflections are also evident but are not nearly as persistent and are small in amplitude.

Equivalent Radius of Cavity

Three zones or cavities became apparent in measuring post-shot cavities. All linear array charges had a length-to-diameter ratio between 1:1 and 4:1. The first zone then would have a radius, r, equal to the radius of the charge. This radius is known before the shot. A second zone or measured post-shot cavity with a radius, r_c, would represent the zone of crushing from which the crushed material is removed by compressed air. The third zone would be a highly fractured zone with radius a, which was not measurable. Figure 37 illustrates the three zones apparent in the salt. From a theoretical solution of uniform pressure pulse, applied to a spherical cavity in an infinite homogenous medium, it is possible to calculate an equivalent radius of cavity, a, (3), (4), by means of the following equation:

$$a = \frac{C}{2\pi f} \cdot \frac{(1-2\nu)^{1/2}}{(1-\nu)} \qquad (15)$$

where

a= equivalent radius of cavity

C= propagation velocity of the medium

f= frequency

ν= Poisson's ratio

The equivalent radius of cavity, a, is assumed to be the distance from the center of charge where the magnitude of the pressure equals the strength of the rock. Beyond this radius the applied pressure is less than the strength and no fracturing takes place. From r to r_c, the pressure from the explosion greatly exceeds the strength of the rock and crushing takes place. As the pressure decreases with distance, only cracking takes place until a distance of a is reached, beyond which the medium behaves elastically.

The frequency of the strain pulse in the salt medium is inversely proportional to the cube root of the charge weight. Using the constant from equation (3) and the elastic constants given in table 18 and substituting in equation (15),

$$a = 1.28\ W^{1/3} \qquad (16)$$

As a typical example for Shot 4-S1-2, an 8.2 pound Pelletol charge,

$$r = .18 \text{ ft.}$$

$$r_c = .34 \text{ ft.}$$

$$a = 2.58 \text{ ft.}$$

No cavities with radii as large as a, were measured. However, cavities were not cleaned to the limit of fracture. Fracturing undoubtedly has taken place well beyond any radius calculated from cavity measurements.

Summary

Small scale tests can be used to predict results from large scale tes Additional testing is needed to evaluate the degree of extrapolation that is permissible. Since particle velocity, acceleration, displacement and strain data are all inter-related, small scale tests designed to establish propagation laws for any one quantity, give useful information for the others. Small scale testing is invaluable in making predictions for large scale shots. The rapidity and economy of the linear array type of testing is especially useful for prediction purposes as linear array tests yield a large volume of data over a wide range of scaled distances.

CRATER STUDIES

Introduction

In previous investigations (2), (5), it has been shown that the crater formed by detonating an explosive near a rock surface results from the reflection at the free surface of the compressive pulse generated by the detonation. This pulse reflects in tension, and as the tensile strength of the rock is much less than the compressive strength, the rock is broken in tension progressively from the surface toward the shot point. Because the rock fails in tension the dynamic tensile breaking strength of the rock can be determined from crater tests.

FIGURE 38. - Typical Crater Before Cleaning.

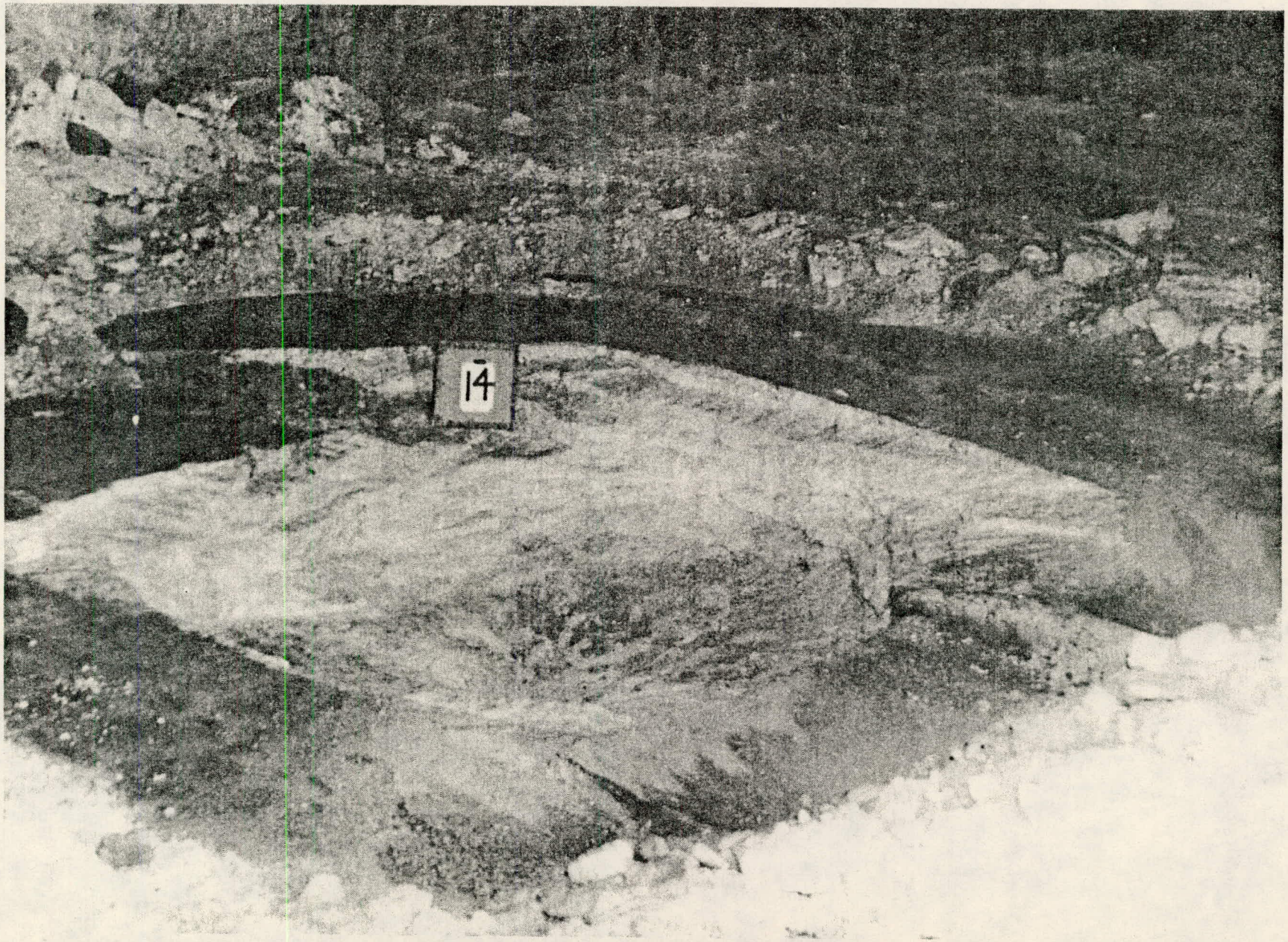

FIGURE 39. - Typical Crater After Cleaning.

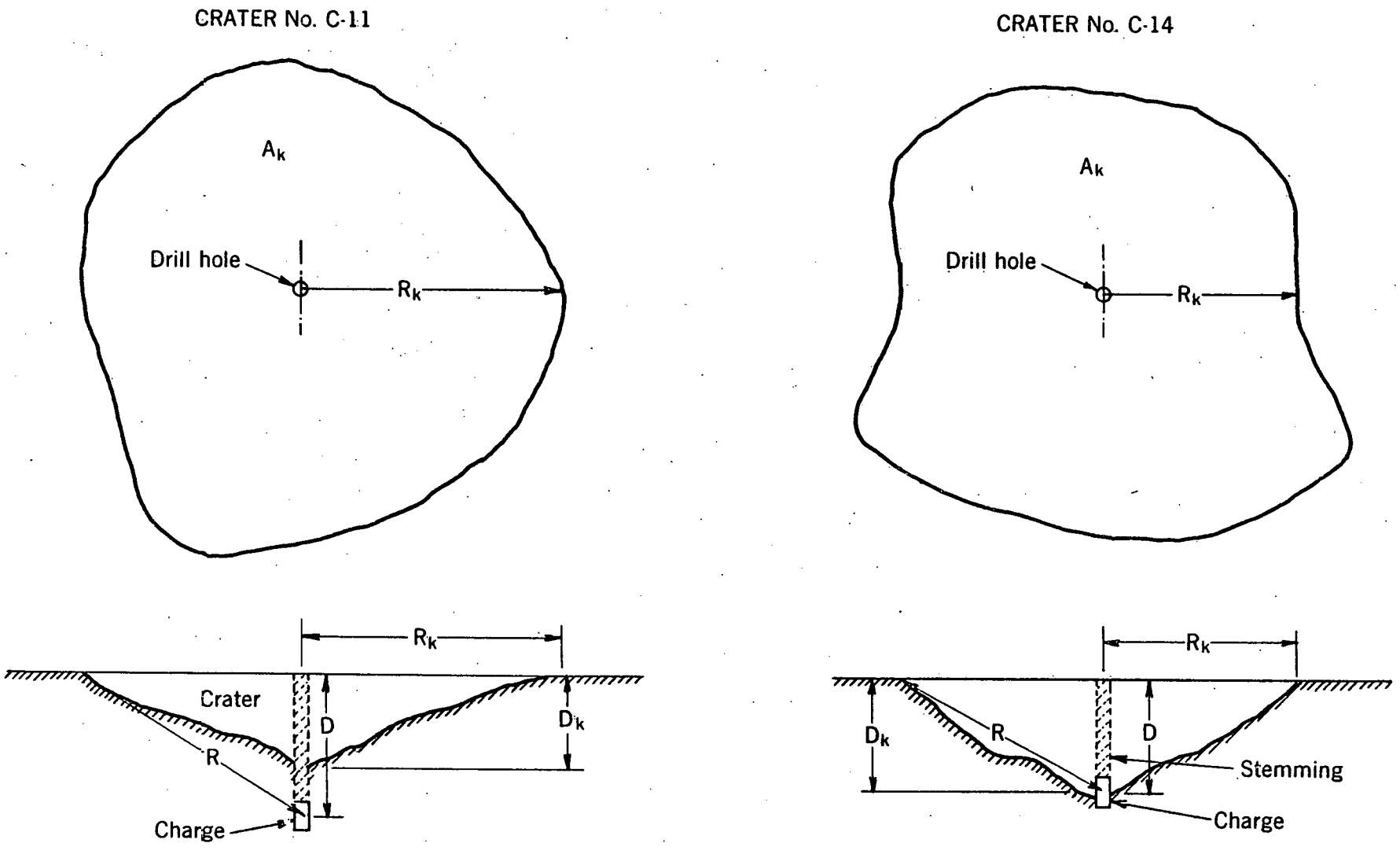

FIGURE 40. - Plan and Section Views of Two Crater Types.

Procedure

A series of fifteen shots were fired in the area shown in figure 10. Eight-pound charges of Gelamite 2 were fired in 5-inch diameter vertical holes, at depths varying from 1 to 10 feet. All holes were stemmed to the surface.

None of the crater shots were instrumented with any type of gage or recording equipment. After each shot was fired a visual inspection was made of the crater area for particle size, slab thickness, and general crater outline. Photographs were taken before any salt was removed. The crater then was cleaned of all loose and broken salt to the extent that a new face of fresh, unbroken salt was exposed. Each cleaned crater was then rephotographed. Figures 38 and 39 are photographs of a typical crater before and after cleaning.

In some cases the hole did not crater to the full depth of the charge. Craters of this type consisted of an unbroken portion of original drill hole separating the surface crater and the cavity produced by the detonation of the charge.

All of the charges did not produce craters. When the center of gravity of the charge was deeper than 6 feet, a small crater at the collar of the shot hole was produced. This may have been caused by gas or sand stemming as it was blown from the hole. The volume of salt removed from these craters was too small to be considered in the data analysis.

After cleaning the crater of broken rock, the periphery of the crater at the surface was mapped and the crater surface area, A_k, was measured (2). Figure 40 shows plan and vertical sections of two craters. The crater radius, R_k, was computed from the crater area by assuming the crater area to be a circle:

$$R_k = \sqrt{A_k / \pi} \qquad (17)$$

Six vertical cross-sections of the crater were mapped, from which the crater volume, V_k, was computed by rotating half of each cross-section through 30°, thus:

$$V_k = \frac{\pi}{2} (r_1 A_1 + r_2 A_2 + \ldots\ldots r_{12} A_{12}), \qquad (18)$$

where A_1, $A_2 \ldots\ldots A_{12}$, are the areas of each half cross-section and

r_1, r_2.....r_{12}, are the radii to their respective centers of gravity. The crater angle ϕ was computed from the crater radius R_k, and crater depth D_k by the equation:

$$\tan \frac{\phi}{2} = \frac{R_k}{D_k} \tag{19}$$

A radius of rupture, R, was computed from the charge depth and crater radius by the equation:

$$R = \sqrt{D^2 + R_k^2} \tag{20}$$

The radius of rupture is the average distance from the center of the charge to the periphery of the crater at the surface.

Crater Data and Analysis

Crater data are presented in table 10. These data are divided into three categories: (1) charge data; describing size, shape and position of the charge: (2) crater data; which describes the physical dimensions and geometry of the crater: and (3) computed and scaled data.

For crater C-2 two sets of data are given; the data, C-2a, showing the smaller volume are based on the cleaned crater and the data, C-2b, based on cracking noted at a radius of 8 feet around the original hole. Compressed air blown into the hole vented through the cracks 8 feet away. The detonation of the charge may have created a slab but lacked sufficient energy at this depth to break the slab.

Figure 41 shows plots of scaled crater radius as a function of scaled charge depth. The data has a characteristic pattern similar to that previously seen in other rock types.

Scaled crater depth is plotted as a function of scaled charge depth in figure 42. This figure shows that for scaled charge depths less than 1.5, the scaled charge depth, and the scaled crater depth are approximately equal. For larger scaled charge depths, the scaled crater depth is smaller than the scaled charge depth. For these shots the crater lies above the original charge point, with unbroken rock between the crater zone and the charge point.

Figure 43 shows a plot of scaled crater volumes as a function of scaled crater depths. This curve resembles the scaled crater radius and scaled crater depth curves.

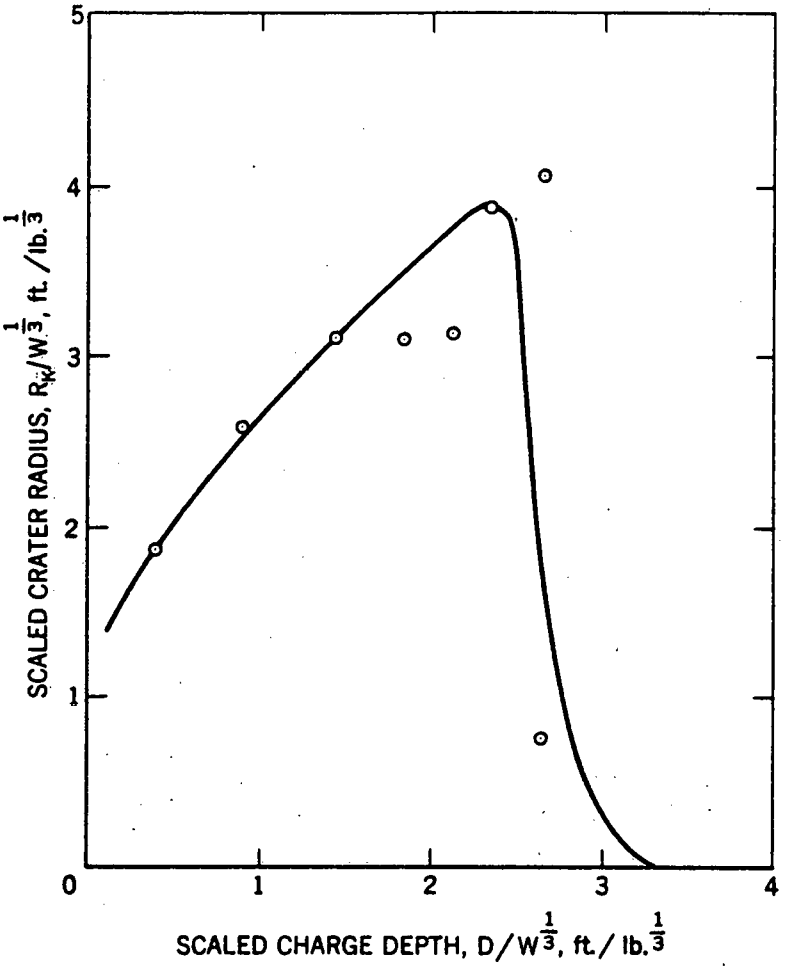

FIGURE 41. - Scaled Crater Radius vs. Scaled Charge Depth.

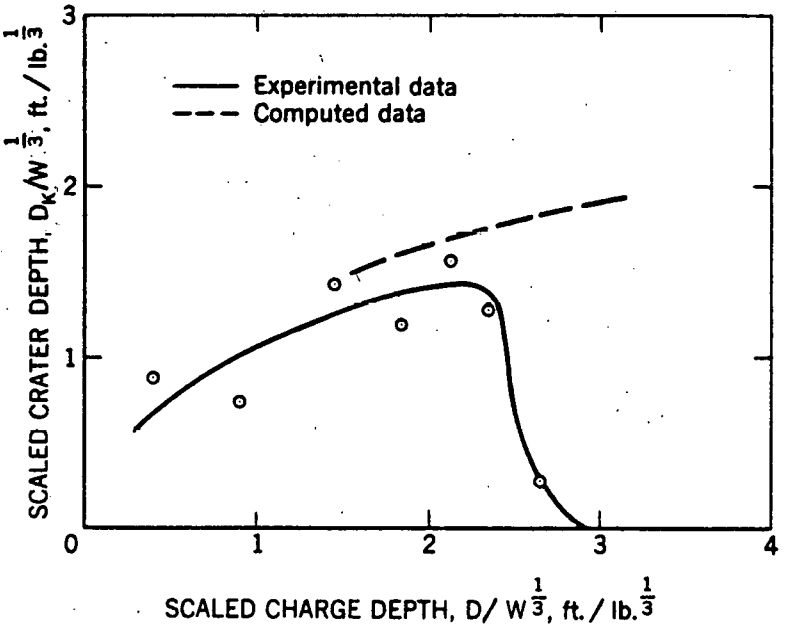

FIGURE 42. - Scaled Crater Depth vs. Scaled Charge Depth.

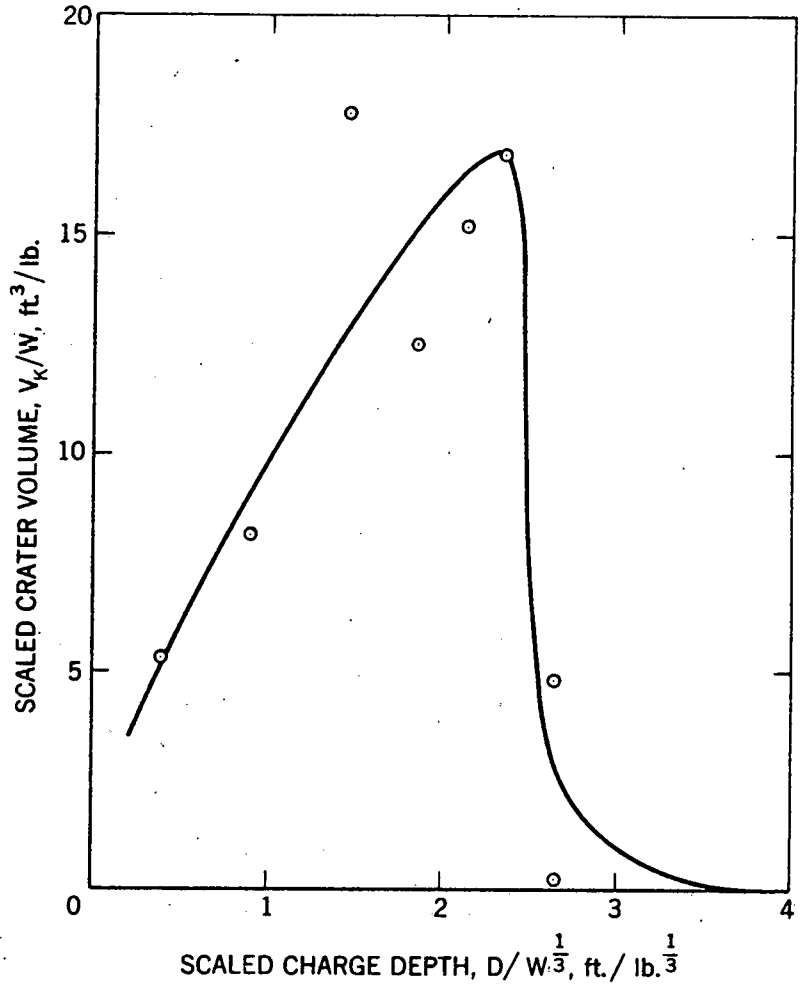

FIGURE 43. - Scaled Crater Volume vs. Scaled Charge Depth.

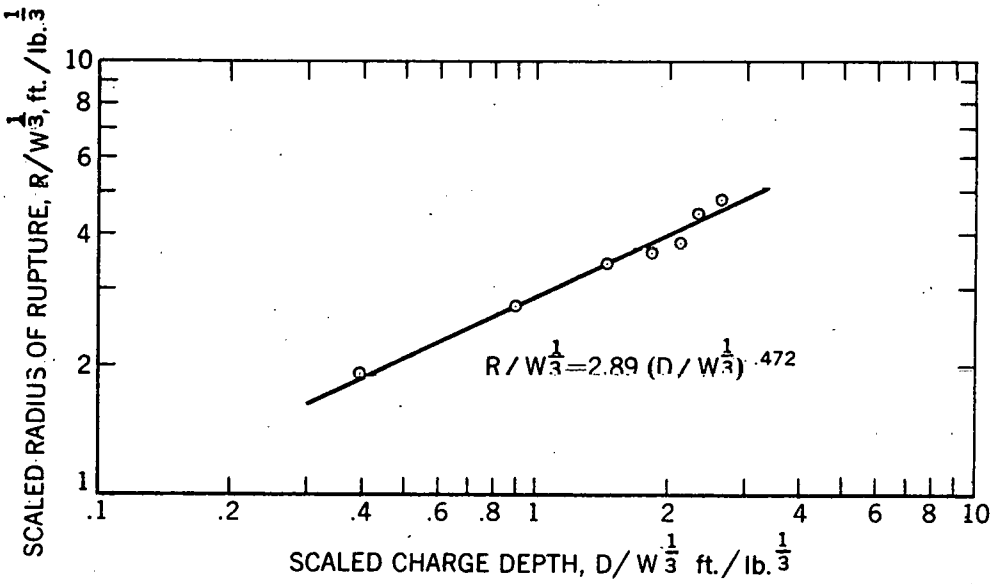

FIGURE 44. - Scaled Radius of Rupture vs. Scaled Charge Depth.

TABLE 10.- Crater test data

Charge data					Crater data				Computed and scaled data						
Shot No.	Weight lb	Depth ft	Length ft	Diameter ft	Radius ft	Depth ft	Angle degree	Volume ft^3	Scaled factor	Scaled charge depth	Charge length to diam. ratio	Scaled crater radius	Scaled crater depth	Scaled radius of rupture	Scaled crater volume
	W	D	l	d	R_k	D_k	ϕ	V_k	$W^{1/3}$	$D/W^{1/3}$	l/d	$R_k/W^{1/3}$	$D_k/W^{1/3}$	$R/W^{1/3}$	V_k/W
C-4	8.2	0.8	0.8	0.42	3.77	1.80	129	44	2.02	.40	1.9	1.87	.89	1.91	5.37
C-12	8.1	1.8	.8	.42	5.20	1.50	148	66	2.01	.90	1.9	2.59	.75	2.74	8.15
C-14	8.0	2.9	.8	.42	6.23	2.85	131	142	2.00	1.45	1.9	3.11	1.43	3.44	17.75
C-11	8.1	3.7	.8	.42	6.23	2.4	138	101	2.01	1.84	1.9	3.10	1.19	3.61	12.47
C-1	7.7	4.2	.8	.42	6.29	3.1	128	117	1.97	2.13	1.9	3.14	1.57	3.84	15.19
C-10	8.1	4.7	.8	.42	7.78	2.55	144	136	2.01	2.34	1.9	3.87	1.27	4.52	16.79
C-2a	7.7	5.2	.8	.42	1.49	.55	139	2	1.97	2.64	1.9	.76	.28	2.75	.26
C-2b	7.7	5.2	.8	.42	8.0	.55	172	37	1.97	2.64	1.9	4.06	.28	4.84	4.81
C-6	8.2	6.1	.8	.42	No crater				2.02	3.02	1.9	No crater			
C-13	8.1	6.3	.8	.42	Do				2.01	3.13	1.9	do			
C-3	8.1	6.6	.8	.42	Do				2.01	3.28	1.9	do			
C-8	8.1	7.2	.8	.42	Do				2.01	3.58	1.9	do			
C-5	8.2	7.7	.8	.42	Do				2.02	3.81	1.9	do			
C-9	8.1	8.2	.8	.42	Do				2.01	4.07	1.9	do			
C-7	8.1	8.7	.8	.42	Do				2.01	4.32	1.9	do			
C-15	8.0	10.0	.9	.42	Do				2.00	5.00	2.1	do			

Figure 44 shows the scaled radius of rupture versus scaled charge depth. The scaled radius of rupture can be represented as a power function of scaled charge depth. The equation in this figure was determined by least-square analysis and is valid only in the region where the scaled radius of rupture is greater than the scaled crater depth, as required by the definition of the radius of rupture.

Interpretation of Results

The fall length of a strain pulse is defined as the product of the fall time, t_f, and the longitudinal propagation velocity C. The value for C can be obtained from the linear array data and the fall time from figure 22 for Gelamite 2. If half of the fall length is less than the charge depth and if the fall strain is several times the tensile breaking strain the depth of the crater should be approximately one-half of the fall length of the strain pulse. Table 11 lists the computed one-half fall lengths. Lack of fall time data for small scaled distances prevents calculation of fall lengths for C-4 and C-12.

TABLE 11. - Measured and computed crater depths

Crater No.	One-half fall length ft	Measured crater depth ft
C-14	2.89	2.85
C-11	3.22	2.4
C-1	3.44	3.1
C-10	3.54	2.55
C-2	3.68	0.55

If the charge depth is less than one-half of the fall length of the pulse, the rock is broken from the free surface back to the crushed zone around the charge. This condition is apparent from craters C-4 and C-12. For crater C-14, the charge depth, crater depth, and estimated crater depth are nearly equal.

Scaled crater depths were computed from the half fall length data given in table 11 and are shown plotted as a function of scaled charge depth (dashed line) in figure 42. For scaled charge depths of 1.5 or less, the scaled crater depths should equal the scaled charge depths. For scaled charge depths greater than 2.3, the measured scaled crater depth decrea abruptly, whereas the computed scaled crater depth continues to increas

This result is to be expected because the fall strain is being attenuated with distance and becomes insufficient to break the rock in tension.

A visual inspection of the craters before cleaning indicated two slabs were produced at charge depths up to 4.7 feet, and slab thickness varied from 1 foot to 1.5 feet. For crater C-2, only one slab was produced indicating that maximum crater depths occurred when two slabs were produced. The formation of two slabs at maximum crater depths is evidence that the fall strain was at least twice the breaking strain of the rock. The dynamic tensile breaking strain and stress of the rock may be calculated from the crater data and the linear array data. The scaled crater depth plus scaled charge depth is the total travel distance of the strain pulse. The fall strain at this distance is read from the dashed curve in figure 18. The average value of the half of the fall strain is the estimated dynamic tensile breaking strain for the salt as given in table 12. Tensile breaking stress is computed from the dynamic modulus of elasticity obtained from wave velocity measurements.

TABLE 12.- Estimated tensile breaking strain and stress

Crater No.	Scaled charge depth $ft/lb^{1/3}$	Scaled crater depth $ft/lb^{1/3}$	Scaled travel distance $ft/lb^{1/3}$	Fall strain μ in /in	One-half fall strain μ in/in	Stress p.s.i.
C-4	.4	.9	1.3	-	-	-
C-12	.9	.8	1.7	920	460	2340
C-14	1.5	1.4	2.9	600	300	1530
C-11	1.8	1.2	3.0	580	290	1480
C-1	2.1	1.6	3.7	460	230	1170
C-10	2.3	1.3	3.6	480	240	1220
C-2	2.6	.3	2.9	600	300	1530

The average tensile breaking strain is 310 microinches/inch and the average tensile breaking stress is 1560 pounds per square inch.

The good agreement between experimental crater depths and computed crater depths from half fall lengths indicates that the entire fall strain was available as tensile strain and the estimated tensile breaking strain determined represents a good estimate.

TABLE 13.- Velocity spread data

Shot number	Explosive type	Charge size W lb.	Gage position	Type of gage	Distance R ft.	Time of arrival P wave 10^{-3}sec.	Time of arrival S wave 10^{-3}sec.
1	Gel.2	0.4	G 11	Acc.	113	8.12	-
			G 12	Vel.	150	10.60	18.70
			G 13	Acc.	188	13.18	21.35
			G 14	Vel.	227	16.10	26.25
2	Gel.2	0.2	G 11	Acc.	111	8.13	-
			G 12	Vel.	148	10.55	-
			G 13	Acc.	186	13.11	21.50
			G 14	Vel.	225	15.65	26.18
4	Gel.2	0.1	G 12	Acc.	144	10.25	17.39
			G 13	Acc.	182	12.72	21.61
			G 14	Vel.	221	15.54	26.85
			G 15	Vel.	343	23.79	41.30
5	Gel.2	0.1	G 12	Acc.	142	10.16	17.78
			G 13	Acc.	180	12.53	21.70
			G 14	Vel.	219	15.38	27.05
			G 15	Vel.	341	23.60	41.10
6	Red HL	0.06	G 12	Acc.	140	9.78	16.90
			G 13	Acc.	178	12.38	21.40
			G 14	Vel.	217	15.22	26.20
			G 15	Vel.	339	23.20	40.40
7	Red HL	0.06	G 13	Acc.	176	12.38	21.75
			G 14	Vel.	215	15.11	26.45
			G 15	Vel.	337	23.25	40.00
			G 16	Acc.	428	29.30	49.30
8	Red HL	0.06	G 13	Acc.	174	12.30	-
			G 14	Vel.	213	15.08	25.50
			G 15	Vel.	335	23.05	39.45
			G 16	Acc.	426	29.37	50.45
9	Red HL	0.06	G 13	Acc.	172	12.08	-
			G 14	Vel.	211	14.67	25.70
			G 15	Vel.	333	22.80	39.25
			G 16	Acc.	424	28.95	50.20

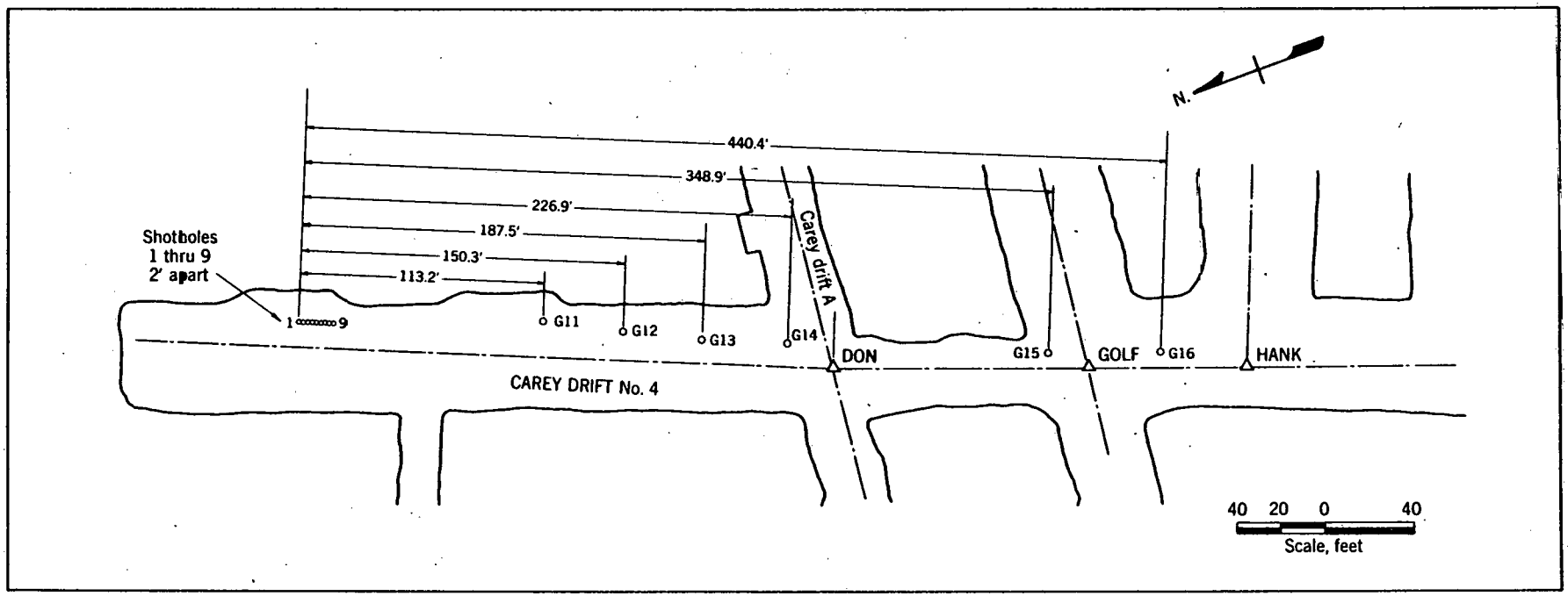

FIGURE 45. - Plan View, Velocity Study Area.

VELOCITY SPREAD No. 5
EXPLOSIVE 0.1 LB. GELAMITE 2

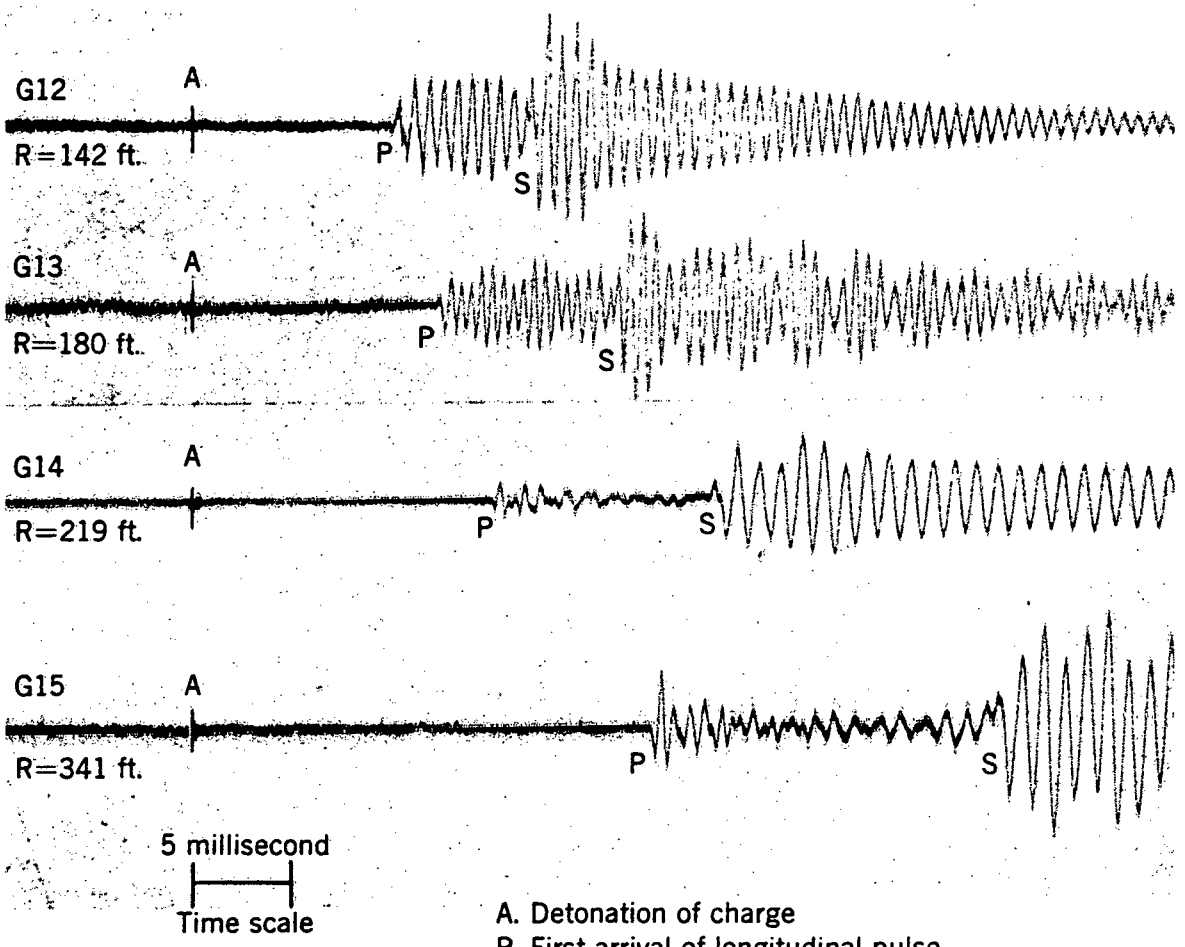

A. Detonation of charge
P. First arrival of longitudinal pulse
S. First arrival of transverse pulse
G12-G15. Gage position
R. Distance from shotpoint to gage

FIGURE 46. - Typical P and S Arrivals.

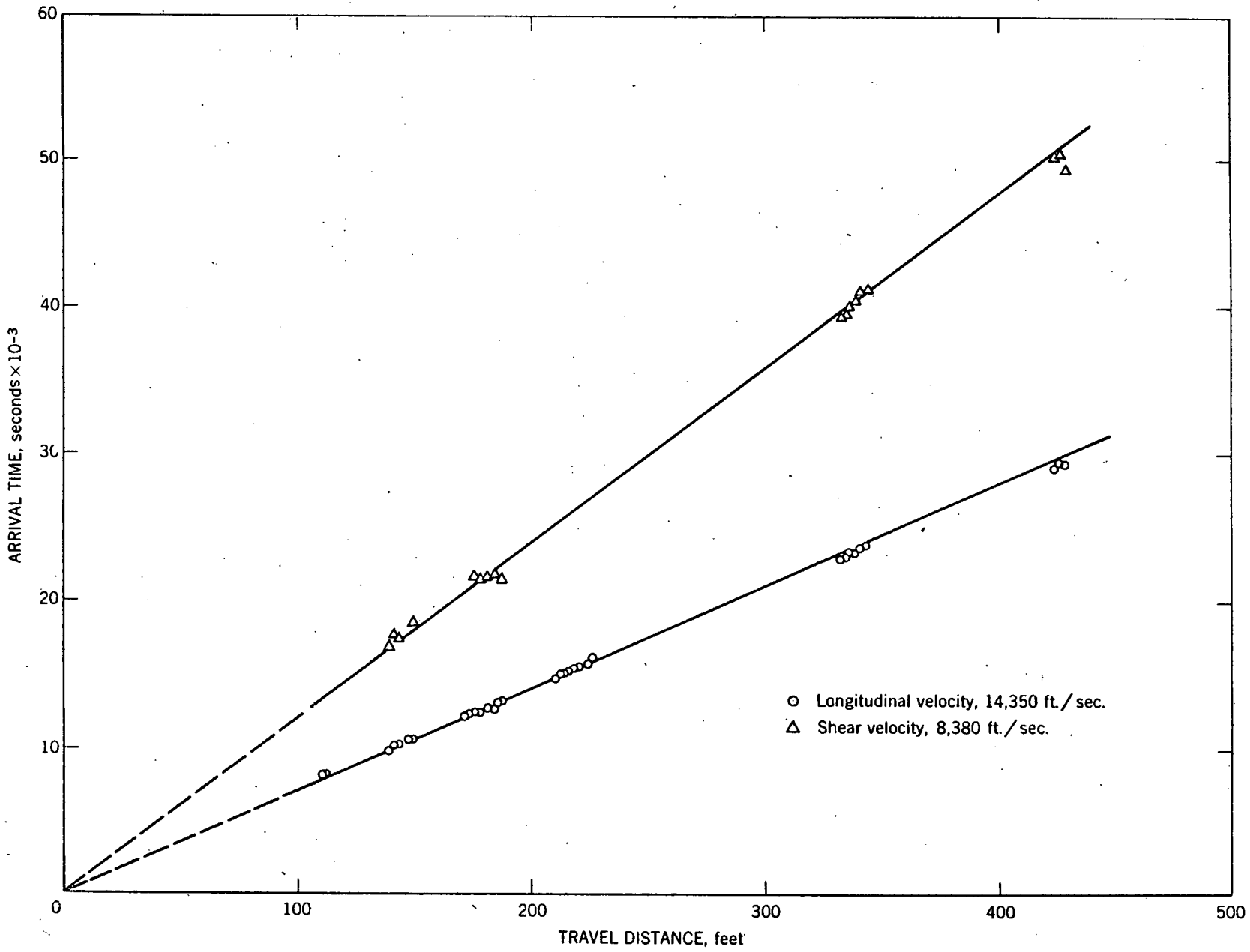

FIGURE 47. - P and S Propagation Velocity Data.

VELOCITY STUDIES IN SITU

Procedure

To determine P and S wave velocities a total of 9 shot holes and 6 gage holes were drilled in Carey Drift No. 4. Figure 45 is a plan of the velocity array area. All holes were shallow vertical holes, the average depth being 8 inches. Of the 9 shots eight were satisfactory and one (the third) misfired. The horizontal component of particle motion perpendicular to a line from shotpoint to gage was measured with MB velocity gages and Endevco accelerometers mounted on grouted studs. Four gages were used on each shot and these gages were moved progressively to greater shot-to-gage distances as testing proceeded.

Conventional electric blasting caps were used to detonate small charges, ranging from 0.06 to 0.4 pounds of explosives. The quantity of explosive was decreased as testing proceeded, so as to yield better P and S wave separation.

Velocity Data and Analysis

Table 13 lists shot-to-gage distances and longitudinal and shear propagation arrival times. Figure 46 shows the seismic records from Shot No. 5. These records are typical except at close distances some records exhibit air-blast phenomena. A gage mount ringing problem which precludes any possibility of frequency analysis or particle velocity or acceleration amplitude studies is evident from the records in figure 46.

A plot of P (longitudinal) and S (shear) wave arrival times versus shot-to-gage distances is shown in figure 47. The velocities shown in the figure and the reciprocal velocity lines drawn through the data have been calculated by least squares analysis. The greater scatter in the shear wave arrival times is attributed in part to the ringing in the gage mounts which tends to obscure the initial arrival time break.

Table 14 shows the results of the P and S wave velocity calculations.

TABLE 14. - Velocity Results

Wave type	Velocity
P- Longitudinal	14,350 ± 100 ft/sec.
S- Shear	8,380 ± 100 ft/sec.

The measurement of longitudinal and shear wave velocities for the

COWBOY salt in situ permits the calculation of various elastic constants which are given in table 15.

TABLE 15. - Dynamic Elastic Constants

Constant	Value
E= Modulus of elasticity	5.09×10^6 p.s.i.
μ= Modulus of rigidity	2.05×10^6 p.s.i.
λ= Lame's constant	1.91×10^6 p.s.i.
k= Bulk modulus	3.28×10^6 p.s.i.
ν= Poisson's ratio	.241
λ / μ	.931

DYNAMIC CORE TESTS

Introduction

Seismic wave propagation in long cylindrical cores has been studied by other investigators (6), (7), (8). Small explosive charges are detonated on one end of the core. A longitudinal compressional wave travels the length of the core and is reflected at the free end as a tensile pulse. The core fails at the shot end in compression and at the free end in tension. Strain gages mounted along the core give strain amplitudes as the wave traverses the core. Dynamic breaking strength or stress at failure can be computed from the strain curve and the dynamic modulus of elasticity.

Procedure

Four 2.5-to-4-ft. lengths of NX core of COWBOY salt were tested. Each core was instrumented with eleven C-7 resistance type strain gage elements. These gages were cemented at various distances along the core, coated with wax, and waterproofed. A typical core (Core No. 1) is shown in figure 48 before final assembly. In this figure the left end of the core is the shot end and the black spots are strain gages. The copper foil shown at the left end was slid two or three inches beyond the end of the core and was used as an explosive container.

The core was placed in a vertical position into a one foot diameter hole and stemmed with sand. The free end of the core extended one to two

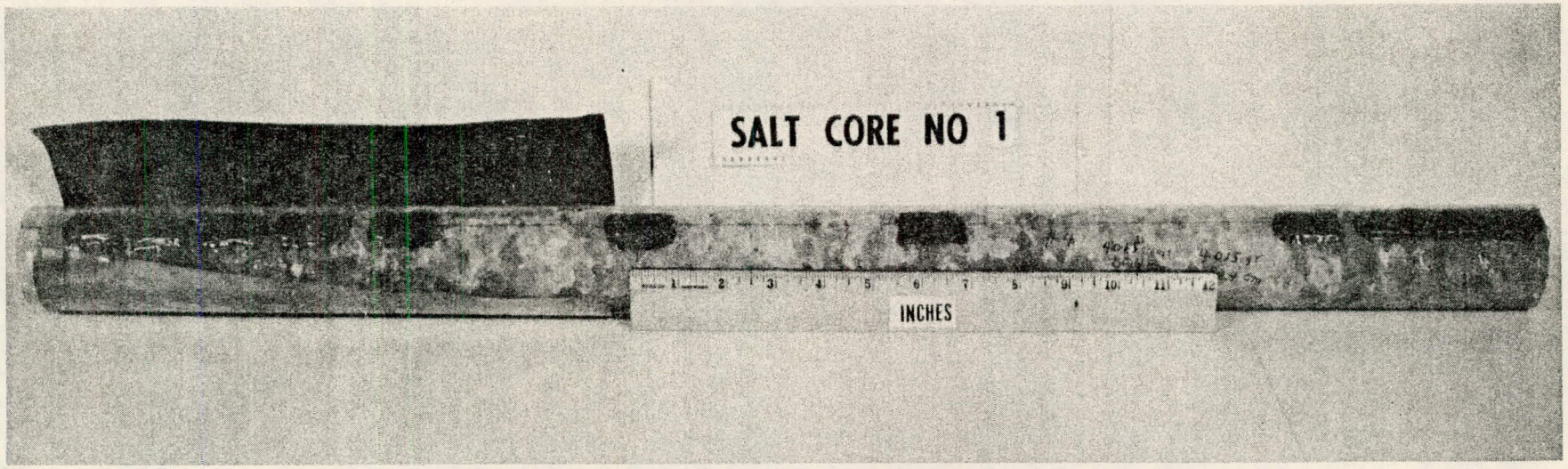

FIGURE 48. - Core No. 1 Before Shooting.

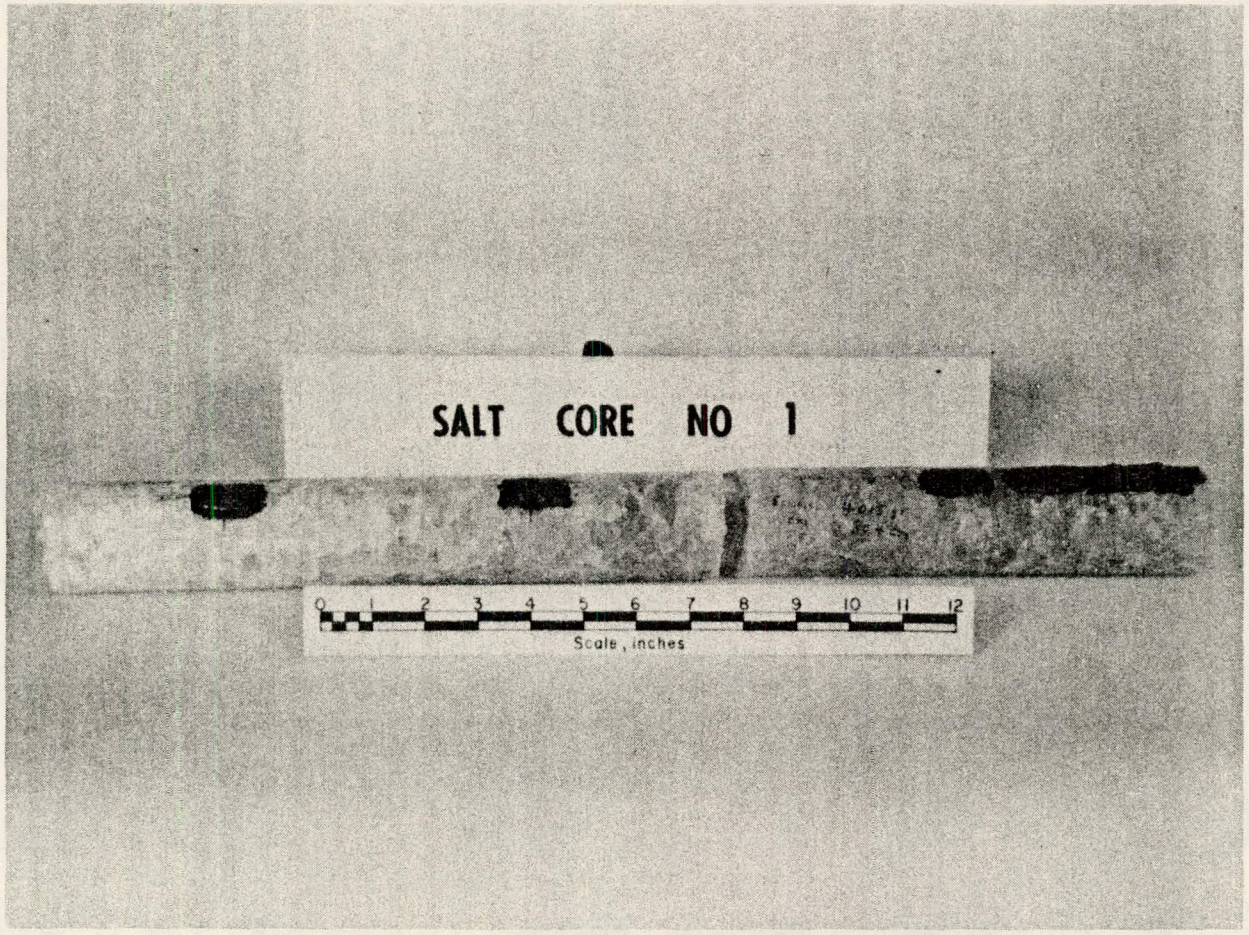

FIGURE 49. - Core No. 1 After Shooting.

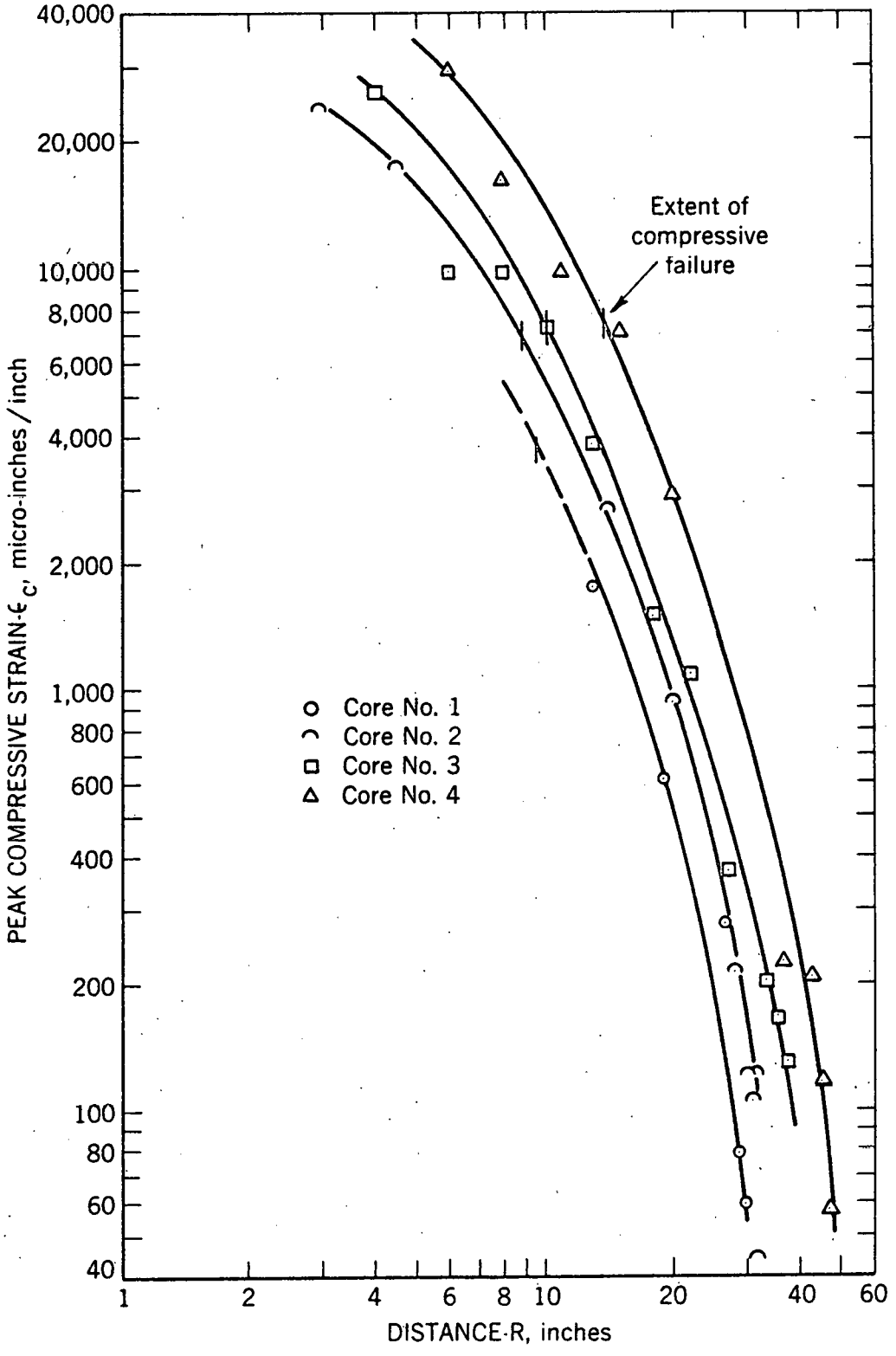

FIGURE 50. - Peak Strain vs. Distance.

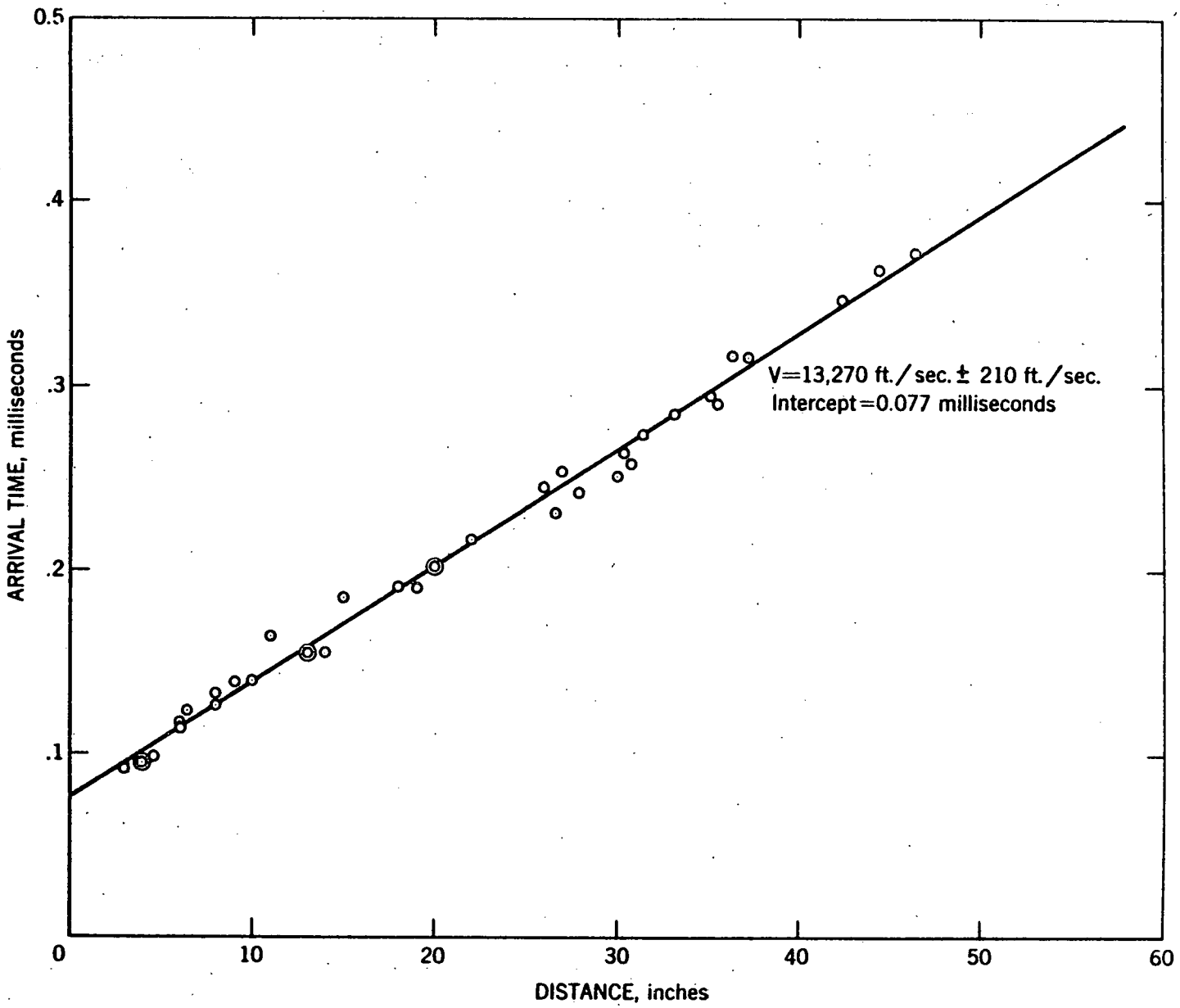

FIGURE 51. - Core Test Arrival Times vs. Distance.

feet above the stemming depending on the length of the core. The charge was detonated and strain data recorded.

After each shot the core was examined for compressive and tensile failures. Figure 49 shows Core No. 1 after shooting.

Data and Analysis

Table 16 lists the data from the four tests. No pieces of core were broken from the free end indicating that there was no tensile failure. The length of the core crushed in compression at the shot end is shown in the table.

Figure 50 shows the relationship between peak compressive strain and distance. The separation of the data by shot probably results from using different charge weights. The steep portion of the curves (data from gages at free end of core) results from the arrival of the reflected tensile pulse before the arrival of the peak of the direct compressive strain wave. Since the two waves are additive and out of phase, the gage responds only to the difference.

A necessary condition for tensile failure of this type is that the wave length of the strain wave be shorter than the length of the core. The average wave length generated was more than five feet indicating that no tensile failure could have occurred. The stemming in the hole may have held up the pressure from the explosion sufficiently long to result in long wave lengths. As a result, the reflected tensile strain wave was not large enough to cause failure in tension and no estimates of the dynamic tensile breaking strength can be made.

A plot of the strain wave arrival times versus gage distance is shown in figure 51. The velocity of the longitudinal wave computed by least squares is 13,270 feet per second. The fact that this curve does not pass thru the origin may result from either or both of two possibilities. (1) The detonation time is obtained from a target which is taped to the blasting cap. The target may pick up the "make" of the cap current. This would give a premature zero time. (2) Because these are regular (not seismic) blasting caps, the time difference may result from a delay between the cap bridge rupturing and the detonation of the cap.

Interpretation of Results

The peak compressive strain at the point of failure is indicated in figure 50. From the peak compressive strain and the dynamic modulus of

TABLE 16. - Dynamic core test data

Gage No.	Distance R in.	Arrival time T_A x10^{-3} sec.	Peak strain ϵ_c in/in.
Core No. 1 Explosive- 1 lb. Gel. 2			
1	1.5	-	-
2	3	-	-
3	4.5	-	-
4	6	-	-
5	8	-	-
6	13	.155	1,730
7	19	.191	609
8	26.6	.233	278
9	28.6	-	79
10	29.6	.257	60
11	30.6	-	-
Length of core 31.6 inches Crushing 9.6 inches			
Core No. 2 Explosive- .05 lb. Gel. 2			
1	3	.093	23,400
2	4.5	.099	17,050
3	6	.115	-
4	9	.140	-
5	14	.155	2,667
6	20	.202	936
7	27.9	.242	213
8	29.9	.251	121
9	30.4	.264	106
10	30.9	.257	121
11	31.4	.274	44
Length of core 31.9 inches Crushing 8.9 inches			
Core No. 3 Explosive- .15 lb. Gel. 2			
1	4	.096	25,700
2	6	.118	9,820
3	8	.127	9,800
4	10	.140	7,130
5	13	.155	3,810
6	18	.192	1,490
7	22	.217	1,090
8	27	.254	369
9	33.2	.285	203
10	35.2	.295	168
11	37.2	.316	130
Length of core 39.2 inches Crushing 10.2 inches			
Core No. 4 Explosive- .4 lb. Gel. 2			
1	4	.096	-
2	6	.124	29,100
3	8	.133	16,100
4	11	.164	9,970
5	15	.186	7,060
6	20	.202	2,910
7	26	.245	-
8	36.4	.316	227
9	42.4	.347	208
10	44.4	.363	117
11	46.4	.372	58
Length of core 48.4 inches Crushing 11.9 inches			

elasticity the dynamic strength of the rock in compression can be computed. These data are given in table 17.

TABLE 17.- Dynamic strengths from core testing

Core No.	Charge weight	Length crushed	Peak compressive strain	Dynamic compressive breaking strength
	lb.	in.	micro-in/in.	$lb/in.^2$
1	.1	9.6	3700	18,800
2	.05	8.9	6700	34,100
3	.15	10.2	7100	36,200
4	.4	13.9	7500	38,200
Average			6250	31,800

PHYSICAL PROPERTIES

A summary of the physical properties of the COWBOY salt, salt grout, and Hydrostone is shown in table 18.

The results from dynamic field tests include data from the linear array tests, velocity studies, core tests and crater tests. Also, static tests were made in the laboratory for comparison. These static tests were made according to standardized procedures (8).

The most significant result is the disparity in the dynamic and static strengths in tension and compression. The dynamic compressive and tensile strengths are, respectively, 7 and 25 times the static values.

TABLE 18. - Physical properties

Property		COWBOY Salt			Salt grout			Hydrostone		
		Value	No. of readings	S_E	Value	No. of readings	S_E	Value	No. of readings	S_E
Weight density	lb/ft^3	135	11	±1.3	125	13	±8.7	124	4	±2.1
Longitudinal velocity										
Linear array test	ft/sec	14,400	217	±240						
Velocity study	ft/ sec	14,350	32	±100						
Core tests	ft/ sec	13,270	37	±210						
Laboratory	ft/ sec	12,810	11	±510	10,000	3	±200	8,990	4	±160
Shear velocity										
Velocity study	ft/ sec	8,380	27	±100						
Laboratory	ft/ sec	8,800	11	±230	6,720	3	±210	5,770	4	±360
Modulus of elasticity										
Velocity study	lb/in^2x10^6	5.09								
Laboratory	lb/in^2x10^6	4.79	11	±.38	2.76	3	±.08	2.16	4	±.05
Modulus of rigidity										
Velocity study	lb/in^2x10^6	2.05								
Laboratory	lb/in^2x10^6	2.26	11	±.12	1.23	3	±.09	.87	4	±.04
Poisson's Ratio										
Velocity study		.241								
Laboratory		.059	11	±.045	.125	3	±.046	.245	4	±.030
Compressive strength										
Core tests	lb/in^2	31,800	4							
Laboratory	lb/in^2	4,620	45	±370	3,830	23	±1140	280	9	±20
Tensile strength										
Crater tests	lb/in^2	1,560	6							
Laboratory	lb/in^2	62	11	±28				250	6	±50

BIBLIOGRAPHY

1. OBERT, LEONARD and DUVALL, WILBUR I., A Gage and Recording Equipment for Measuring Dynamic Strain in Rock, Bureau of Mines Report of Investigations 4581, 1949, 11 pp.

2. DUVALL, WILBUR I. and ATCHISON, THOMAS C., Rock Breakage by Explosives, Bureau of Mines Report of Investigations 5356, 1957, 52 pp.

3. BLAKE, F. G., Spherical Wave Propagation in Solid Media: The Journal of the Acoustical Society of America, Vol. 24, No. 2, March 1952, pp 211-215.

4. SHARPE, J. A., The Production of Elastic Waves by Explosion Pressures, I, Theory and Empirical Field Observations: Geophysics, Vol. 7, April 1942, pp 144-154.

5. HINO, KUMAO, Theory of Blasting with Concentrated Charge, Jour. Ind. Explosives Soc., Japan.

6. HINO, KUMAO, Fragmentation of Rock Through Blasting, Jour. Ind. Explosives, Soc., Japan, Vol. 17, No. 1, 1956, pp 2-11.

7. GRINE, D. R., Finite Amplitude Stress Waves in Rocks, Stanford Research Institute Lab. Tech. Report 011-59, October 1, 1959, 51 pp.

8. OBERT, LEONARD, WINDES, S. L., and DUVALL, WILBUR I., Standardized Tests for Determining the Physical Properties of Mine Rock, Bureau of Mines Report of Investigations 5891, 1946, 67 pp.

Int. --Bu. Mines, Pgh., Pa. 1924

SUMMARY OF SHOT DATA-PROJECT COWBOY

SHOT NO.	DATE	TIME (CST)	YIELD (lbs)	STATION	TYPE
1	17 Dec.	0015	20	1.2	Coupled- 45' hole
2	17 Dec.	0045	20	1.1	Decoupled- 12' diam. sphere
3	19 Dec.	0000	100	1.1	Decoupled- 12' diam. sphere
4	19 Dec.	0015	100	1.3	Coupled- 45' hole
5	23 Jan.	0000:00.113	198.35	2.1	Decoupled- 30' diam. sphere
6	30 Jan.	0001:00.112	200.0	2.1	Decoupled- 30' diam. sphere
7	30 Jan.	0101:00.112	199.65	2.2	Coupled- 110' hole
8	6 Feb.	0001:00.115	477.4	2.1	Decoupled- 30' diam. sphere
9	6 Feb.	0101:00.113	499.7	2.3	Coupled- 110' hole
10	13 Feb.	1901:00.113	954.0	2.1	Decoupled- 30' diam. sphere
11	13 Feb.	2001:00.114	1003.0	2.4	Coupled- 110' hole
12	20 Feb.	0001:00.112	929.0	1.1	Decoupled- 12' diam. sphere
13	20 Feb.	0100:59.614	987.6	2.5	Coupled- 110' hole
14	27 Feb.	0001:00.127	1902.4	1.1	Decoupled- 12' diam. sphere
15	28 Feb.	0401:00.131	936.2	2.6	Coupled- 110' hole
16	3 Mar.	2301:00.128	199.5	1.4	Coupled- 45' hole
17	4 Mar.	0001:00.130	199.8	1.3-1	Coupled- 45' hole

NOTE 1) All times for shots 5 through 17 are derived from comparisons with WWV. Accuracies are $\pm$ 0.001 sec, except for shot 15, which is $\pm$ 0.003 sec.

2) All yields include "Nitramon" booster and detonator weights of either 2 or 3 pounds.

(Distribution List) for Project COWBOY Final Reports

No. of Copies	Addressee
1	E. N. Parker, DASA, Washington, D.C.
1	A. D. Starbird, DMA, AEC, Washington, D.C.
10	I. Maddock, OBE, AWRE (thru DMA)
1	W. S. Long, BJSM (thru DMA)
1	W. J. Manning, DMA, AEC, Washington, D.C.
5	Department of State (thru DMA)
2	G. B. Kistiakowsky (thru DMA)
10	J. Rosen, DMA, AEC, Washington, D.C.
1	C. H. Reichardt, DI, AEC
5	C. F. Romney (thru DMA)
25	J. G. Lewis, DASA, Washington, D.C.
5	I. D. Brent, II (thru DMA)
3	J. R. Balsley, U.S. Geological Survey, Washington, D.C.
3	D. S. Carder, USCand G S, Washington, D.C.
5	J. E. Crawford, Bureau of Mines, Washington, D.C.
20	J. E. Reeves, ALOO
3	L. S. Ayers, SFOO
3	W. K. Cloud, USCandGS, San Francisco, California
10	B. F. Murphey, SC, Albuquerque, New Mexico
2	R. J. Tockey, SC, Livermore, California
2	R. B. Vaile, Jr., SRI, Menlo Park, California
2	R. M. Foose, SRI, Menlo Park, California
5	N. E. Bradbury, LASL
1	F. Press, California Institute of Technology, Pasadena
1	J. E. Oliver, Columbia University, New York
4	W. G. McMillan, Rand Corp., Santa Monica, California
1	H. A. Bethe, Cornell University, Ithaca, New York
1	S. B. Smith, Holmes and Narvar, Los Angeles, Calif.
1	H. E. Grier, ECandG, Las Vegas, Nevada
1	F. B. Porzel, Armour Research Foundation, Chicago, Ill.
1	W. B. Heroy, Sr., The Geotechnical Corp., Dallas, Texas
2	L. Strickland, Texas Instruments Inc., Dallas, Texas
1	W. R. Mitchell, National Geophysical Corp., Dallas, Tex.
1	J. T. Wilson, University of Michigan
1	H. Benioff, Calif. Institute of Technology, Pasadena, Cal.
1	R. F. Hautley, Sprengnether Instrument Co. St. Louis, Mo.
1	D. N. Tocher, University of California
1	T. C. Poulter, SRI, Menlo Park, California
1	P. D. Trask, University of California, Berkeley, Calif.
1	B. Sussholz, STL, Inglewood, California
50	A. V. Shelton, jr. Lawrence Radiation Laboratory

Titles for Final Project COWBOY Reports

AGENCY	TITLES	AUTHORS
SC, ABQ	Particle Motions near Explosions in Halite	B. F. Murphey et. at.
USC and GS	Seismic Ground Effects from Coupled and Decoupled Shots in Salt	D. S. Carder et. al.
APRL	1. Dynamic Strain Measurements in Salt - Part I	L. A. Obert and/ or associates
	2. Dynamic Strain Measurements in Salt - Part II	
	3. Static Stress Measurements in Salt	
BuMines PIT	Investigations Relating to Gas-Phase Detonations	R. W. VanDolah and/ or associates
WES	Drilling and Grouting Support	J. M. Polatty
SRI	Investigations of On-Site Inspection Techniques for High-Explosive Tests in a Salt Mine	R. B. Hoy and associates
SC, Livermore	High Explosives -- Arming and Firing	R. J. Tockey and associates
LRL	Seismic Decoupling in Spherical Cavities	W. M. Adams and D. S. Carder
LRL	Permanent Deformation	W. A. Hamilton et. al.
LRL	Close-in Pressure Measurements with Tourmaline Crystals on Tamped Detonations	W. F. Lindsay et. al.
EGandG, BOS	Timing and Firing of High Explosives	S. R. Hamilton et. al.
LRL	Instrument Chart and Miscellaneous Engineering Information	R. B. Petrie et. al.
LRL	Interpretation of the Seismic Data	R. F. Herbst and G. C. Werth
LRL	Analysis and Interpretation of Blose-in Measurements	J. H. Nuckolls
LRL	Physical Properties of Salt Samples	S. E. Warner et. al.